University of Sussex

Quantum Gravity and the Renormalisation Group.

From the UV to the IR

Author:
Raul Antonio Cuesta Ramos

Supervisor:
Dr. Daniel Litim

Submitted for the degree of Doctor of Philosophy in Particle Physics

University of Sussex

January 2016

UNIVERSITY OF SUSSEX

Raul Antonio Cuesta Ramos, Doctor of Philosophy

Quantum Gravity and the Renormalisation Group
From the UV to the IR

Summary

General relativity is the successful classical theory describing gravitational interactions from cosmological scales down to the sub-millimetre scale. It has remained an open challenge to combine the principles of general relativity with those of the quantum world. A promising avenue has been put forward by Steven Weinberg, known as the asymptotic safety conjecture for gravity. It stipulates that a quantum field theory of gravity may very well exist as a fundamental and predictive theory up to highest energies. The central ingredient of this scenario is the existence of an interacting ultraviolet fixed point under the renormalisation group running of gravitational couplings. In this thesis, we study several aspects of asymptotic safety for gravity. Firstly, we offer a detailed qualitative and quantitative analysis of modern renormalisation group equations for Einstein-Hilbert gravity by contrasting different implementations of a Wilsonian momentum cutoff in combination with either heat kernel techniques or spectral sums. Secondly, we analyse in some depth the scale-dependence of gravitational couplings in the low-energy regime of Einstein-Hilbert gravity, where indications for the existence of an interacting infrared fixed point are found. Finally, we extend our analysis of renormalisation group trajectories to $f(R)$-type theories of gravity, and investigate how an interacting UV fixed point is connected with the classical low-energy regime. Implications of our findings are discussed.

Acknowledgements

I would like to thank and express my appreciation for my supervisor Daniel Litim for encouraging me constantly, without him this project wouldn't be possible. Thanks to Kevin for all the discussions, parties, etc. Also, thanks to my family and my accomplice of life for putting up with me all the time, in good and bad times. Literally I would not be here without them. Thanks to my office mates as well, and in general to all the students and academics of the department of physics.

Finally I want say thank you to the Mexican National Council for Science and Technology (CONACyT) scholarship scheme for giving me the opportunity to study in the UK.

Contents

List of Tables

List of Figures

Chapter 1

Introduction

Quantum field theory is the modern theory describing the phenomena occurring at the very small lengths. In spite of not explaining the gravitational phenomena, it successfully describes three of the four fundamentals forces in nature: strong and electroweek interactions. Moreover, it is applicable to topics that range from particle physics to condensed matter. With it, the description of a particle arises directly from the degrees of freedom under consideration, and hence it provides a fundamental description of the building blocks of matter.

On the other side of the spectrum, we find general relativity, describing gravity, which in turn is for sure one of the most intriguing phenomena in nature. General relativity is based on the idea that matter modifies the structure of the space-time while at the same instant, space-time dictates the dynamics of matter.

Combining these two fundamental blocks of modern physics has been a challenge for a long time now, and it still is. In contrast with other approaches that try to give a reliable quantum description for gravity, Steven Weinberg's asymptotic safety proposal is a minimal one, in the sense that only requires a slight generalisation on the notion of the perturbative approach for quantising a theory[91] without touching the principles governing general relativity.

Wilson's renormalisation group [94, 96] has proven to be a useful tool for the purpose of studying asymptotic safety for gravity. In its modern approach, Martin Reuter provided the first computations towards proving the existence of a fixed point in $2 + \epsilon$ and four dimensions[80], and from there, a vast amount of results have been found to this days. By now, these results group into studies on Einstein-Hilbert theory [51, 80, 30, 81, 20, 81], inclusions of matter [75, 39, 29], $f(R)$ gravity [19, 33, 26, 61, 9, 8, 38, 74], and some phenomenological studies [82, 59, 58, 55, 21, 37]. Much of these works were enabled, on

the technical side, by optimisation techniques, which have allowed for explicit analytical renormalisation group equations [53, 54].

Despite of the large amount of results and insights found by now, a number of open challenges remain. In this thesis, we will analyse in some depth the following aspects of quantum gravity and its renormalisation group flow. Firstly, finding a complex conjugate pair of scaling exponents is a common result. It has been conjectured that a complex exponent is a sign for a degeneracy within the theory. They are generated by the off-diagonal elements of the stability matrix, in contrast to Gaussian fixed points for which their stability matrix is diagonal or triangular. Then, it remains to be understood whether complex exponents are an artefact of neglecting some interactions, or whether they are a feature of the physical theory. As a starting point, we point out that studies on higher order derivatives keep finding complex critical exponents. Hence, our main new addition here will be to change the the way to compute the running of the couplings. Most studies rely on the use of the so called heat kernel techniques, which amounts to a expansion around small curvature. Instead, we will use spectral sum techniques without any kind of approximation. This will allow us to explore other regimens of the curvature. As a complement of the spectral sums, we will implement an idea to interpolate between both schemes.

Secondly, we will analyse the renormalisation group trajectories which connect the interacting UV fixed point with the deep IR regime of the theory. Thus far this has been done in approximations including up to R^2 interactions [79, 50]. We will improve upon this by including interactions in general $f(R)$ theories. The necessity for this arises because R^2 theory thus far have lead to an unphysically large scaling exponent for the R^2 interaction. The effect of it in the UV in negligible. However, the addition of higher order operators to the theory account to take down the value of the critical exponent to a physically acceptable one. The price to pay is that many more higher order interactions need to be taken into consideration. Here, we will put forward an approach which encodes the higher order terms indirectly, thus allowing for a physically acceptable eigenvalue of the R^2 interaction.

Finally, we put forward the idea that gravity might display an interacting IR fixed points. We explain why the conventional RG equations lead to a degeneracy, and with the help of tools from dynamical systems we will lift it, leading to new infrared fixed points in quantum gravity. These fixed points might play some role for the late-time acceleration of cosmology.

The outline of the thesis is as follows. We start in chapter 2 introducing the general tools and concepts needed for the rest of the thesis. In chapter 3 we will study the spectral sums as mentioned before. For that purpose, we introduce a special parametrisation that will help us to get simple expressions. After that we introduce the notion of spectral sum and projection of the renormalisation group equations. After getting the fixed point and critical exponents of the theory we present the available improvements to the anomalous dimension. Next, in chapter 4 we integrate numerically the RG equations for the R^2 system, and comment on the large critical exponent found. Then, we introduce a new idea in order to compute encode information of higher order couplings into the R^2 flow. Finally in chapter 5 we introduce ideas from dynamical systems in order to disentangle a degenerate fixed point, which on top of it, present a singularity. We find two new fixed points. After that, we define new type of trajectories in theory space to finally show the gauge independence of the result. We will conclude with a brief discussion in chapter 6.

Chapter 2

Renormalisation Group

If general relativity is treated as a usual effective quantum field theory, then Newton's constant, and the cosmological constant must be treated as energy dependent couplings of the system, hence an important task is to study their behaviour for different energy scales. One possibility for this is using the tools and assumptions presented in this chapter.

In particular, we present the way to deduce the flow equation [92] for the quantum Einstein gravity (QEG) as presented in several works [80, 51, 50]. This equation is the essential ingredient in later chapters in order to compute beta functions, fixed points and critical exponents.

2.1 Wilsonian Renormalisation Group

Along this thesis we will be working within a coarse graining-like procedure, as the one formulated by Wilson [94, 96, 67, 77, 6, 76, 98]. This procedure is based on the introduction of an infrared adjustable cut-off scale k, and an ultraviolet (UV) cut-off Λ. Also let us represent high momentum modes by $\phi_>$ ($\Lambda^2 > p^2 > k^2$), and low momentum modes by $\phi_<$ ($k^2 > p^2$). Then the Wilsonian effective action S_k is defined by

$$e^{-S_k[\phi]} \equiv \int_{k^2<p^2<\Lambda^2} \mathcal{D}\phi_> e^{-S[\phi_>+\phi]}, \tag{2.1}$$

from this definition note that this is an implicit definition where we have integrated high energy modes, and then the effective action S_k does not depend on the high energy modes anymore, so we will get the same result for the long distance physics. Note that from (2.1) we can get the Wilsonian action at some lower scale $k'^2 < k^2$

$$e^{-S_{k'}} = \int_{k'^2<p^2<k^2} \mathcal{D}\phi_> e^{-S_k[\phi_>+\phi]}, \tag{2.2}$$

where now the high momentum modes are those defined for the mass shell $k'^2 < p^2 < k^2$.

Finally, with this we can now write the functional integral as

$$\begin{aligned} Z &= \int_{p^2<\Lambda^2} \mathcal{D}\phi e^{-S[\phi]} \\ &= \int_{p^2<k^2} \mathcal{D}\phi_< \int_{k^2<p^2<\Lambda^2} \mathcal{D}\phi_> e^{-S[\phi_>+\phi_<]}, \end{aligned} \tag{2.3}$$

finally, by renaming $\phi_< \to \phi$ we get

$$Z = \int_{p^2<k^2} \mathcal{D}\phi e^{-S_k[\phi]}. \tag{2.4}$$

Now, with this functional integral we can compute correlation functions (or the effective average action) by integrating out quantum fluctuations a momentum shell δk at a time.

2.2 Asymptotic safety

The asymptotic safety scenario was introduce by Weinberg [91] as an extension of asymptotic freedom. The latter, is based on the assumption that all the coupling constants of a well defined quantum field theory (like QCD, the theory of strong interactions) end in a fixed point in the limit of high energies $k \to \infty$ [95, 45, 78]. The QCD case for asymptotic freedom works in a weakly coupled regime where perturbation theory works at its best, in other words the dimensionless gauge coupling is small as we increase the energy towards infinity: $g_s \to 0$ when $k \to \infty$, for such a limit, the theory is free.

However, it is well stablished that quantisation of gravity by means of perturbation theory is not realisable, that asymptotic freedom as in the case for the strong force cannot be achieved. One argument is that just with dimensional arguments we find that the dimensionless Newton's constant $g = k^2 G_k$ grows when we increase the energy, meaning that the theory is strongly coupled in the UV. Another general argument is that, gravity as a non-renormalisable theory in the standard picture, leads to UV divergences that have to be absorbed in several counterterms in the Lagrangian, e.g for the Einstein-Hilbert case we would need to add terms proportional to higher orders of the Ricci scalar R^n, the square of the Ricci tensor $(R_{\mu\nu}R^{\mu\nu})^n$, and the square of the Riemann tensor $(R_{\mu\nu\rho\sigma}R^{\mu\nu\rho\sigma})^n$. In particular, at two loops the Goroff-Sagnotti term $R_{\mu\nu}{}^{\rho\sigma}R_{\rho\sigma}{}^{\lambda\tau}R_{\lambda\tau}{}^{\mu\nu}$ [44] is encountered needing a non-trivial counter term, this proves general relativity as perturbatively non-renormalisable. Also, once matter content is introduced, it makes gravity non-renormalisable at one-loop [90].

Instead, a promising option is Weinberg's proposal [91] to accept that the quantisation of gravity is modified through an interacting UV fixed point, instead of a free one. In order to illustrate how a non-trivial interacting ultraviolet fixed point might arise in gravity,

consider the Gell-Mann-Low equation [43] for Newton's coupling. With just dimensional arguments the general form of this beta function can be found to be

$$\beta_g = \partial_t g = (2 + \eta_N)g.$$

The first term occurs due to the canonical mass dimension of G, while the second term is generated due to quantum fluctuations. Evidently, and without knowing the specific details of the anomalous dimension η_N, this beta function accepts two types of fixed points. First, we have the Gaussian fixed point $g = 0$, at which both terms vanish. Note then that no quantum effects were necessary for it to occur, it follows then that this is a fixed point related to the classical theory. Second, as long as the anomalous dimension exactly cancels with the canonical dimension of g, the theory displays another fixed point. And then the relation $\eta_N = -2$ provides us with an implicit equation for the gravitational fixed point.

Certain toy models are known to achieve this asymptotic safety mechanism, these include gravity in $2 + \epsilon$ dimensions [49, 3, 72, 18], Gross-Neveu models[42, 86, 14], Yang Mill theories above four dimensions[60, 57], and self interacting scalar theories with non-linearly realised symmetry.

A non-Gaussian fixed point is just one of the two ingredients that an asymptotically safe theory must accomplish. In general, if we work with a Wilsonian effective action, we have to include all the possible interactions allowed by the symmetries of our theory (in the case of gravity, invariance under diffeomorphism). A good way to have control over all the coupling constants of a theory, is by defining them as a series expansion in the action over some basis operators $\mathcal{O}$

$$S_k = \sum_i g_i \mathcal{O}_i,$$

with this in mind, the second requirement for a theory to be asymptotically safe is that the dimensionless couplings $\bar{g}_i = k^{d_i} g_i$ (where d_i is the canonical dimension of each coupling) actually sit on a trajectory that hits the fixed point for $k \to \infty$. These class of trajectories will define the ultraviolet critical surface, and the number of free parameters of an asymptotically safe theory will be the dimensionality of this critical surface. If the dimension D of the critical surface is infinite, then we would need to measure an infinite number of free parameters to fully determine our theory. Hence, the second condition for having a asymptotically safe theory is for the dimensionality of the critical surface D to be greater than zero but finite.

An exact analytical way to determine D is given by analysing the neighbourhood of the fixed point g_i^*. Expanding the beta functions to first order around the fixed point we

have

$$\partial_t g_i = \beta_i = \sum_j \left.\frac{\partial \beta_i}{\partial g_j}\right|_{g_l^*} (g_j - g_j^*), \tag{2.5}$$

$$= \sum_j M_{ij}(g_j - g_j^*) \tag{2.6}$$

where M_{ij} is called the stability matrix. The general solution of this system is given by

$$g_i(k) = g_i^* + \sum_K C_K V_i^K k^{-\theta_K}, \tag{2.7}$$

here V_i^K, and $-\theta_K$ are the eigenvectors and eigenvalues of M_{ij} respectively. If $\theta_K < 0$, then in the limit $k \to \infty$ the couplings will never reach the fixed point (the couplings related to this set of eigenvalues are called irrelevant). And therefore, the dimension of the critical surface is the number of positive critical exponents (the corresponding couplings are called relevant). The D constants C_K for which $\theta_k > 0$ are the free parameters of the theory to be determined by initial conditions at some energy k_0 as

$$C_K = \sum_j (S^{-1})_{Kj}(g_j(k_0) - g_j^*), \quad S = (V_1, \ldots, V_D), \tag{2.8}$$

the C_K corresponding to irrelevant couplings are set to zero. Now, assume we have n couplings, from which D are relevant ones, then by removing the cutoff k from the solution of the linearised system, we have D relations between D free parameters, and D relevant couplings. Then, we can solve for all the C_K in terms of the relevant couplings, to finally substitute this values on the remaining $n - D$ relations (corresponding to the irrelevant couplings), and end up with $n - D$ irrelevant couplings in terms of D relevant ones. This defines our UV critical surface in theory space.

2.3 Effective action

In the context of quantum field theory (QFT), a theory, with an Euclidean action $S[\varphi]$, is said to be solved whenever we find all the correlation functions, defined through the Feynman path integral in Euclidean space as

$$\langle \varphi(x_1) \cdots \varphi(x_n) \rangle = \mathcal{N} \int \mathcal{D}\varphi \varphi(x_1) \cdots \varphi(x_n) e^{-S[\varphi]}, \tag{2.9}$$

where $\mathcal{N}$ is a normalisation constant, and the assumption of a well defined regularised measure $\int_\Lambda \mathcal{D}\varphi$, with a UV cut-off Λ. Either, we take S as the Wilsonian effective action S_Λ by integrating out high energy modes, or the limit $\Lambda \to \infty$ is well defined, which means the theory is well defined in the continium.

In terms of the generation functional $Z[J]$

$$Z[J] = \int \mathcal{D}\varphi \exp\left[-S[\varphi] + \int d^d x J(x)\varphi(x)\right] \tag{2.10}$$

with $J(x)$ playing the role a source term which is to be considered as an external field, (2.9) is written as

$$\langle \varphi(x_1)\cdots\varphi(x_n)\rangle = \frac{1}{Z[0]}\frac{\delta^n Z[J]}{\delta J(x_1)\cdots\delta J(x_n)}\bigg|_{J=0}. \tag{2.11}$$

Also, in the context of a perturbative expansion, we can express connected Feynman diagrams out of the so called Schwinger functional $W[J] = \ln Z[J]$. And, the expectation value $\phi(x)$ of a field $\varphi(x)$ at a point x is

$$\phi(x) = \langle\varphi(x)\rangle = \frac{\delta W[J]}{\delta J(x)} = \frac{1}{Z[J]}\frac{\delta Z[J]}{\delta J(x)}. \tag{2.12}$$

Now, we can define the Legendre transform of $W[J]$:

$$\Gamma[\phi] = \sup_J \left\{-W[J] + \int d^d x J(x)\phi(x)\right\}, \tag{2.13}$$

this is the effective action (or generating functional of one-particle irreducible correlation functions), and the $\sup_J$ means that the right hand side (RHS) is taken at $J = J_{sup}[\phi]$ by taking the supremum. As a consequence of this, if $W[J]$ is a convex functional so too is $\Gamma[\phi]$, and thus the latter enjoys the property

$$\frac{\delta^2\Gamma}{\delta\phi\delta\phi} \geq 0, \tag{2.14}$$

and can be viewed as the quantum counterpart of the classical action $S[\varphi]$, in fact if one takes the functional derivative of (2.13) we get the quantum equation of motion

$$\frac{\delta\Gamma[\phi]}{\delta\phi(x)} = J(x), \tag{2.15}$$

however, unlike its classical counterpart, (2.15) takes into account all quantum fluctuations averaged over in the functional integral.

2.4 Functional renomalisation for gravity

Here, we recall Wilson's (functional) renormalisation group idea, which is based on the notion of an average effective action Γ_k which connects the bare action $\Gamma_{k\to\infty} = S$ with an IR action $\Gamma_{k\to 0} = \Gamma$. Here, k is the renormalisation group momentum scale, and it dictates the scale down to which modes have been integrated out in the path integral.

Following [51, 68, 65, 64], we start with the modified functional for connected Green's functional

$$\exp\{W_k[t^{\mu\nu}]\} = \int \mathcal{D}\gamma_{\mu\nu} \exp\{-S[\gamma] - \Delta S_k[\gamma] + S_{source}\}, \tag{2.16}$$

where $S_{source} = \int d^dx \sqrt{\gamma}\gamma_{\mu\nu}t^{\mu\nu}$, the integration is over all Euclidean signature real Riemannian metrics, and $S[\gamma]$ is the classical euclidean form of some general gravity theory (e.g. Einstein-Hilbert, f(R), etc.). The crucial part that make $W_k[\gamma]$ a scale-dependent quantity is the Wilsonian infrared (IR) cutoff $\Delta_k S$, which has the form of a mass term

$$\Delta S_k[\gamma] = \frac{1}{2}\int d^dx \frac{1}{32\pi G}\sqrt{\gamma}\gamma_{\mu\nu}R_k^{\mu\nu\rho\sigma}\gamma_{\rho\sigma}. \tag{2.17}$$

The cutoff operator $R_k^{\mu\nu\rho\sigma}$ (not to be confused this with the Riemann tensor) appearing in (2.17) is such that eigenmodes of the covariant Laplacian $-\nabla^2$ with eigenvalues $p^2 \gg k^2$ are kept in (2.16), while small eigenvalues $p^2 \ll k^2$ are suppressed, i.e. (2.17) describe the transition from the high-momentum regime to the low-momentum regime, i.e.

$$R_k(p^2) = k^2 \ \text{ for } \ p^2 \ll k^2, \qquad R_k(p^2) = 0 \ \text{ for } \ p^2 \gg k^2 \tag{2.18}$$

As usual with gauge field theories, the measure $[\mathcal{D}\gamma_{\mu\nu}]$ in (2.16) is overdetermined by the gauge freedom of our theory. In our case this freedom is dictated by the symmetry under diffeomorphisms

$$\delta_\epsilon\gamma_{\mu\nu} = \nabla_\mu\epsilon_\nu + \nabla_\nu\epsilon_\mu = \frac{1}{2}\nabla^\lambda\epsilon_\lambda\gamma_{\mu\nu} + (L\epsilon)_{\mu\nu}, \tag{2.19}$$

where the operator L maps vectors into symmetric trace-free tensors

$$(L\epsilon)_{\mu\nu} = \nabla_\mu\epsilon_\nu + \nabla_\nu\epsilon_\mu - \frac{1}{2}\gamma_{\mu\nu}\nabla_\lambda\epsilon^\lambda. \tag{2.20}$$

In order to extract this overdetermination, we need to choose a gauge fixing condition

$$F_\mu - l_\mu = 0, \tag{2.21}$$

with l_μ being arbitrary functions over space-time.

The way to introduce this gauge fixing condition into our generating functional (2.16), we use the Faddev-Popov trick. We first multiply the functional unit element

$$1 = \int \mathcal{D}\epsilon\delta[F_\nu(\gamma^\epsilon_{\mu\nu}) - l_\nu]\det(\frac{\delta F_\nu(\gamma^\epsilon_{\mu\nu})}{\delta\epsilon^\rho}) \tag{2.22}$$

where γ^ϵ is the transformed metric

$$\gamma^\epsilon_{\mu\nu} = \gamma_{\mu\nu} + \delta_\epsilon\gamma_{\mu\nu}. \tag{2.23}$$

We will be considering gauge conditions which are linear in the metric field, hence F_μ takes the form $F_\mu = \mathcal{F}_\mu^{\alpha\beta}\gamma_{\alpha\beta}$. For this kind of gauge condition, inserting (2.22) into the functional integral and performing the change of variable $\gamma^\epsilon \to \gamma$ we get

$$\int \mathcal{D}\epsilon \int \mathcal{D}\gamma_{\mu\nu} e^{-S[\gamma]} \delta[F_\nu(\gamma_{\mu\nu}) - l_\nu] det\left(\mathcal{F}_\nu^{\alpha\beta}(\gamma_{\alpha\rho}\nabla_\beta + \gamma_{\beta\rho}\nabla_\alpha)\right). \tag{2.24}$$

Here the integral over ϵ can be identify as volume of the group $Vol\mathcal{G}$, and can be factored out. Also, by introducing an arbitrary non-degenerated functional $G_{\mu\nu}[\gamma_{\alpha\beta}]$, such that

$$1 = det^{1/2} G_{\alpha\beta} \int \mathcal{D}l_\nu exp\left[-\int d^d x \frac{1}{2} l^\alpha G_{\alpha\beta} l^\beta\right], \tag{2.25}$$

and integrating (2.24) over l_ν with such a weight, we can write (by discarding the constant $Vol\mathcal{G}$, and using the functional delta)

$$\int \mathcal{D}\gamma_{\mu\nu} e^{-S[\gamma]} = \int \mathcal{D}\gamma_{\mu\nu} e^{-S[\gamma]-S_{gf}} \det M_{\mu\nu} (\det G_{\mu\nu})^{1/2} \tag{2.26}$$

where,

$$S_{gf} = \frac{1}{2}\int d^d x F^\mu G_{\mu\nu} F^\nu, \tag{2.27}$$

is the gauge fixing action, and

$$M_{\mu\nu} = \mathcal{F}_\mu^{\alpha\beta}(\gamma_{\alpha\nu}\nabla_\beta + \gamma_{\beta\nu}\nabla_\alpha) \tag{2.28}$$

is the Faddeev-Popov operator. These determinants can be expressed in terms a pair of complex conjugate anti-commuting ghost fields z_μ and $\bar{z}_\mu$ and a third real ghost b_μ.

Finally, we can write our modified generating functional (2.16) as

$$exp\{W_k[j]\} = \int \mathcal{D}\gamma_{\mu\nu}\mathcal{D}\bar{C}_\mu \mathcal{D}C_\mu \mathcal{D}b_\mu e^{-S[\gamma]-S_{gf}[\gamma]-S_{gh}[\bar{z},z,b]-S_{source}-\Delta S_k[\gamma,\bar{z},z,b]}, \tag{2.29}$$

where j encodes all the external sources for the different fields, and ΔS_k includes a regulator for each fluctuating field. Then, following the steps of last section, we get the effective action

$$\begin{aligned} \Gamma_k[\phi] &= \bar{\Gamma}_k - \Delta S_k, \\ &= \sup_J \left\{-W_k[j] + \int d^d x \sqrt{g} j(x)\cdot\phi(x)\right\} - \Delta S_k, \end{aligned} \tag{2.30}$$

where the product $\cdot$ means summation over field and indices, also $\phi = \{\bar{g}_{\mu\nu}, C_\mu, \bar{C}_\mu, B_\mu\}$ are the expectation values of the integral variables $\varphi = \{\gamma_{\mu\nu}, z_\mu, \bar{z}_\mu, b_\mu\}$.

In order to maintain the invariance under diffeomorphisms along our treatment and construct the regulators we use the background gauge fixing technique [41], for which we expand the metric $\bar{g}_{\mu\nu}$ around a fixed background field $g_{\mu\nu}$. With this, the regulator will be a function of a differential operator Δ defined on the background metric.

Now, let us consider the connected two point function (propagator)

$$(G_k)_{ij}(x,y) = \frac{1}{\sqrt{g(x)g(y)}}\frac{\delta^2 W_k}{\delta j_i \delta j_j} = \langle \varphi_i(x)\varphi_j(y)\rangle - \phi_i(x)\phi_j(y), \tag{2.31}$$

and also note that the propagator may be written as $G_k(x,y) = (1/\sqrt{g(y)})\delta\phi(x)/\delta j(y)$, hence it follows that

$$\int d^d y\sqrt{g(y)}G_k(x,z)\frac{\delta j(y)}{\delta\phi(z)} = \delta(x-z). \tag{2.32}$$

Next, by taking the second functional derivative of (2.30) respect the fields ϕ, one finds a relationship between $\delta j/\delta\phi$ and the Hessian of the effective action. All these mean that the propagator is related to the Hessian of the effective action and the regulator as

$$(G_k(x,y))_{ij} = \left[\frac{\delta^2\Gamma_k}{\delta\phi_i\delta\phi_j} + R_k\right]^{-1}(x,y). \tag{2.33}$$

Finally, we take the scale derivative of the effective action Γ_k at constant fields

$$\begin{aligned} k\partial_k\Gamma_k &= k\partial_k W_k - \frac{1}{2}\phi\cdot k\partial_k R_k\cdot\phi \\ &= \frac{1}{2}\langle\varphi\cdot k\partial_k R_k\cdot\varphi\rangle - \frac{1}{2}\langle\varphi\rangle\cdot k\partial_k R_k\langle\varphi\rangle \\ &= \frac{1}{2}S\mathrm{Tr}[k\partial_k R_k\cdot G_k], \end{aligned} \tag{2.34}$$

and finally, we get

$$\partial_t\Gamma_k[\phi;g] = \frac{1}{2}S\mathrm{Tr}\left[\frac{1}{\Gamma_k^{(2)}[\phi;g]+R_k[g]}\cdot\partial_t R_k[g]\right] \tag{2.35}$$

which is referred as the flow equation (or Wetterich equation). Here the super trace $S\mathrm{Tr}$ means we have to sum over all indices, fields, and integrate over space-time. And, since our momentum is defined by a background metric, then we need to take the limit $g_{\mu\nu} = \bar{g}_{\mu\nu}$ at the end of any calculation.

The flow equation (2.35) is an exact functional differential equation for Γ_k, for which finding a solution is a formidable task. This equation give rise to a flow in a usually infinite dimensional space spanned by the couplings associated with the operators in the action respecting the symmetries of our theory. As it is impossible to solve (2.35) exactly, in order to extract physical information out of it, we need to turn into reliable approximations for our effective action Γ_k. In particular as we will be working with the background field method, it means we will be considering three metrics into account: the background metric $g_{\mu\nu}$, the fluctuating metric field $h_{\mu\nu} \equiv \bar{g}_{\mu\nu} - g_{\mu\nu}$, and the full classical metric $\bar{g}_{\mu\nu}$. Then, our first approximation is to take into account effective actions of the form

$$\Gamma_k[\bar{g},g,C,\bar{C}] = \bar{\Gamma}_k[\bar{g}] + \hat{\Gamma}_k[\bar{g},g] + S_{gf}[h;g] + S_{gh}[h,C,\bar{C};g], \tag{2.36}$$

the first term here encodes interaction monomials built from the classical action only

$$\bar{\Gamma}_k[\bar{g}] = \Gamma_k[\bar{g}, \bar{g}, 0, 0] \tag{2.37}$$

while $\hat{\Gamma}_k$ contains the deviations from $\bar{g} = g$ (or the remainder terms), and by definition $\hat{\Gamma}_k[\bar{g}, \bar{g}] = 0$. Since the beginning the proposal was to neglect $\hat{\Gamma}_k$ [80], and within this approximation it has been stablished the existence of a non-gaussian fixed point with a finite number of relevant operators as it is required for the asymptotic safety program [9, 20, 30, 36, 50, 51, 61, 81]. However, recently, while trying to tackle the background independence problem, it was introduced the so called bimetric truncations in which the term $\hat{\Gamma}_k$ is no longer discarded and hence the flow equation is capable of discerning between invariants built with the total metric and the background one [62, 63]. Nevertheless, in this thesis we will focus on the single metric case.

Chapter 3

Functional Renormalisation and Spectral Sums

In this chapter we will focus on quantum gravity in the Einstein-Hilbert theory. The principal aim is to evaluate the functional integral using spectral sums techniques, rather than the widely-used heat kernel expansion. The main motivation for this are:

Firstly, the heat kernel expansion used in the context of asymptotic safety is an approximation scheme bound to regions of small curvature. Spectral sums in principle should provide a way to explore other regions with a non-small curvature giving rise to good results.

Secondly, the vast majority of studies have found interacting fixed points in the Einstein-Hilbert theory provided with a pair of complex scaling exponents. As it was first explained in [36], the presence of complex exponents indicate a degeneracy due to the approximation. It is possible that the degeneracy gets unfolded once more interactions are taken into account. Alternatively, the degeneracy might be lifted once quantum fluctuations are resummed in a more accurate way.

Thirdly, in many previous studies RG equations have been derived by expanding the quantum effective action around vanishing background Ricci curvature. But in principle, fixed point solutions should be valid for all curvature values. In fact, is was shown recently that the sensitivity to gauge fixing parameters is reduced provided the functional integral is evaluated on the equations of motion[7, 9]. Therefore, we will study RG equations in settings where the evolution of couplings is derived from non-trivial background curvature.

Finally, we wish to explore more generally the extent to which spectral sum methods are practical and useful for advanced investigations in quantum gravity.

With these goals in mind, this chapter is organised as follows. First in sections 3.1,

3.2,3.3, and 3.4 we will review the key methods and explain how they are used in quantum gravity. Then, in section 3.5 we will contrast heat kernel and spectral sum methodologies using all types of Wilsonian momentum cutoffs introduced in the literature. Furthermore, in 3.6, 3.7, and 3.8 we will systematically analyse the background curvature dependence of the results, and the effect of spectral sums on the existence of fixed points and the eigenvalue spectrum. Much of our work will use numerical tools, while some other results are achieved analytically.

3.1 Gauge fixing and field decomposition

Our main motivation is the one-loop result (semi-classical approximation)[64, 65, 68], where at the level of the generation functional (2.10) when we apply the equations of motion $R = 4\Lambda$, we are left with the $(d-2)(d+1)/2$ transverse-traceless fluctuations, a constant mode and $d-1$ degrees of freedom coming from the Jacobian arising after the decomposition of the metric into its irreducible components. Also, in this approximation [35], with the Faddeev-Popov method, the gauge fixing action is explicitly cancelled by the ghosts action.

The first step is invoking the background gauge fixing technique [1, 2]. For this, we decompose the metric $\gamma_{\mu\nu}$ into a fixed background metric and a fluctuation $\bar{h}_{\mu\nu}$

$$\gamma_{\mu\nu} = g_{\mu\nu} + \bar{h}_{\mu\nu}. \tag{3.1}$$

This split of the metric changes the integration variables of the functional integral (2.16) as $\int \mathcal{D}\gamma_{\mu\nu} = \int \mathcal{D}\bar{h}_{\mu\nu}$. Also, the gauge condition F_μ from (2.27) was linear in the whole metric $\gamma_{\mu\nu}$, but after the split will turn into a linear functional of the fluctuation field $F_\mu = \mathcal{F}_\mu^{\alpha\beta}\bar{h}_{\alpha\beta}$, where $\mathcal{F}$ now depends solely on the background metric. Finally, everything else will be written in terms of the expectation value of the fluctuation field $h_{\mu\nu} = \langle\bar{h}_{\mu\nu}\rangle$, and the covariant derivative D_μ compatible with the background metric.

We will use the gauge fixing term

$$S_{gf} = \frac{Z_k}{2\alpha}\int d^dx\sqrt{g}F_\mu F^\mu, \tag{3.2}$$

this means that in (2.27) $G_{\mu\nu} = Z_k\sqrt{g}g_{\mu\nu}/\alpha$, Z_k is the wave function renormalisation and

$$F_\mu = D^\nu h_{\mu\nu} - \frac{1+\rho}{d}D_\mu h.$$

Here, α measures the strength of the gauge fixing term while ρ gives rise to different gauges. $\rho = \frac{d}{2} - 1$ corresponds to the harmonic gauge whilst for $\rho = 0$ we have the

geometric gauge. We will be working with the latter after showing a way to cancel the gauge degrees of freedom in the flow equation (2.35).

The transverse-traceless decomposition for the metric fluctuation $h_{\mu\nu}$ [97] is given by

$$h_{\mu\nu} = h^{\perp}_{\mu\nu} + D_\mu \xi_\nu + D_\nu \xi_\mu + D_\mu D_\nu \sigma + \frac{1}{d} g_{\mu\nu} h - \frac{1}{d} g_{\mu\nu} D^2 \sigma, \tag{3.3}$$

which will help us to write the hessian and the gauge fixing action into a diagonal form. In (3.3) $h^{\perp}_{\mu\nu}$ is the traceless transverse part of the fluctuation, h is its trace part, and the longitudinal traceless part of it is formed by the transverse vector ξ_μ and the scalar σ. Hence, the following properties follow

$$D^\mu h^{\perp}_{\mu\nu} = 0, \quad h^{\perp\mu}_{\mu} = 0, \quad D_\mu \xi^\mu = 0, \quad h = h^\mu_\mu \tag{3.4}$$

By decomposing the gauge vector ϵ_μ into its transverse and longitudinal parts ($\epsilon_\mu = \epsilon^{\perp}_{\mu} + D_\mu \epsilon$, with $D_\mu \epsilon^{\perp\mu} = 0$), symmetry (2.19) translate into

$$\begin{aligned} h^{\perp}_{\mu\nu} &\to h^{\perp}_{\mu\nu}, \quad \xi_\mu \to \xi_\mu + \epsilon^{\perp}_{\mu}, \\ \sigma &\to \sigma + 2\epsilon, \quad h \to h + 2D^2 \epsilon. \end{aligned} \tag{3.5}$$

From here and (3.3) we can see that the field redefinition of h

$$\bar{h} = h - D^2 \sigma, \tag{3.6}$$

mixes the trace and trace-free parts of the metric to give rise to a gauge invariant mode $\bar{h}$.

From here on we will start using maximally symmetric spaces as background, hence, Riemann and Ricci tensors can be written as

$$R_{\mu\nu\rho\sigma} = \frac{R}{d(d-1)} (g_{\mu\rho} g_{\nu\sigma} - g_{\mu\sigma} g_{\nu\rho}), \quad R_{\mu\nu} = \frac{R}{d} g_{\mu\nu}, \tag{3.7}$$

where the Ricci scalar R is a constant.

Using (3.3), (3.6), and (3.7) in (3.2), we get

$$\begin{aligned} S_{gf} = \frac{Z_k}{2\alpha} \int d^d x \sqrt{g} \Big(& \xi_\mu \Delta_1^2 \xi^\mu + \bar{h} \frac{\rho}{d^2} \left[((d-1-\rho)\Delta - R)\, \Delta \sigma + \rho \Delta \bar{h} \right] \\ & + \sigma \frac{1}{d^2} ((d-1-\rho)\Delta - R) \left[((d-1-\rho)\Delta - R) \Delta \sigma + \rho \Delta \bar{h} \right], \end{aligned} \tag{3.8}$$

here, $\Delta_1 = -D^2 - R/d$, and $\Delta = -D^2$. Also, note that in the geometric gauge ($\rho = 0$), there are no mixing terms for the gauge fixing action. Another way to get rid of the mixing terms is by redefining the scalar mode σ, by introducing the new field $\bar{\sigma}$ as

$$\bar{\sigma} = \sigma + \frac{\rho}{(d-1-\rho)\Delta - R} \bar{h}. \tag{3.9}$$

Finally with all these, we end up with two gauge dependent fields (corresponding to d degrees of freedom, $d-1$ from the traverse vector ξ_μ and 1 from the scalar mode $\bar{\sigma}$),

$$S_{gf} = \frac{Z_k}{2\alpha}\int d^dx\sqrt{g}\left[\xi_\mu\Delta_1^2\xi^\mu + \bar{\sigma}\Delta_L^2\Delta\bar{\sigma}\right], \tag{3.10}$$

with the gauge dependent differential operator acting on scalars as

$$\Delta_L\phi = \frac{1}{d}\left((d-1-\rho)\Delta - R\right)\phi. \tag{3.11}$$

3.2 Hessians

As explained in chapter 2, after taking the second functional derivative of the effective action, we need to evaluate the flow equation at $\bar{g}_{\mu\nu} = g_{\mu\nu}$. Hence, the hessian in matrix notation can be expressed as

$$(\Gamma_k^{(2)})^{ij} \equiv \frac{1}{\sqrt{g}}\frac{\delta^2\Gamma_k}{\delta\phi_i\delta\phi_j}, \tag{3.12}$$

where $\phi_i = \{h^\perp_{\mu\nu}, \xi_\mu, \bar{\sigma}, \bar{h}, C_\mu, \bar{C}_\mu, B_\mu\}$ are the expectation values of the metric fluctuations (after the TT decomposition) and the ghosts.

For the Einstein-Hilbert theory

$$\Gamma_k = \frac{1}{16\pi G_k}\int d^dx\sqrt{g}\left[-R + 2\Lambda_k\right] + S_{gf} + S_{gh}, \tag{3.13}$$

where we can identify the wave function renormalisation Z_k with the gravitational coupling G_k by $Z_k = 1/(16\pi G_k)$, and defining the inverse propagator plus the gauge fixing term $\bar{\Gamma}_k = \Gamma_k - S_{gh}$, the quadratic part of the effective action due to the metric fluctuation is

$$\begin{aligned}\frac{1}{2}h_{\mu\nu}\bar{\Gamma}_k^{(2)\mu\nu\rho\sigma}h_{\rho\sigma} = Z_k\int d^dx\sqrt{g}[&-\frac{1}{4}h_{\mu\nu}D^2h^{\mu\nu} + \frac{1}{8}(R-2\Lambda_k)(2h_{\mu\nu}h^{\mu\nu} - h^2)\\ &+\frac{1}{2}hR_{\mu\nu}h^{\mu\nu} - \frac{1}{2}h_{\mu\nu}R^\nu_\rho h^{\mu\rho} - \frac{1}{2}h_{\mu\nu}R^\nu{}_\rho{}^\mu{}_\sigma h^{\rho\sigma} + \frac{1+\alpha}{2\alpha}h_{\mu\nu}D^\nu D_\rho h^{\rho\mu}\\ &+\frac{2(1+\rho)-d\alpha}{2d\alpha}hD_\mu D_\nu h^{\mu\nu} + \frac{d^2\alpha - 2(1+\rho)^2}{4d^2\alpha}hD^2h].\end{aligned} \tag{3.14}$$

After substituting (3.3) and (3.6) into (3.14), we get the quadratic part for the TT symmetric tensor part

$$\begin{aligned}h^\perp_{\mu\nu}\bar{\Gamma}^{(2)}_{h_\perp h_\perp}h^{\perp\mu\nu} &= \frac{1}{4}h^\perp_{\mu\nu}\left(\Delta + \frac{2}{d(d-1)}R\right)h^{\perp\mu\nu} + \left(R - \frac{2d}{d-2}\Lambda_k\right)\frac{d-2}{4d}h^\perp_{\mu\nu}h^{\perp\mu\nu}\\ &= \frac{1}{4}h^\perp_{\mu\nu}\Delta_2 h^{\perp\mu\nu} + \left(R - \frac{2d}{d-2}\Lambda_k\right)\frac{d-2}{4d}h^\perp_{\mu\nu}h^{\perp\mu\nu}\end{aligned} \tag{3.15}$$

with $\Delta_2 = -D^2 + \frac{2R}{d(d-1)}$ as the Lichnerowicz Laplacian restricted to spheres. Also, for the transverse vector part we get

$$\xi_\mu\bar{\Gamma}^{(2)}_{\xi\xi}\xi^\mu = \frac{1}{2\alpha}\xi_\mu\Delta_1^2\xi^\mu + \left(R - \frac{2d}{d-2}\Lambda_k\right)\frac{d-2}{2d}\xi_\mu\Delta_1\xi^\mu, \tag{3.16}$$

and the scalar contributions

$$\sigma\bar{\Gamma}^{(2)}_{\sigma\sigma}\sigma = \frac{1}{2\alpha d^2}\sigma\left[(d-1-\rho)\Delta - R\right]^2\Delta\sigma + \left(R - \frac{2d}{d-2}\Lambda_k\right)\frac{d-2}{8d^2}\sigma(d\Delta - 2R)\Delta\sigma, \quad (3.17)$$

$$\bar{h}\bar{\Gamma}^{(2)}_{\bar{h}\bar{h}}\bar{h} = \frac{\rho^2}{2\alpha d^2}\bar{h}\bar{h} - \frac{d-2}{4d^2}\bar{h}\left[(d-1)\Delta - R\right]\Delta\bar{h} - \left(R - \frac{2d}{d-2}\Lambda_k\right)\frac{(d-2)^2}{8d^2}\bar{h}\bar{h}, \quad (3.18)$$

and the mixing term

$$\sigma\bar{\Gamma}^{(2)}_{\sigma\bar{h}}\bar{h} = \bar{h}\bar{\Gamma}^{(2)}_{\bar{h}\sigma}\sigma = \bar{h}S^{(2)}_{gf}\sigma + \frac{(d-2)^2}{8d^2}\left(R - \frac{2d}{d-2}\Lambda_k\right)\sigma\Delta\bar{h}. \quad (3.19)$$

Next, we still need to substitute (3.9) into all the quadratic parts of the effective action. This change of variables leaves the $h^\perp h^\perp$, $\xi\xi$, and $\bar{\sigma}\bar{\sigma}$ sectors unchanged, while the mixing and the $\bar{h}\bar{h}$ parts are

$$\bar{\sigma}\bar{\Gamma}^{(2)}_{\bar{\sigma}\bar{h}}\bar{h} = \bar{h}\bar{\Gamma}^{(2)}_{\bar{h}\bar{\sigma}}\bar{\sigma} = \frac{(d-2)^2}{8d^2}\left(R - \frac{2d}{d-2}\Lambda_k\right)(d-2-2\rho)\bar{h}\frac{(d-1)\Delta - R}{(d-1-\rho)\Delta - R}\Delta\bar{\sigma}, \quad (3.20)$$

and

$$\begin{aligned}\bar{h}\bar{\Gamma}^{(2)}_{\bar{h}\bar{h}}\bar{h} &= -\frac{d-2}{4d^2}\bar{h}\left[(d-1)\Delta - R\right]\bar{h} + \left(R - \frac{2d}{d-2}\Lambda_k\right)X, \\ &= -\frac{(d-2)(d-1)}{4d^2}\bar{h}\Delta_0\bar{h} + \left(R - \frac{2d}{d-2}\Lambda_k\right)X,\end{aligned} \quad (3.21)$$

with $\Delta_0 = -D^2 - R/(d-1)$, and

$$X = -\frac{d-2}{8d^2}\bar{h}\left[(d-1)\Delta - R\right]\frac{(d-2)((d-1)\Delta - R) - 2\rho^2\Delta}{\left[(d-1-\rho)\Delta - R\right]^2}\bar{h} \quad (3.22)$$

At this point it is convenient to summarise the different Laplacians defined so far

$$\Delta_2 = -D^2 + \frac{2R}{d(d-1)}, \qquad \Delta_1 = -D^2 - \frac{R}{d}, \qquad \Delta_0 = -D^2 - \frac{R}{d-1}. \quad (3.23)$$

Now, it is clear that with the field redefinitions (3.3), (3.6) and (3.9), whenever we work on-shell, i.e. $R = \frac{2d}{d-2}\Lambda_k$, the whole Hessian matrix is diagonal, and the unique gauge dependent parts are those for the transverse vector ξ_μ (which is fourth order in derivatives) and the scalar $\bar{\sigma}$ (which is sixth order in derivatives).

3.3 Ghosts, auxiliary fields and Jacobians

3.3.1 Ghosts

We start writing down the ghost action. For this purpose, we exploit our freedom to write the determinant of the Faddeev-Popov operator (2.28) as $\det M = \left(\det M^2\right)^{1/2} = \det(M^2)(\det M^2)^{-1/2}$. This choice introduces the usual anti-commuting ghosts $\bar{C}_\mu$, C_μ, and a third ghosts B_μ which is a real commuting field first introduced in [7]. Be careful

with the latterreal field since this is not the same field arising from the operator $G_\mu\nu$ appearing in chapter 2 and[15, 40]. Also, in a similar fashion to decomposition (3.3), here we perform the transverse decomposition of the ghosts

$$\bar{C}_\mu = \bar{C}^\perp_\mu + D_\mu \bar{C}, \quad C_\mu = C^\perp_\mu + D_\mu C, \quad B_\mu = B^\perp_\mu + D_\mu B \tag{3.24}$$

Now, at the level of the effective action by remembering the form of the Faddeev-Popov operator, we get the ghost action from (2.26)

$$\begin{aligned}
\Gamma_{gh} =& \frac{Z_k}{\alpha}\int d^dx\sqrt{g}\bar{C}_\mu(M^2)^{\mu\nu}_\lambda C_\nu + \frac{Z_k}{2\alpha}\int d^dx\sqrt{g}B_\mu(M^2)^{\mu\nu}B_\nu \\
=& \frac{Z_k}{\alpha}\int d^dx\sqrt{g}\Bigg[\bar{C}^{\perp\mu}\left(\Delta - \frac{R}{d}\right)^2 C^\perp_\mu + 4C\left(\frac{d-1-\rho}{d}\Delta - \frac{R}{d}\right)^2 \Delta C + \\
&+ B^{\perp\mu}\left(\Delta - \frac{R}{d}\right)^2 B^\perp_\mu + 4B\left(\frac{d-1-\rho}{d}\Delta - \frac{R}{d}\right)^2 \Delta B\Bigg] \\
=& \frac{Z_k}{\alpha}\int \sqrt{g}[\bar{C}^{\perp\mu}\Delta_1^2 C_\mu + 4\bar{C}\Delta_L^2\Delta C + B^{\perp\mu}\Delta_1^2 B_\mu + 4B\Delta_L^2\Delta B]
\end{aligned} \tag{3.25}$$

3.3.2 Jacobians

Here we take into account the various field redefinitions (3.24), (3.3). In appendix A it is shown that the TT decomposition gives rise to two Jacobians

$$J_0 = (\det{}''\Delta_0)^{1/2}, \qquad J_1 = (\det{}'(\Delta_1))^{1/2}, \tag{3.26}$$

where $\Delta_0 = \Delta - R/(d-1)$ and $\Delta_1 = \Delta - R/d$, and the primes indicate that we need to remove zero modes or negative modes. Also, from the decomposition of the ghosts we get the Jacobian

$$J_{gh} = (\det\Delta)^{-1/2}, \tag{3.27}$$

one way to avoid including the auxiliary field coming from J_{gh} is to rescale the longitudinal modes $\psi_L = \{\bar{\sigma}, B, C, \bar{C}\}$ according to $\psi_L \to (1/\sqrt{-D^2})\psi_L$. This rescaling also prevents the Jacobian J_0 from being fourth order in derivatives. Finally, redefinitions (3.6) and (3.9) give rise to trivial Jacobians, and then they do not introduce new auxiliary fields.

3.3.3 Auxiliary fields

Using the standard Gaussian integration, we can rewrite the contributions of the Jacobians as

$$S_{aux} = \int d^dx\sqrt{g}\left[2\bar{c}^{\perp\mu}\Delta_1 c^\perp_\mu + \left(\frac{d-1}{d}\right)\bar{c}\Delta_0\Delta c + 2\phi^{\perp\mu}\Delta_1\phi^\perp_\mu + \left(\frac{d-1}{d}\right)\phi\Delta_0\phi\right], \tag{3.28}$$

similar to the ghost sector, here $c^\perp_\mu$ and c (and the corresponding barred fields) are complex Grassmann fields, while $\phi^\perp_\mu$ and ϕ are real commuting ghosts.

Spin s	Eigenvalue $\omega(l,s)$	Multiplicity $m(l,s)$
0	$\frac{l(l+d-1)}{d(d-1)}R;\ l=0,1,\ldots$	$\frac{(l+d-2)!(2l+d-1)}{l!(d-1)!}$
1	$\frac{l(l+d-1)-1}{d(d-1)}R;\ l=1,2,\ldots$	$\frac{(l+d-3)!l(l+d-1)(2l+d-1)}{(l+1)!(d-2)!}$
2	$\frac{l(l+d-1)-2}{d(d-1)}R;\ l=2,3,\ldots$	$\frac{(l+d-3)!(d+1)(d-2)(l+d)(l-1)(2l+d-1)}{2(l+1)!(d-1)!}$

Table 3.1: Eigenvalues of the Laplacian on the d-sphere and their corresponding multiplicities [84, 85].

It is important to note that each transverse vector $\xi_T = \{\xi_\mu, B_\mu^\perp, \bar{C}_\mu^\perp, C_\mu^\perp\}$, and each longitudinal scalar ψ_L share the same number of components of Δ, also, ξ_T and ψ_L have the same number of commuting and anti-commuting fields.

3.4 Wilsonian cutoff Schemes

The general form of the regulator (2.17) will be

$$R_k = Z_k r_k(z), \tag{3.29}$$

here, the cutoff function r_k vanishes in the limit $k \to 0$ for all the eigenvalues z of a differential operator of the form $z = -D^2 + U$.

The inverse propagator $\Gamma_k^{(2)}$ in general is a differential operator of the form $\Delta = -D^2 + \mathbf{E}$, where $\mathbf{E}$ is a linear map acting on quantum fields, and in our case it contains linear curvature terms, and the couplings of the effective action (cosmological constant in the Einstein-Hilbert case). Using the terminology of [20], we split $\mathbf{E} = \mathbf{E}_1 + \mathbf{E}_2$, here $\mathbf{E}_1$ does not contain any couplings, while $\mathbf{E}_2$ does.

1. If the cutoff operator r_k is only a functions of the Laplacian, we will call it type I cutoff (i.e. $U = 0$).

2. If the cutoff operator r_k is only a functions of the kinetic operator $-D^2 + \mathbf{E}_1$, we will call it type II cutoff (or $U \equiv U(R)$).

   (a) Cutoff II type a.- This is such that, the integrand keeps a part proportional to the on-shell condition $(d-2)R/2d - \Lambda_k$

   (b) Cutoff II type b.- Takes the whole $\mathbf{E_1}$ into the cutoff.

3. And if the cut off operator is a function of the full operator $\Delta = -D^2 + \mathbf{E}$, then it will be called type III (for Einstein-Hilbert theory this means $U \equiv U(R, \Lambda_k)$).

One important feature of the field parametrisation introduced, (i.e., $\{h^{\perp}_{\mu\nu}, \xi_\mu, \bar{h}, \bar{\sigma}\}$) in the structure of the quadratic part of the effective action (with components (3.15), (3.16), (3.17), (3.20) and (3.21)) is that when the background field goes on-shell $R = \frac{2d}{d-2}\Lambda_k$, the Hessian is completely diagonal (another way to accomplish this is by setting the limit $\alpha \to 0$), and therefore we will only regulate those modes that survive on-shell (i.e., the diagonal part of the Hessian).

The on-shell condition has no effect on the auxiliary and ghosts fields, and hence, this will be regulated in a standard way as fluctuating fields.

Finally, we will choose the cutoff R_k in such a way to implement in the Hessian the rule

$$\Delta_i \to P_{k,i} \equiv \Delta_i + r_{k,i}(\Delta_i/k^2), \tag{3.30}$$

but only on the fields that survive after imposing the on-shell condition.

3.5 Spectral sums

We start here by normalising all our fields such that all components of the differential operator

$$\Delta_i \equiv 16\pi G_k \Gamma^{(2)}_{k,i} \tag{3.31}$$

have the form $\Delta_i = -D^2 + \cdots$, and $\Delta_i = (-D^2)^2 + \cdots$ for the fourth order parts (here the subindex i corresponds to the fields the operator act on (metric fluctuation, auxiliary and ghosts fields)) . Then, with this definition, and noting that at the level of the super trace on (2.35), each Grasmannian complex field contributes with a -1, and $-1/2$ for each real Grasmannian field, while for real scalar, vector or tensor fields the contribution is $1/2$, we conclude that all the gauge dependence of the metric fluctuation cancels with the ghosts contributions when we go on-shell or in the $\alpha \to 0$ gauge, while from the auxiliary fields we will get a scalar and a vector contribution on the right hand side of (2.35).

Finally, we need to take special care of the conformal mode $\bar{h}$, since it gives rise to the well known unboundedness problem. This problem arrises due to the overall negative sign in front of the corresponding quadratic part of the effective action (3.21) after imposing the on shell condition. From the functional measure this can be solved by Wick rotating $\bar{h} \to i\bar{h}$ the modes for which $\Delta_0 \geq 0$ [64, 65]. The resulting right hand side of the flow equation (2.35) has the form

$$\begin{aligned}\frac{1}{V}\mathcal{S} =&\frac{1}{V}\sum_i S_i = \frac{1}{2V}\mathrm{Tr}\left[\frac{\partial_t R_{\perp,k}}{\frac{1}{4}Z_k(-D^2+\frac{2}{d(d-1)}R+2(\frac{d-2}{2d}R-\Lambda_k))+R_{\perp,k}}\right]\\ &+\frac{1}{2V}\mathrm{Tr}''\left[\frac{\partial_t R_{\bar{h},k}}{\frac{(2-d)(d-1)}{4d^2}Z_k[-D^2-\frac{R}{d-1}+\frac{d}{d-1}(\frac{d-2}{2d}R-\Lambda_k)]+R_{\bar{h},k}}\right]\\ &-\frac{1}{2V}\mathrm{Tr}''\left[\frac{\partial_t R_{0,k}}{\frac{(d-1)}{d}Z_k[-D^2-\frac{R}{d-1}]+R_{0,k}}\right]\\ &-\frac{1}{2V}\mathrm{Tr}'\left[\frac{\partial_t R_{1,k}}{2Z_k[-D^2-\frac{R}{d}]+R_{1,k}}\right]+\frac{1}{2V}\left[\frac{\partial_t R_{-,k}}{Z_k a_- + R_{-,k}}\right],\end{aligned} \tag{3.32}$$

the last term corresponds to a single negative mode of $\bar{h}_-$ (lowest mode) happening on the d-sphere for which $-\Delta_{\bar{h}}$ has an eigenvalue $a_- = \frac{R}{d-1} - \frac{d}{d-1}\left(\frac{d-2}{2d}R-\Lambda_k\right)$. The latter mode is the last term in (3.32), its inclusion in the following analysis do not change the overall picture of the results to be shown. Also, V is the volume of the d-sphere

$$V = \int d^dx\sqrt{g} = (4\pi)^{d/2}\left(\frac{d(d-1)}{R}\right)^{d/2}\frac{\Gamma(d/2)}{\Gamma(d)}, \tag{3.33}$$

and we can define the modified Laplacians

$$\begin{aligned}\Delta_\perp &= \Delta_2 + 2\left(\frac{d-2}{2d}R-\Lambda_k\right), \quad \Delta_2 = -D^2+\frac{2}{d(d-1)}R,\\ \Delta_{\bar{h}} &= \Delta_0 + \frac{d}{d-1}\left(\frac{d-2}{2d}R-\Lambda_k\right), \quad \Delta_0 = -D^2-\frac{R}{d-1},\\ \Delta_1 &= -D^2-\frac{R}{d},\end{aligned} \tag{3.34}$$

Note that when we apply the equations of motion $R = \frac{2d}{d-2}\Lambda_k$, $\Delta_{\bar{h}} = \Delta_0$, and since the corresponding traces have opposite signs, for cutoff type III, the contributions proportional to the anomalous dimension of the second and third traces in (3.32) cancel each other, while for cutoff type II the whole traces of these modes cancel each other. Beside, let us note as well that the modified eigenvalues for the vector and scalar 0-mode for the type II and III cutoffs are the same for any dimension. Using the spherical harmonics for transverse vectors and scalars (3.38), the values on Table (3.1) and (3.34)

$$\begin{aligned}\Delta_1 T_\mu^{lm} &= \left(-D^2-\frac{R}{d}\right)T_\mu^{lm} = \frac{(l+d)(l-1)}{d(d-1)}T_\mu^{lm}\\ \Delta_0 T^{lm} &= \left(-D^2-\frac{R}{d-1}\right)T^{lm} = \frac{(l+d)(l-1)}{d(d-1)}T^{lm},\end{aligned} \tag{3.35}$$

for all d and l, this will simplify the computation of the traces with spectral sums. Hence, the traces for this modes are proportional to each other after performing the spectral sums.

Using all these definitions, (3.30), and (3.31), the right hand side of the flow equation

(3.32) takes the simple form

$$\begin{aligned}\frac{1}{V}\partial_t\Gamma_k = \mathcal{S} = \frac{1}{V}\sum_i S_i \equiv \frac{1}{2V}\mathrm{Tr}\left[\frac{\partial_t r_{k,\perp}}{Z_k\Delta_\perp + r_{k,\perp}}\right] + \frac{1}{2V}\mathrm{Tr}''\left[\frac{\partial_t r_{k,\bar{h}}}{Z_k\Delta_{\bar{h}} + r_{k,\bar{h}}}\right] \\ - \frac{1}{2V}\mathrm{Tr}''\left[\frac{\partial_t r_{k,0}}{Z_k\Delta_0 + r_{k,0}}\right] - \frac{1}{2V}\mathrm{Tr}'\left[\frac{\partial_t r_{k,1}}{Z_k\Delta_1 + r_{k,1}}\right] + \frac{1}{2V}\left[\frac{\partial r_{k,-}}{Z_k a_- + r_{k,-}}\right]\end{aligned} \tag{3.36}$$

the primes on the traces of (3.32) and (3.36) indicate excluded modes. For the vector part, we only exclude its zero mode (lowest mode), for the scalar 0 part we exclude the negative mode (lowest one), and the zero mode; also, for the conformal part $\bar{h}$ we exclude the zero mode (second mode when we go on shell), and the constant mode explained above.

Along this chapter we will be using the exponential cutoff function

$$R_k(z) = Z_k r_k(z), \quad r_k(z) = \frac{zk^2}{\exp(z/k^2) - 1}, \qquad z = \Delta_i, \tag{3.37}$$

the advantage of using this cutoff over the optimised one [53, 54] is to avoid the problems arising when handling numerics with a distribution instead of a function.

Let the covariant Laplacian $\Delta = -D^2$ be a Hermitian, positive semidefinite operator with

$$\Delta T^{l,m}_{\mu_1\ldots\mu_s}(x) = \omega(l,s)T^{l,m}_{\mu_1\ldots\mu_s}, \tag{3.38}$$

$\{T^{\mu\nu}_{\mu_1\ldots\mu_s}\}$ is a complete set of orthonormal eigenfunctions, and $\{\omega(l,s)\}$ the corresponding eigenvalues of the covariant Laplacian with relative multiplicities $\{m(l,s)\}$. In the case where the Laplacian acts on a d-dimensional sphere this eigenspectrum is reported on Table 3.1 [84, 85].

The functional trace is of the form

$$\mathrm{Tr}'_s[W(\Delta)] = \int d^dx\sqrt{g}\,\langle x|\,W(\Delta)^{\mu_1\ldots\mu_s}_{\mu_1\ldots\mu_s}\,|x\rangle\,, \tag{3.39}$$

where W is any smooth function whose argument is replaced with the covariant Laplacian, and inherits the matrix structure from the corresponding Laplacian, also the prime means that we need to take care of the unphysical modes for each type of field. Then, using the orthonormal eigenfunctions of Δ in the form $T^{l,m}_{\mu_1\ldots\mu_s}(x) = \langle x|l,m\rangle_{\mu_1\ldots\mu_s}$, and using the completeness relation (with $\mathbf{1}_{\mu_1\ldots\mu_s,\nu_1\ldots\nu_s}$ being the unit matrix in the spin field space s)

$$\mathbf{1}_{\mu_1\ldots\mu_s,\nu_1\ldots\nu_s}\frac{\delta(x-y)}{\sqrt{g(x)}} = \frac{1}{2}\sum_l\left(T^{l,m}_{\mu_1\ldots\mu_s}(x)T^{l,m}_{\nu_1\ldots\nu_s}(y) + T^{l,m}_{\nu_1\ldots\nu_s}(x)T^{l,m}_{\mu_1\ldots\mu_s}(y)\right), \tag{3.40}$$

we can write (3.39) as

$$\begin{aligned}\mathrm{Tr}'W(\Delta) &= \int d^dx\sqrt{g}\sum_{l=n_0}^{\infty}\langle x|\,W(\Delta)^{\mu_1\ldots\mu_s,\nu_1\ldots\nu_s}\,|l,m\rangle_{\mu_1\ldots\mu_s}\,\langle l,m|x\rangle_{\nu_1\ldots\nu_s} \\ &= \sum_{l=n_0}^{\infty} m(l,s)W(\omega(l,s))\int d^dx\sqrt{g}\,\langle x|l,m\rangle\,\langle l,m|x\rangle\,,\end{aligned} \tag{3.41}$$

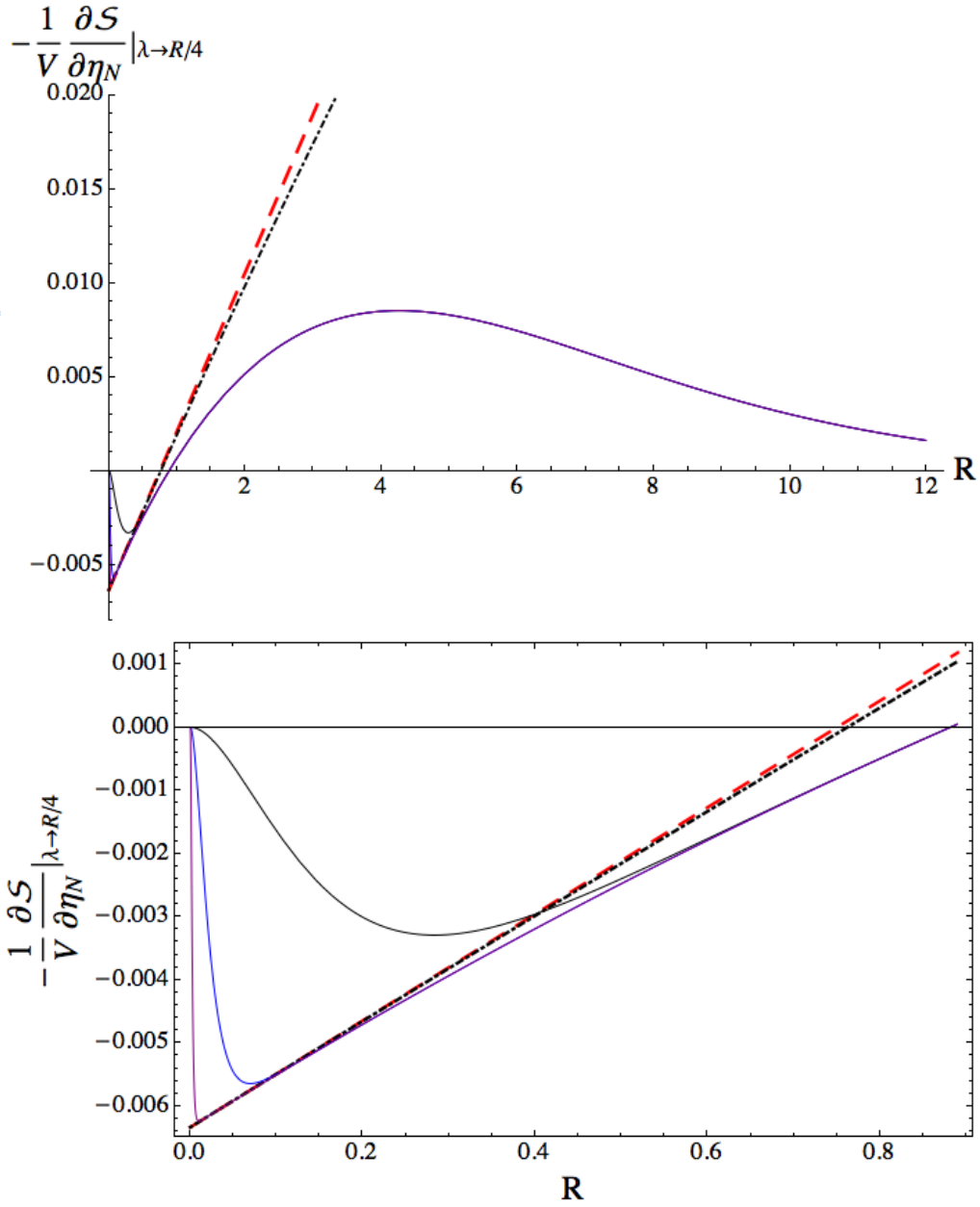

Figure 3.1: Comparison of the RHS of the flow equation (3.36) proportional to the anomalous dimension for different values n_{max} (various colours) for the spectral sums, using the heat kernel expansion up to linear terms in R (red dashed line), and using the heat kernel expansion up to R^2 terms. Black line corresponds to $n_{max} = 10$, the blue one to $n_{max} = 30$ and the purple to $n_{max} = 50$. The upper panel shows the behaviour of the RHS for big values of R. The bottom panel shows the differences for values small R.

and finally using the orthonormality of the eigenfunctions we have

$$\mathrm{Tr}' W(\Delta) = \sum_{l=n_0}^{\infty} m(l,s) W(\omega(l,s)), \tag{3.42}$$

where n_0 refers to the first mode included for each type of field.

Using (3.37) each trace S_i has the form

$$S_i = -\frac{\eta_N}{2}\mathrm{Tr}\left[\frac{r_{k,i}}{\Delta_i + r_{i,k}}\right] + \frac{1}{2}\mathrm{Tr}\left[\frac{\dot{r}_{k,i}}{\Delta_i + r_{i,k}}\right] + \dot{U}_i \frac{1}{2}\left[\frac{r'_{k,i}}{\Delta_i + r_{i,k}}\right], \tag{3.43}$$

the dot means derivative respect the RG time t and the prime means derivative respect the arguments. Also, the "potential" term U_i is the difference between the usual laplacian $\Delta = -D^2$ and the modified one Δ_i (3.34), i.e. $U_i = \Delta_i - \Delta$.

In order to highlight the benefits of using spectral sums instead of heat kernels, let us compute the trace of the RHS proportional to the anomalous dimension for a type III cutoff and compare both results. In [34] the traces were computed to first order using heat kernel techniques because that was enough to find the beta functions. Here we computed the right hand side of of the flow equation (3.36) in the heat kernel case, up to R^2 terms for $d = 4$ (see Appendix B)

$$\begin{aligned}\frac{1}{V}\mathcal{S} = &\frac{-120\left(49\lambda^2 + 51\lambda + 9\right) - 757R^2 + 30(146\lambda + 99)R}{17280\pi^2}\eta_N + \\ &+ \frac{68640\lambda^2 + 10843R^2 - 53040\lambda R - 720\gamma(73R - 196\lambda) + 12240\pi^2 - 73440}{207360\pi^2}\beta_\lambda + \\ &+ \frac{(10843\lambda + 9084)R^2 - 240\lambda(221\lambda + 219\gamma + 219)R - 180\pi^2(33R - 136\lambda)}{103680\pi^2} + \\ &+ \frac{480\left(143\lambda^3 + 147(1+2\gamma)\lambda^2 - 153\lambda + 54\zeta(3)\right)}{103680\pi^2}\end{aligned} \tag{3.44}$$

we used a dimensionless Ricci scalar ($R \to k^2 R$), and a dimensionless cosmological constant $\lambda = k^{-2}\Lambda_k$. γ is Euler's constant, and $\zeta(x)$ is the Riemann zeta function, these two factor arise after integrating the threshold functions (B.11) with the exponential cutoff (3.37).

Meanwhile, from (3.43) and truncating our spectral sum up to an n_{max} value, we get

$$-\frac{\partial S_i}{\partial \eta_N} = \frac{1}{2}\sum_{n=n_0}^{n_{max}} m(n,i)\frac{r_{k,i}(\omega(n,i,R,\Lambda_k))}{\omega(n,i,R,\Lambda_k) + r_{k,i}(\omega(n,i,R,\Lambda_k))}. \tag{3.45}$$

As we are using the cutoff type III, we need to modify the eigenvalues of Table 3.1 by adding by subtracting the corresponding "potential" terms $U(R,\Lambda_k)$ associated with each type of field ($\Delta_i = -D^2 + U_i$). With this we note that the eigenvalues of the Laplacian on the d-sphere are linear in R and Λ_k, hence

$$-\frac{\partial S_i}{\partial \eta_N} = \frac{1}{2}\sum_{n=n_0}^{n_{max}} m(n,i)\frac{r_{k,i}(\omega(n,i,R,\Lambda_k))}{a(n,i)R + b(i)\Lambda_k + r_{k,i}(\omega(n,i,R,\Lambda_k))}, \tag{3.46}$$

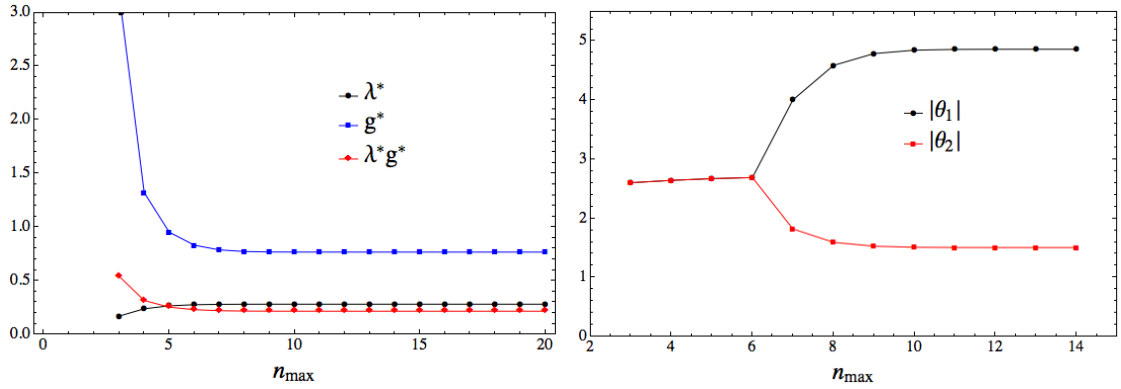

Figure 3.2: Values of the fixed point and the absolute value of the critical exponents for different values of n_{max}. The critical exponents are a conjugated pair of complex values, and for $n_{max} = 3$ the value for the real part of θ_1 is negative. This plots were obtained with the cutoff type III and $c = 1$.

where $a(n, i)$ and $b(i)$ are number coming from the eigenvalues of the operator Δ_i.

The results are plotted in Figure 3.1 using dimensionless quantities $R \to k^2 R$, $\lambda = k^{-2}\Lambda_k$, and the on-shell condition $R = 4\lambda$ in $d = 4$. The main things to note here are:

a) It does not matter how big n_{max} is, the limits $R \to 0$ and $R \to \infty$ the trace divided by the volume will vanish for the spectral sum provided n_{max} is finite, but the heat kernel will give non-zero value for the $R \to 0$ limit. Remember that the regulator vanishes at large momentum, but thanks to the spectral sum, now the momentum is replaced by R, which is the dimensional Ricci scalar divided by the momentum cutoff k, hence the limit $R = \bar{R}/k^2 \to \infty$ can be understood as the limit $k \to 0$ and finite $\bar{R}$, i.e. it is the infrared limit. From figure 3.1 we observe that in this limit we are left only with the left hand side of (2.35) (the vanishing of the right hand side of the flow equation occurs due to the definition of the cutoff operator (2.18)), which in turn produce the classic scaling for the couplings;

b) the heat kernel method comprises the small R behaviour, meanwhile the spectral sum gets information for different values of R;

c) the only way for the spectral sum to reproduce the heat kernel method is by computing the traces for a sufficiently big n_{max}. This can be noted from the bottom panel of figure 3.1, where the spectral sum is clearly different for each n_{max} chosen. Meanwhile, the top panel shows a rapid convergence for values $R > 1$, this means that in this regime we only need to take few modes into account to compute beta functions, fixed points and critical exponents.

This behaviour of the spectral sum will be important for performing the projection of

the flow equation and to analyse the convergence properties of the different approximations.

3.6 Projection

By projecting the flow equation we mean that we project the RG flow from an infinite dimensional space of all actions onto some finite dimensional subspace, and hence, (2.35) becomes an ODE for a finite set of generalised couplings which are the coordinates on this subspace.

The most general way to perform this is by expanding both sides of (2.35) around some arbitrary value R_0 and match both sides by comparing orders of $(R-R_0)$. By performing this in the Einstein-Hilbert theory in its dimensionless form, the LHS gives

$$\frac{1}{V}\partial_t\Gamma_k = \frac{-2g+\beta_g}{16\pi g^2}(R-R_0) + \frac{(R_0-2\lambda)\beta_g + 2g(-R_0+4\lambda+\beta_\lambda)}{16\pi g^2} \tag{3.47}$$

Note that the dependence of the flow equation on R_0 only come from the RHS, and the term proportional to $(R-R_0)^0$ in the left hand side.

From here, two particular cases have beenexploited in literature

- $R_0 = 0$ [80, 50, 61] (and many other references).

  Since the heat kernel describes the $R \to 0$ limit, this is the correct way of computing and projecting the traces. It is also possible to compute the UV divergences appearing in perturbation theory [20] by computing heat kernel coefficients for operators with four derivatives of the metric (e.g. R^2, $R_{\mu\nu}R^{\mu\nu}$, C^2).

- **On shell,** $R_0 = 4\lambda$ [7, 9, 30, 34, 73].

  In this case (3.47) is,

  $$\frac{1}{V}\partial_t\Gamma_k = \frac{-2g+\beta_g}{16\pi g^2}(R-4\lambda) + \frac{\lambda\beta_g + g\beta_\lambda}{8\pi g^2}, \tag{3.48}$$

  also, several cancelations occur on the RHS for the cutoff type III (Appendix B) and all the gauge dependence gets factorised as shown in [7]. In this case, in [34], heat kernels are used, while in [7, 9], spectral sums are implemented.

- **Interpolating between** $R_0 = 0$ **and on-shell.** $R_0 = 4c\lambda$

  Here we introduce a constant c to help us to interpolate between the first and the second case. Due to the presence of c, no cancelations occur in (3.47) as in the on-shell case, but instead we get

  $$\frac{1}{V}\partial_t\Gamma_k = \frac{-2g+\beta_g}{16g^2\pi}(R-4c\lambda) + \frac{(2c-1)\lambda\beta_g + g(\beta_\lambda - 4\lambda(c-1))}{8g^2\pi} \tag{3.49}$$

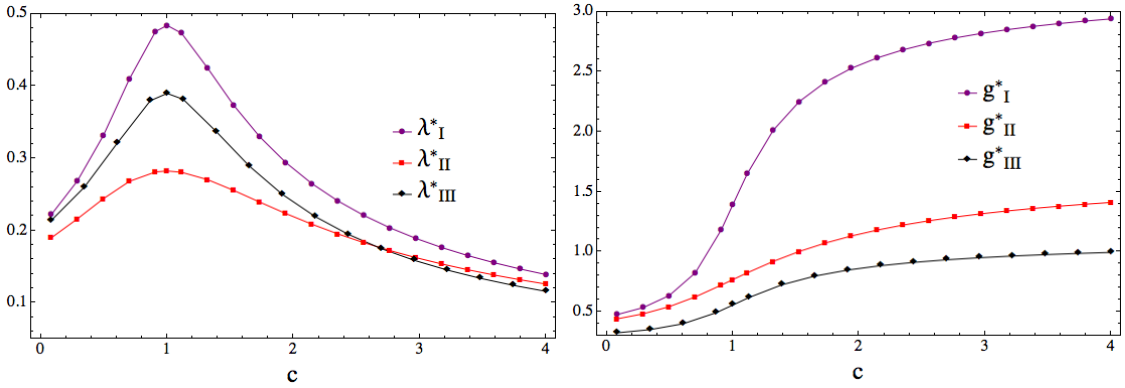

Figure 3.3: Fixed points values for the different cutoff schemes.

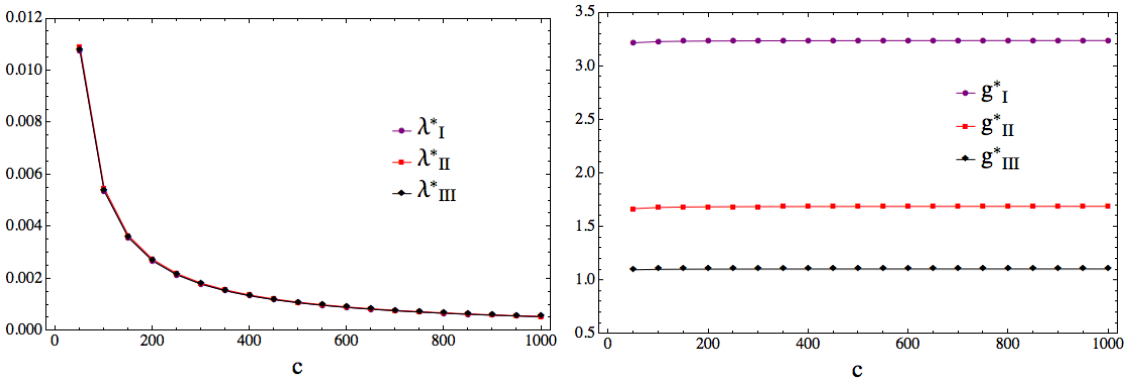

Figure 3.4: Fixed points values for the dimensionless cosmological constant (left), and Newton's constant for all three cutoff types, using large values for the interpolating parameter c (see disscucion after (3.68)).

In this case, if we use the field parametrisation of [51] in the limit $c \to 0$ we recover the exact values for the fixed points and the complex conjugated pair of critical exponents, while it is impossible to find a fixed point for values above $c = 1/4$ (this result is not shown here). As discussed before, whenever we try to reach the limit $c \to 0$ we need to increase the number of modes in the spectral sum n_{max}.

3.7 Fixed points and critical exponents

Considering both sides of the flow flow equation (2.35), let us call

$$E = \frac{1}{\tilde{V}}\partial_t \Gamma_k - \frac{1}{\tilde{V}}\mathcal{S} = 0. \tag{3.50}$$

where $\tilde{V} = k^4 V$ is the dimensionless volume.

It is easy to see that from the general form of the flow equation and the way we implement our regulator, (3.50) is linear in the beta functions, and then it is possible to

write (3.50) as

$$E = A(g_i, R) + B_k(g_i, R)\beta_k(g_i) = 0, \quad i, k = 0, 1, \tag{3.51}$$

where we use Einstein convention on the index k, we use the notation $g_0 = \lambda$, $g_1 = g$, $\beta_0 = \beta_\lambda$, and $\beta_1 = \beta_g$, A and B are complicated functions of g_i and the background Ricci scalar R.

In order to project the flow equation we use for each order of $R - R_0$ an equation of the form

$$E_n = \frac{\partial^{(n)}}{\partial R^{(n)}} E\Big|_{R\to R_0} = A^{(n)}(g_i, R_0) + B_k^{(n)}(g_i, R_0)\beta_k(g_i) = 0 \tag{3.52}$$

then the beta functions in a matrix form are

$$\beta_k = -(B_k^{(n)})^{-1} A^{(n)} \tag{3.53}$$

The condition to find a fixed point is $\beta_i(g_i^*) = 0$, hence the fixed point equation from (3.52) is

$$E_n^* = A^{(n)}(g_i^*, R_0) = 0, \quad n = 0, 1, \tag{3.54}$$

this yield a system of 2 coupled equations to find λ^* and g^*.

To find the critical exponents, we first need the stability matrix

$$M_{ij} = \frac{\partial \beta_i}{\partial g_j}\Big|_{g_m = g_m^*} = \partial_j \beta_i\Big|_{g_m = g_m^*}, \tag{3.55}$$

At this stage we need to be careful with the different kind of projections described in the previous section. On the one hand, when the expansion parameter R_0 is a function of the couplings in the system (as in the on-shell, and the interpolating cases), then we get contributions depending on the couplings that have to be taken into account for computing the stability matrix. On the other hand, R_0 being just a number will give no contributions over the derivative respect the couplings, and hence, if one wants to compare both results, one will find same value for the fixed points but different critical exponents.

Now by taking the derivative with respect to g_k of the vector E_n in (3.52) we get

$$\partial_{g_k} E_n|_* = \partial_k E_n|_* = \partial_k A_n(g_m^*, R_0) + B_{ni}(g_m^*, R_0) M_{ik} = 0 \tag{3.56}$$

in matrix form, after solving for the stability matrix M_{ik} we get finally

$$M_{kj} = -B_{ki}^{-1} A_{ij}, \tag{3.57}$$

with $A_{ij} = \partial_j A^{(i)}(g_i^*, R_0)$ and $B_{ij} = B_i^{(n)}(g_i^*, R_0)$.

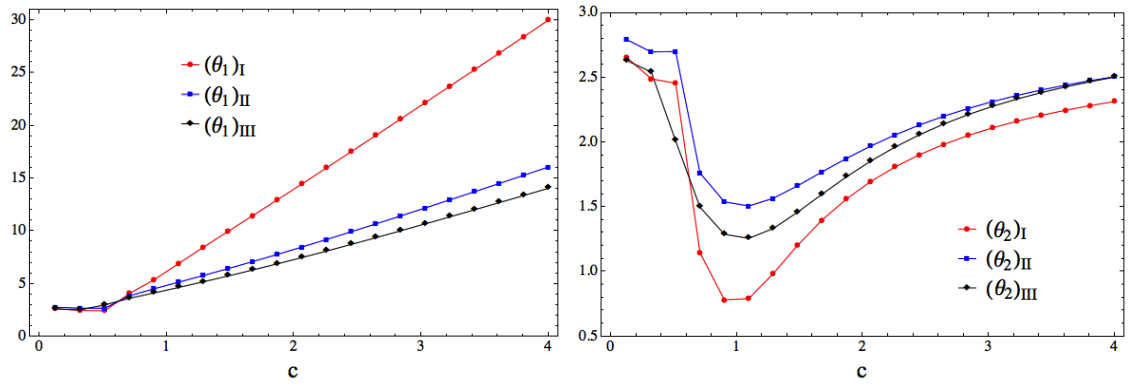

Figure 3.5: Critical exponents for different cutoff schemes. Note that the critical exponents from $c = 0$ to $c = 0.5$ are a complex conjugated pair with a positive real part.

3.7.1 Fixed Points

Explicitly, our fixed point equation (3.54) for the interpolating case has the form

$$\begin{aligned} \frac{\lambda^*(1-c)}{2\pi g^*} &= \mathcal{S}|_{R=4c\lambda^*} \equiv F^*(R = 4c\lambda^*, \lambda^*) \\ -\frac{1}{8\pi g^*} &= \frac{\partial}{\partial R} F^*(R = 4c\lambda^*, \lambda^*) \equiv F_1^*(R = 4c\lambda^*, \lambda^*), \end{aligned} \tag{3.58}$$

where the asterisk on F and F_1 means we have set $\beta_\lambda = \beta_g = 0$, and $\eta_N = -2$. Now, substituting the second equation into the first, and reordering we get

$$C(R = 4c\lambda^*, \lambda^*) \equiv 4\lambda^*(1-c)F_1^*(R = 4c\lambda^*, \lambda^*) + F^*(R = 4c\lambda^*, \lambda^*) = 0. \tag{3.59}$$

This is a single equation depending only on λ^* and c, and hence, by choosing different values for c we can solve it numerically for λ^*. Once we get the value for λ^*, we can go back to (3.58) to find g^*. Let us remember here that the functions F and F_1, are the traces and the derivative with respect to R of the traces of the RHS of the flow equation (3.32). We have computed this traces with the spectral sums as described in section 3.5, then, F and F_1 depend also on our upper maximum value n_{max} on the sums. The fast convergence for λ^*, g^*, and $\lambda^* g^*$ is shown in the left panel of figure 3.2 for the cutoff type III and $c = 1$.

The results for different cutoff types are shown in figure 3.3 for values of c ranging from 0 to 4, and in figure 3.4 for large values of c (where $n_{max} \approx 100$) . Close to $c = 0$ (with $n_{max} \approx 50$), λ^* is about 0.2 for all the different cutoffs, and g^* is about 0.5. Also whenever we increment the value of c, λ^* tends towards zero, while g^* converges to 3.2398 for type I, 1.6924 for type II, and 1.1065 for type III. This last limit is shown in figure 3.4, where c ranges from 50 to 1000 and $n_{max} \approx 50$

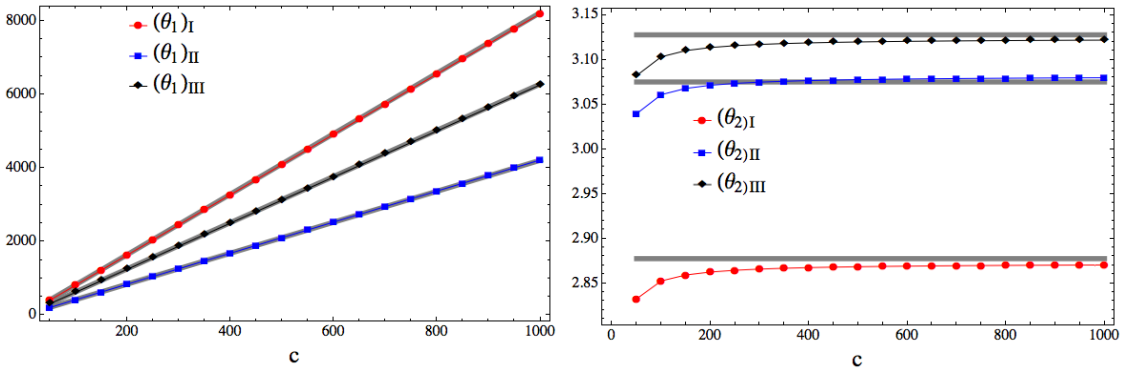

Figure 3.6: Critical exponents in the large c limit. c ranges from 50 to 1000 with $n_{max} = 50$. Dots, squares and diamonds correspond to numerical values, while grey lines correspond to the fits appearing on table 3.3

From figure 3.3 we observe that there is a maximum for λ^* at $c = 1$, and that can be proven as follows: first we take the total derivative of (3.59) respect c, hence

$$\frac{dC(R = 4c\lambda^*, \lambda^*)}{dc} = \frac{\partial \lambda^*}{\partial c}\frac{\partial C}{\partial \lambda^*} + \frac{\partial C}{\partial c} = 0, \tag{3.60}$$

which is equally zero by definition. From here, we can solve for $\partial\lambda^*/\partial c$

$$\frac{\partial \lambda^*}{\partial c} = -\frac{\partial C/\partial c}{\partial C/\partial \lambda^*}, \tag{3.61}$$

hence, the condition for a maximum/minimum value for λ^* is give by equation (3.61) to be zero and solving it for c. This means that $\partial C/\partial c$ must be zero, and from (3.59) we can take explicitly the derivative respect c

$$\begin{aligned}\frac{\partial C}{\partial c} =& -4\lambda^* F_1^*(R = 4c\lambda^*, \lambda^*) + 4\lambda^*(1-c)\frac{\partial F_1^*(R = 4c\lambda^*, \lambda^*)}{\partial c} + \\ &+ \frac{\partial F^*(R = 4c\lambda^*, \lambda^*)}{\partial c} = 0,\end{aligned} \tag{3.62}$$

next, we need to consider that λ^* is only a function of c (given by solving (3.59)) and not of R, then the following relationship between F_1^* and $\partial F^*/\partial c$ holds,

$$\frac{\partial F^*(R = 4c\lambda^*, \lambda^*)}{\partial c} = 4\lambda^*\frac{\partial F^*(R = 4c\lambda^*, \lambda^*)}{\partial R} = 4\lambda^* F_1^*, \tag{3.63}$$

with this, the first and the third terms in (3.62) cancel each other, leaving us with

$$\frac{\partial C}{\partial c} = 4\lambda^*(1-c)\frac{\partial F_1^*(R = 4c\lambda^*, \lambda^*)}{\partial c} = 0. \tag{3.64}$$

Then, finally this is true either if $\partial F_1^*/\partial c = 0$ or $c = 1$. And thus, $c = 1$ corresponds to a maximum for $\lambda^*(c)$.

n_{max}	3	4	5	6	7	8	100
θ_1	$-1.213 - 2.513i$	$0.4969 - 2.440i$	$1.507 - 1.853i$	$2.170 - 0.923i$	3.554	4.141	4.409
θ_2	$-1.213 + 2.513i$	$0.4969 + 2.440i$	$1.507 + 1.853i$	$2.170 + 0.923i$	1.557	1.335	1.255

Table 3.2: Critical exponents for different n_{max} values for cutoff type III and $c = 1$. Note that for values up to 3 the real part of the critical exponents is negative (irrelevant), then after 3 they change to a real positive part and they converge quickly for grater values. The relative error between 7 and 100 is 19.39%, between 8 and 100 is 6.08%, and between 9 and 100 it is just 1.59%. Also after $n_{max} = 6$ the pair of complex conjugated pair bifurcates into two relevant and real critical exponents.

3.7.2 Critical Exponents

For the critical exponents in the interpolation case, we need to construct first the stability matrix (3.55). By taking the derivative of (3.49) with respect to λ and g, and imposing the fixed point condition $\beta_\lambda = \beta_g = 0$ and $\eta_N = -2$, we get the following set of equations

$$\begin{aligned}
M_{00}\left[\frac{1}{8\pi g^*} - \frac{\partial F^*}{\partial \beta_\lambda}\right] + M_{10}\left[\frac{(2c-1)\lambda^*}{8\pi g^{*2}} - \frac{\partial F^*}{\partial \beta_g}\right] &= \frac{\partial F^*}{\partial \lambda} + 4c\frac{\partial F^*}{\partial R} + \frac{c-1}{2\pi g^*} \\
M_{01}\left[\frac{1}{8\pi g^*} - \frac{\partial F^*}{\partial \beta_\lambda}\right] + M_{11}\left[\frac{(2c-1)\lambda^*}{8\pi g^{*2}} - \frac{\partial F^*}{\partial \beta_g}\right] &= \frac{\partial F^*}{\partial g} + \frac{(1-c)\lambda^*}{2\pi g^{*2}} \\
M_{00}\left[\frac{\partial F_1^*}{\partial \beta_\lambda}\right] + M_{10}\left[\frac{\partial F_1^*}{\partial \beta_g} - \frac{1}{16\pi g^{*2}}\right] &= -\frac{\partial F_1^*}{\partial \lambda} - 4c\frac{\partial F_1^*}{\partial R} \\
M_{01}\left[\frac{\partial F_1^*}{\partial \beta_\lambda}\right] + M_{11}\left[\frac{\partial F_1^*}{\partial \beta_g} - \frac{1}{16\pi g^{*2}}\right] &= -\frac{\partial F_1^*}{\partial g} + \frac{1}{8\pi g^{*2}}
\end{aligned} \tag{3.65}$$

which are four equations for the four entries of the stability matrix. In this case the asterisk on F and F_1 means $\beta_\lambda = \beta_g = 0$, and $\eta_N = -2$ after taking the respective derivatives. The solution of the system is

$$\begin{aligned}
M_{00} &= \frac{A_2C_1 - A_1C_2}{A_0C_1 - A_1C_0}, \qquad M_{01} = \frac{B_2C_1 - A_1D_2}{A_0C_1 - A_1C_0} \\
M_{10} &= \frac{A_2C_0 - A_0C_2}{A_1C_0 - A_0C_1}, \qquad M_{11} = \frac{B_2C_0 - A_0D_2}{A_1C_0 - A_0C_1}
\end{aligned} \tag{3.66}$$

with

$$\begin{aligned}
A_0 &= \frac{1}{8\pi g^*} - \frac{\partial F^*}{\partial \beta_\lambda}, \quad A_1 = \frac{(2c-1)\lambda^*}{8\pi g^{*2}} - \frac{\partial F^*}{\partial \beta_g}, \quad A_2 = \frac{\partial F^*}{\partial \lambda} + 4c\frac{\partial F^*}{\partial R} + \frac{c-1}{2\pi g^*}, \\
B_2 &= \frac{\partial F^*}{\partial g} + \frac{(1-c)\lambda^*}{2\pi g^{*2}}, \quad C_0 = \frac{\partial F_1^*}{\partial \beta_\lambda}, \quad C_1 = \frac{\partial F_1^*}{\partial \beta_g} - \frac{1}{16\pi g^{*2}}, \\
C_2 &= -\frac{\partial F_1^*}{\partial \lambda} - 4c\frac{\partial F_1^*}{\partial R} \qquad D_2 = -\frac{\partial F_1^*}{\partial g} + \frac{1}{8\pi g^{*2}}.
\end{aligned} \tag{3.67}$$

Let us note that for cutoff types I and II we have $\partial F/\partial \beta_\lambda = \partial F_1/\partial \beta_\lambda = 0$, and hence $C_0 = 0$, and $A_0 = 1/(8\pi g^*)$.

	Type I	Type II	Type III
λ^*	$0.5376/c$	$0.5468/c$	$0.4405/c$
g^*	3.2559	1.6835	1.1105
θ_1	$3.8593 + 8.2206c$	$4 + 4.2c$	$6.0882 + 6.2773c$
θ_2	2.8774	3.1	3.1277
$R_* = 4c\lambda^*$	2.1496	2.1872	1.762

Table 3.3: Fixed point values for λ^* and g^* and critical exponents in the limit $c \to \infty$ for the different cutoff types.

As in the fixed points case, here, the quantities A_i, B_i, C_i, and D_i depend also on the number of modes included in each spectral sum (n_{max}). Then, we find that for $n_{max} = 3, 4, 5, 6$ they are a complex conjugated pair, giving rise to a irrelevant direction for $n_{max} = 3$, as shown on table 3.2, and the right panel of figure 3.2 for cutoff type III and $c = 1$. After $n_{max} = 6$, we start getting a fast converging pair of real critical exponents. This convergence can be seen since the relative errors between $n_{max} = 7, 8, 9$ and $n_{max} = 100$ are 19.39%, 6.08%, and 6.08% respectively.

Going back to (3.59), we can solve for λ^*, and from the second equation in (3.58) we can solve for g^* as follows,

$$\lambda^* = \frac{F^*}{4(c-1)F_1^*}, \qquad g^* = -\frac{1}{8\pi F_1^*}, \tag{3.68}$$

in the limit for large c, from figure 3.4 we note that λ^* is inversely proportional to c while g^* is just a constant. These mean that in this limit, from the first equation of (3.68) we get that F_0^*/F_1^* is order zero in c, making λ^* order c^{-1}. While from the second equation of (3.51) we get that F_1^* is order zero when $\lambda^* \propto 1/c$. These asymptotic values are reported on table 3.3 for the different cutoff types. The last line of table 3.3 contains the maximum value for the Ricci scalar we can explore within the present framework: for cutoff type I we have $R^* = 2.1506$, for type II $R^* = 2.1871$, and for type III $R^* = 1.7619$.

From the previous analysis, in the large c limit we can establish now the c-scaling of the different quantities (3.67), and, therfore the c-scaling for the components of the stability matrix. Only A_2 and C_2 are proportional to c, and all other quantities are order zero in c. Also, these two quantities are the responsible for the unphysical growing of θ_1. The way to find the values of table 3.3 was first by adjusting λ^* as a/c (with a constant value a), then with this value is possible to find g^* by inserting the former value of lambda in (3.68) and taking the limit $c \to \infty$, and as expected this is a constant value. Next, we use

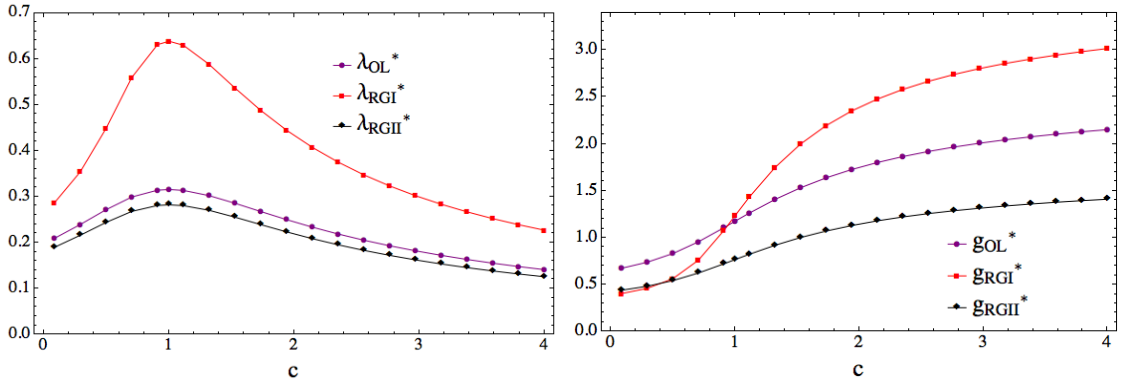

Figure 3.7: Cutoff type II. Fixed points values for the different improvements. OL means $\eta_N = \eta_J = 0$, RG improvement I is $\eta_J = 0$, and RG improvement II $\eta_J = \eta_J$.

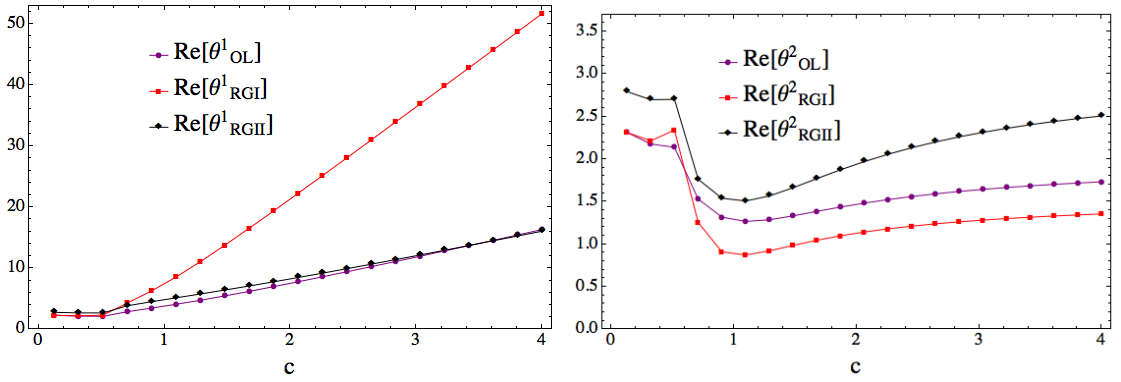

Figure 3.8: Cutoff type II. Real part of the critical exponents for the different improvements. OL means $\eta_N = \eta_J = 0$, RG improvement I is $\eta_J = 0$, and RG improvement II $\eta_J = \eta_J$.

this values for λ^* and g^* and the same limit to find the values (3.67), to finally compute the stability matrix. For all cutoff types, the stability matrix has the form

$$M_{ij} = \begin{pmatrix} a_{00} + b_{00}c & a_{01} \\ a_{10} + b_{10}c & a_{11} \end{pmatrix}, \tag{3.69}$$

in the large c limit the eigenvalues of (3.69) are

$$(\theta_1)_{I,II,III} = a_{00}\frac{a_{01}b_{10}}{b_{00}} + b_{00}c, \quad (\theta_2)_{I,II,III} = a_{11} - \frac{a_{01}b_{10}}{b_{00}}. \tag{3.70}$$

These confirm the arguments of the previous paragraph. Also, figure 3.6 shows both, the numerical and the fit on table 3.3 for the critical exponents using the different types of cutoffs.

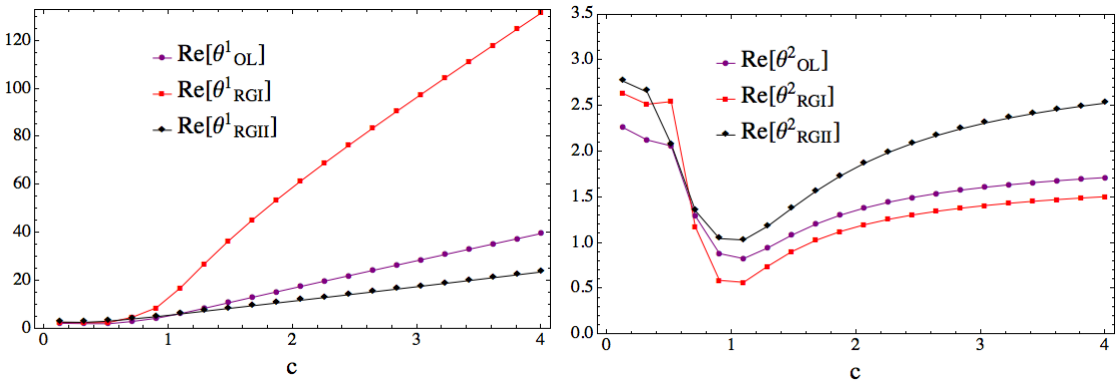

Figure 3.9: Cutoff type III. Real part of the critical exponents for the different improvements. OL means $\eta_N = \eta_J = 0$, RG improvement I is $\eta_J = 0$, and RG improvement II $\eta_J = \eta_J$.

3.8 Anomalous dimension

In definition (3.31) we implicitly defined the laplacian for the auxiliary fields with a Newton's constant coupling as a factor, and by doing so we have got some cancelations when we go on shell, i.e. $\Delta_{\bar{h}} = \Delta_0$. For type III cutoff, this implies that the whole traces corresponding to scalar modes cancel each other.

Instead we could have defined the laplacian corresponding to auxiliary fields as

$$\Delta_0 = \Gamma^{(2)}_{k,cc}/Z_J, \quad \Delta_1 = \Gamma^{(2)}_{k,c^\perp c^\perp}/Z_J, \tag{3.71}$$

hence, the corresponding traces will be of the form

$$S_0 + S_1 = -\frac{1}{2} Tr'_{1T}\left[\frac{-\eta_J r_{k,1} + \dot{r}_{k,1}\dot{U}r'_{k,1}}{\Delta_1 + r_{k,1}}\right] - \frac{1}{2} Tr''_0\left[\frac{-\eta_J r_{k,0} + \dot{r}_{k,0} + \dot{U}r'_{k,0}}{\Delta_0 + r_{k,0}}\right]. \tag{3.72}$$

From here we can choose η_J and η_N in different ways: The first one is the one we adopted in the previous chapters, and we will call it RG improvement II

$$\eta_J = \eta_N = -Z_k \partial_t Z_k. \tag{3.73}$$

This improvement was first used in [34] and it was motivated by the cancelations described at the beginning of the chapter. The second one is just to neglect η_J terms, and will be called RG improvement I

$$\eta_J = 0, \quad \eta_N = -Z_k \partial_t Z_k. \tag{3.74}$$

The last one correspond to the one-loop approximation for which

$$\eta_J = \eta_N = 0 \tag{3.75}$$

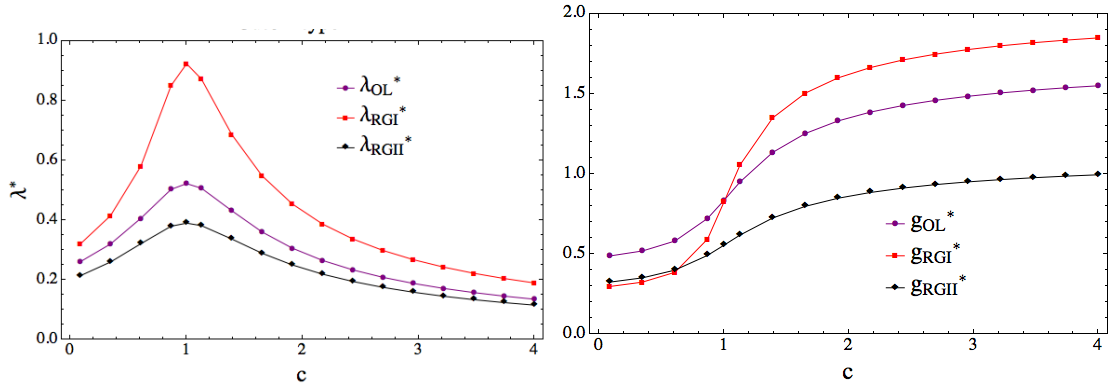

Figure 3.10: Cutoff type III. Fixed points values for the different improvements.

Cutoff type II

In figures 3.7 and 3.8 we compare the different improvements for the cutoff type II. The first thing to note is that for RG improvement I λ^* gets a very big FP value for the on-shell condition $c = 1$, and for g^* both RG improvements I and II give a very similar value for $c \to 0$. For the critical exponents, for RG improvement I we see that at $c = 1$ θ^1 already have a really big eigenvalue before it start growing proportional to c, while all other values are comparable for the different improvements.

Cutoff type III

Similarly, figures 3.10 and 3.9 show the fixed point values and critical exponents respectively for cutoff type III. The same remarks as in the results for cutoff type II are noted.

Finally, as expected from the discussion on the previous section, all the structure shown is preserved for each cutoff type and RG improvement.

3.9 Conclusions

We have derived the flow equation (2.35) for the Einstein-Hilbert theory in a way that only physical modes contribute to the beta functions, fixed points and critical exponents of the theory. Also, we introduced two different RG improvements. One of them consisted of identifying the wave function renormalisation of the auxiliary sector as the newtonian one, the other sets the wave function renormalisation of the auxiliary sector to 1, i.e. $Z_J = 1$ or $\eta_J = 0$.

After that we argued that computing the traces of the flow equation via heat kernels only works for small values of the background Ricci scalar, even if we go on-shell. This was shown in figure 3.1 where we compared the complete right hand side of the flow equation

computed with heat kernels up to second order in the Ricci scalar R and with spectral sums. We learnt that for small values of R we need to truncate our spectral sum with a big n_{max}, while for values $R > 1$ we only need the contribution of few modes on the spectral sum to achieve convergence. Next, we implement a new way for projecting both sides of the flow equation, called interpolating projection. Here we introduced a numeric parameter c such that we expand both sides around c times the on shell curvature, i.e. $R = 4c\Lambda_k$, and by doing so it was possible to compute numerically the fixed points and critical exponents for different values of c.

The first important remark is the lifting of degeneracy for the complex critical exponents. In contrast with the present work, the lifting of the degeneracy was achieved as well in [34] with the help of the heat kernel, but going on shell. Then, the appearance of complex critical exponents might be an artefact not on the field content of the theory, but rather of computing them too far off shell. Care must be presented to this argument, since previous results working on shell and with spectral sums found complex critical exponents [7], the main difference with our work is the way to implement the spectral sums and the different cutoffs.

As a second remark, we found that even though we introduced a unphysical parameter, there is a structure that does not depend on the way we compute the right hand side of (2.35) or even the approximations we use. First, there is a maximum for the λ^* at precisely $c = 1$ where the on-shell condition is met. Second, for $c = 1$ we found a minimum for the critical exponent corresponding to the gravitational coupling G_k. This points out that in a general framework, the renormalisation group equation (2.35) prefers the on-shell condition over all others.

Also, for values beyond the on-shell condition $c \to \infty$ λ^* is inversely proportional to c, g^* gets to a constant value (that depends on the used approach). The critical exponent corresponding to the cosmological constant grows indefinitely proportional to c, and the other critical exponent approaches constant values. Clearly the large-c behaviour is not physical in the current context, but it is intriguing the fact that the critical exponent corresponding to Newton's coupling stabilises at about $\theta_2 \approx 3$, which is the same as the one found by Hamber[47] in numerical lattice studies, and the one found by Falls [35]. Also, it limits the exploration for fixed points for different values of the curvature constant to $R \leq 2$ (see table (3.3)). The proposal for overcoming this difficulties is to perform a similar study with the projection $R = R_0$ with R_0 being a constant, and also to use the exponential parametrisation for the metric fluctuation $h_{\mu\nu}$ [35], instead of the linear

splitting used in the present work.

Furthermore, there is a critical value for c where the critical exponents bifurcate into a pair of real exponents, this in contrast with the usual complex pair found in most of the literature regarding asymptotic safety for gravity. It was believed that the appearance of complex conjugated pairs of critical exponents was due to the fact that Einstein-Hilbert theory or even polynomial truncations on Ricci scalar were not accurate enough in the UV [36].

Chapter 4

The phase diagram of $f(R)$ quantum gravity

4.1 Introduction

One of the current challenges in the asymptotic safety program for quantum gravity is to prove the existence (or non-existence) of an ultraviolet fixed point with a finite-dimensional UV critical surface. Throughout the years, systematically new positive evidence has been found regarding the possibility for gravity to be asymptotically safe. However, little is known about whether strong effects of the renormalisation group can be seen in the infrared limit of the theory. Furthermore, since the information about the precise numerical values of the couplings for the gravitational phenomena come form the classical world, then, it is important to understand how the two regimes, ultraviolet and infrared, talk to each other.

For example, a satisfactory model that explains the exponential expansion of space in the early universe, is given by Starobinky's model [88]. It is based on the inclusion of the term $\frac{1}{96\pi G_N M}R^2$ to the Einstein-Hilbert action without cosmological constant. The experimental value for M is about $10^{13}\ GeV$, and it follows that if the asymptotic safety conjecture and Starobinsky's model is correct, then this value with the addition of the value of Newton's constant would provide an initial condition for the effective gravitational action, opening the possibility to make future predictions based on our theory.

Two more open question regarding higher order theories of gravity are discussed throughout the chapters of this thesis. The first one regards the complex conjugated pair of critical exponents found throughout literature on the topic, and whether is possible to disentangle the couplings near the UV fixed point given a more general theory. And the second regards the unfolding of the singular point $(\lambda = 1/2, g = 0)$ in the deep

infrared of the theory, providing us with a new fixed point that could explain the late acceleration of the universe.

With this ideas in mind, here we will explore the phase space of the R^2 theory with the help of a general renormalisation group equation for $f(R)$ theories, and also we will use to our advantage the remarkable result of the existence of a reliable UV fixed point at least for truncations up to order R^{70}.

4.2 RG equations for f(R) gravity

In order to compute the beta functions of the system we will follow [48, 71, 36, 87]. The starting point is the scale dependent Euclidean effective action

$$\Gamma_k = \int d^4x\sqrt{\bar{g}}F_k(\bar{R}) + S_{gf} + S_{gh} + S_{aux} \tag{4.1}$$

with the corresponding gauge fixing action, ghosts and auxiliary fields. The function $F_k(\bar{R})$ is a polynomial expansion about the dimensionful Ricci scalar $\bar{R}$

$$F_k(\bar{R}) = \sum_{i=0}^{\infty} \bar{g}_i \bar{R}^i. \tag{4.2}$$

In a similar fashion as we did in chapter 3, we start with a maximally symmetric background, and we perform the TT decomposition (3.3) for the metric fluctuation $h_{\mu\nu}$ and the ghost fields.

Also, we use the gauge fixing action (3.2) with the gauge fixing parameters $\alpha = \rho = 0$. The benefits of this gauge is first the decoupling of the scalar fields σ and h at the level of the hessian, and second, only the traces over $h^{\perp}_{\mu\nu}$ and h depend on $F_k(\bar{R})$ with the traces over ξ_μ and σ coming just from the gauge fixing actions.

In order to implement the flow equation (2.35) [92] we need to choose a proper cutoff. Here following [87], we define the cutoff such that in the flow equation explicit poles in the dimensionless curvature sacalar $R = k^{-2}\bar{R}$ are removed. The latter observation was first made in [9]. The observation made here is the generic product-structure of the Hessian

$$\Gamma^{(2)}_{xx} = a\Delta(\Delta_i)^k \tag{4.3}$$

where a is a constant prefactor, i can take the values 0 or 1, k is either 1 or 2, and the modified laplacians Δ_i are

$$\Delta = -D^2, \quad \Delta_0 = \Delta - \frac{\bar{R}}{3}, \quad \Delta_1 = \Delta - \frac{\bar{R}}{4}, \tag{4.4}$$

where Δ_0 act on scalar fields and Δ_1 on transverse vectors. Then, for the transverse vector ξ_μ, the scalar σ, the scalar longitudinal part of the ghost C, and the auxiliary fields upon

which four derivatives act, we implement a cutoff type II with the implicit definition of the regulator R_k^{xx} via the relationship

$$\Gamma^{(2)}_{xx} + R_k^{xx} = a\left[\Delta + r_k(\Delta)\right]\left[\Delta_i + r_k(\Delta_i)\right]^k, \tag{4.5}$$

in which the shape cutoff function r_k will be the optimised cutoff $r_k(q^2) = (k^2 - q^2)\theta(k^2 - q^2)$[53, 54]. For the remaining fields we will use the cutoff type I as explained in 3. This technical detail ensures the that the poles $R = 3$ and $R = 4$ appearing in [48, 36], which come from the choice of regulator (and as they are regulator dependent, the may not be physical poles), do not appear.

Using dimensionless Ricci sacalar $R = k^{-2}\bar{R}$ let us introduce the dimensionless function and dimensionless couplings,

$$f(R) = 16\pi k^{-4} F_k(R), \quad g_i(k) = k^{-d_i}\bar{g}_i(k), \tag{4.6}$$

where d_i is the mass dimension of $\bar{g}_i$.

Hence, equation (2.35) in its dimensionless form take the form

$$\partial_t f - 2Rf' + 4f = I_0[f] + I_1[f]\cdot\partial_t f' + I_2[f]\cdot\partial_t f'', \tag{4.7}$$

where the prime denotes derivation with respect to R and I_n depends explicitly on f, its first three derivatives, and on R (Appendix C). Explicitly (4.7) has the form

$$\begin{aligned}
&384\pi^2(\partial_t f(R) - 2Rf'(R) + 4f(R)) = \\
&\partial_t f'(R)\left(\frac{\frac{311R^3}{3360} - \frac{R^2}{12} - 15R + 30}{3f(R) - (R-3)f'(R)} + \frac{\frac{37R^3}{1512} + \frac{29R^2}{60} + 3R + 6}{(R-3)^2 f''(R) + (3-2R)f'(R) + 2f(R)}\right) \\
&+ \frac{R\left(-\frac{311R^3}{756} + \frac{R^2}{6} + 30R - 60\right)f''(R) + \left(\frac{311R^3}{756} - \frac{R^2}{3} - 90R + 240\right)f'(R)}{3f(R) - (R-3)f'(R)} \\
&\frac{+\partial_t f''(R)\left(-\frac{181R^4}{3360} - \frac{29R^3}{30} - \frac{91R^2}{20} + 27\right)}{(R-3)^2 f''(R) + (3-2R)f'(R) + 2f(R)} + \frac{R\left(\frac{181R^4}{1680} + \frac{29R^3}{15} + \frac{91R^2}{10} - 54\right)f^{(3)}(R)}{(R-3)^2 f''(R) + (3-2R)f'(R) + 2f(R)} \\
&+ \frac{\left(-\frac{37R^4}{756} - \frac{29R^3}{10} - \frac{121R^2}{5} - 12R + 216\right)f''(R) + \left(\frac{37R^3}{756} + \frac{29R^2}{15} + 18R + 48\right)f'(R)}{(R-3)^2 f''(R) + (3-2R)f'(R) + 2f(R)} \\
&+ \frac{422R^2}{45} - 36R - 48
\end{aligned} \tag{4.8}$$

As we can note, this equation contains derivatives of f up to $f^{(3)}$. Then, if we insert the fixed point conditions $\partial_t f = \partial_t f' = \partial_t f'' = 0$, we will end up with a third order non-linear ordinary differential equation. Solving this kind of equations is an open topic nowadays, so we only refer the reader to the next references [8, 74, 48, 87, 9, 61, 20, 19, 24, 26, 27].

Another approach to extract information out of (4.7), is to implement the method used in [36, 48, 87]. Then to find the the beta functions up to order $N-1$ we first need to truncate (4.6) by choosing all the couplings to be zero, from $N+2$ to infinity, i.e.

$$g_l = 0 \quad \forall l > N+2, \tag{4.9}$$

or in other words, truncate our theory up to two orders above of the one desired. Then we simply need to plug (4.6) into (4.7) or (4.8), project the resulting equation, following by setting the initial conditions

$$g_{N,N+1} = 0, \qquad \beta_{N,N+1} = 0, \tag{4.10}$$

and finally solve the remaining $N-1$ equations for the remaining $N-1$ beta functions.

To demonstrate how the argument above works we will state the first steps explicitly for the R^2 theory. Or more, clearly, we want to compute the beta functions for R^2 theory, then we start with $N=3$.

First, we need to substitute $f(R) = \sum_{i=0}^{4} g_i R^i$ into (4.7) to get

$$\sum_{n=0}^{4} (\beta_n R^n + 4g_n R^n - 2n g_n R^n) = I_0[f] + I_1[f] \sum_{n=0}^{4} \left(n\beta_n R^{n-1}\right) + I_2[f] \sum_{n=0}^{4} \left(n(n-1)\beta_n R^{n-2}\right), \tag{4.11}$$

where I_0, I_1, and I_2 are shown in appendix C.

Then, expanding to order R^0, R^1 and R^2 around $R=0$ and equating both sides order by order we get

$$\beta_0 + 4g_0 = I_0^{(0)} + I_1^{(0)}\beta_1 + 2I_2^{(0)}\beta_2, \tag{4.12a}$$

$$\beta_1 + 4g_1 - 2g_1 = I_0^{(1)} + 2I_1^{(0)}\beta_2 + I_1^{(1)}\beta_1 + 2I_2^{(1)}\beta_1 + 2\cdot 3 I_2^{(0)}\beta_3, \tag{4.12b}$$

$$\beta_2 = \frac{1}{2}I_0^{(2)} + 3I_1^{(0)}\beta_3 + 2I_1^{(1)}\beta_2 + \frac{1}{2}I_1^{(2)}\beta_1 + I_2^{(2)}\beta_2 + 3I_2^{(1)}\beta_3 + 6I_2^{(0)}\beta_4. \tag{4.12c}$$

This process is the projection of the flow equation. From here, now we can note that for each order R^n we get a linear term in β_{n+2}, and also note that in terms of the beta functions, this is a linear system of 3 equation with 5 variables. Then, we can always solve

the system for β_2, β_3 and β_4 in terms of β_0 and β_1 and the couplings up to order g_4

$$\begin{aligned}
\beta_2 &= -\frac{-\beta_0 - 4g_0 + I_0^{(0)} + \beta_1 I_1^{(0)}}{2I_2^{(0)}} \\
\beta_3 &= \frac{-I_1^{(0)}\left(\beta_0 + 4g_0\right) + 2g_1 I_2^{(0)} + I_0^{(0)} I_1^{(0)} - I_0^{(1)} I_2^{(0)}}{6I_2^{(0)2}} \\
&\quad \frac{+\beta_1\left(I_1^{(0)2} - I_2^{(0)}(I_1^{(1)} + 2I_2^{(1)} - 1)\right)}{6I_2^{(0)2}} \\
\beta_4 &= \frac{\left(-\beta_0 - 4g_0 + I_0^{(0)} + \beta_1 I_1^{(0)}\right)\left(-I_1^{(0)2} - I_1^{(0)} I_2^{(1)} + 2I_1^{(1)} I_2^{(0)} + I_2^{(0)} I_2^{(2)} - I_2^{(0)}\right)}{12I_2^{(0)3}} \\
&\quad - \frac{(-3I_1^{(0)} - 3I_2^{(1)})\left(-\beta_1 - 2g_1 + I_0^{(1)} + \beta_1 I_1^{(1)} + 2\beta_1 I_2^{(1)}\right)}{36I_2^{(0)2}} \\
&\quad - \frac{I_0^{(2)} + \beta_1 I_1^{(2)}}{12I_2^{(0)}}
\end{aligned} \tag{4.13}$$

Next, with use of the conditions (4.10),

$$\beta_{3,4} = 0, \qquad g_{3,4} = 0, \tag{4.14}$$

then the last two equations of (4.13) can be solved for the values of β_0 and β_1, and with these the first equation of (4.13) is already the solution for β_2. Then, is the equations for the two higher orders the ones used to find β_0, and β_1.

It is convenient to switch to a different parametrisation from the g-couplings

$$g_0 \to \frac{\lambda}{8\pi g}, \quad g_1 \to -\frac{1}{16\pi g}. \tag{4.15}$$

From here, we recognise g as the dimensionless Newton coupling, and λ as the dimensionless cosmological constant. The canonical mass dimensions for the new system are given by $[\Lambda] = [c_0 k^2] = 2$, $[G] = [c_1 k^{-2}] = -2$, and $[\bar{g_n}] = [g_n k^{4-2n}] = (4 - 2n)$. This change of parametrisation will also change the location of the fixed points, however, the critical exponents must remain the same. Consider the general phase space coordinate change $\bar{g}_i = \bar{g}_i(g)$; hence, this will induce a change in the beta functions $\partial_t \bar{g}_i = \bar{\beta}_i = \partial \bar{g}_i / \partial g_j \beta_j$; while the stability matrix will change as

$$\bar{M}_{ij} = \frac{\partial \bar{\beta}_i}{\partial \bar{g}_j}\Big|_* = \frac{\partial \bar{g}_i}{\partial g_k} M_{kl} \frac{\partial g_l}{\partial \bar{g}_j}\Big|_*$$

which means the eigenvalues of $\bar{M}$ and M are the same.

In the vicinity of any FP, the behaviour of the system is governed by the linearised flow equations

$$\partial_t g_i = \beta_i = \sum_{j=1}^{n} M_{ij}(g_j - g_j^*), \tag{4.16}$$

whose solution is

$$g_i(t) = g_i^* + \sum_{\alpha=1}^{n} C_\alpha V_\alpha^i e^{-t\theta_\alpha}. \tag{4.17}$$

C_α are constant to be determined by the initial condition $t = 0$ (corresponding to k_0) given by

$$C_\alpha = \sum_j (S^{-1})_{\alpha j}(g_j(k_0) - g_j^*), \quad S = (V_1, \ldots, V_n) \tag{4.18}$$

V_α and $\vartheta_\alpha = -\theta_\alpha$ are the eigenvectors and eigenvalues of the stability matrix M, respectively.Relevant (irrelevant) directions correspond to those with a negative (positive) real part of $\vartheta = -\theta_\alpha$. For relevant directions we can take safely the limit $k \to \infty$, and they define the UV critical surface, which in turn is obtained by setting $C_\alpha = 0$ for $\theta_\alpha < 0$, solving for the remaining C_α constants in terms of the relevant couplings, and finally substituting these values into the irrelevant ones. We will be using this critical surface to safely define our initial conditions when solving the system of beta functions for the R^3 theory.

As in the Einstein-Hilbert case [51], here we find a pair of complex conjugated eigenvalues, whose eigenvectors are complex as well. However, we can always choose C_α constants such that, solution (4.17) is written only with real terms.

In the next section we will analyse and integrate numerically the system of beta functions for the R^2 theory (4.13). Lastly, as the expression for the beta functions are too long we will not write them down explicitly.

4.3 R^2 theory

Gaussian fixed point

The usual gaussian fixed point (GFP) seems to be absent in this case due to the coupling parametrisation (see (4.23)), and what is found is that β_λ and β_g vanish for vanishing couplings, meanwhile in the linearised system β_2 take the form [50]

$$\beta_2 = \partial_t g_2 = \frac{1117}{4320\pi^2} = \gamma, \tag{4.19}$$

hence, in this regime, g_2 behaves linearly in t. Also, in order to get a better insight about the behaviour near the point $(\lambda = 0, g = 0, g_2 = 0)$, we can make use of the linearised system (4.16), but changing the entry $i = 2$ for $\partial_t g_2 = \gamma + \sum_j M_{2j}(g_2)$. In this case the

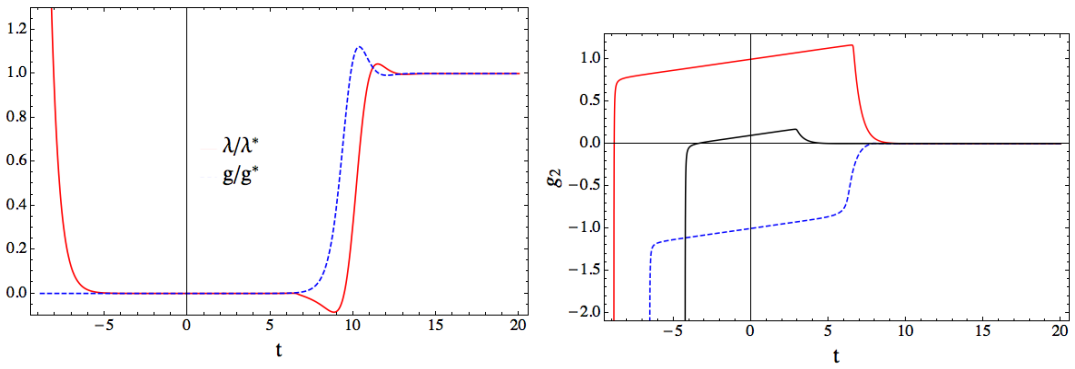

Figure 4.1: Left panel: Running of the λ (solid red line), and g (dashed blue line) couplings for the R^2 theory. Right panel: Running of the g_2 coupling for different initial conditions, the red solid line correspond to $(\lambda_0 = g_0 = 10^{-8}, g_{2,0} = 1)$, the black solid line to $(\lambda_0 = g_0 = 10^{-4}, g_{2,0} = -1/10)$, and the blue dashed line to $(\lambda_0 = g_0 = 0, g_{2,0} = -1)$

stability matrix is given by

$$M = \begin{pmatrix} -2 & \nu = \frac{1}{2\pi} & 0 \\ 0 & 2 & 0 \\ \zeta = \frac{28843}{25920\pi^2} & \tau = \frac{1238387}{3110400\pi^3} & 0 \end{pmatrix}. \tag{4.20}$$

With these, the linearised system of beta functions around the point $(\lambda = 0, g = 0, g2 = 0)$ takes the form

$$\partial_t \lambda = -2\lambda + \nu g, \tag{4.21a}$$

$$\partial_t g = 2g, \tag{4.21b}$$

$$\partial_t g_2 = \gamma + \zeta\lambda + \tau g. \tag{4.21c}$$

The solution of the system is

$$\lambda = \left(\lambda_0 - \frac{\nu}{4} g_0\right)\left(\frac{k_0}{k}\right)^2 + g_0 \frac{\nu}{4}\left(\frac{k}{k_0}\right)^2, \tag{4.22a}$$

$$g = g_0 \left(\frac{k}{k_0}\right)^2, \tag{4.22b}$$

$$g_2 = g_{2,0} + \frac{\zeta}{2}\left(\lambda_0 - \frac{\nu}{4} g_0\right) - \frac{1}{2}\left(\frac{\nu}{4}\zeta + \tau\right) g_0 + \frac{\zeta\nu + 4\tau}{8} g_0 \left(\frac{k}{k_0}\right)^2 - \\ - \frac{\zeta}{2}\left(\lambda_0 - \frac{\nu}{4} g_0\right)\left(\frac{k_0}{k}\right)^2 + \gamma \ln\left(\frac{k}{k_0}\right). \tag{4.22c}$$

Where $\lambda_0 = \lambda(k_0)$, $g_0 = g(k_0)$, and $g_{2,0} = g_2(k_0)$. From (4.22a) and (4.22c), we note that when $k < k_0$, the first term of (4.22a) and the fifth term of (4.22c) start dominating until a point where its value is so big that the linear approximations is not valid anymore, and the limit $k \to 0$ cannot be reached. The only way this limit could be achieved

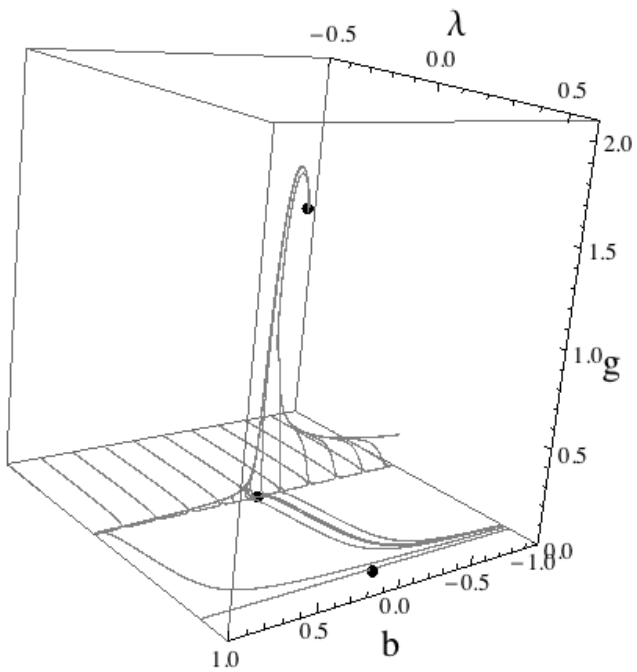

Figure 4.2: Flow for the R^2 system using the initial conditions (4.14). The black dots correspond to the ultraviolet fixed point, the Gaussian fixed point, and the singular point $(\lambda = 1/2, g = 0)$

is when the initial condition are such that $\lambda_0 = \frac{\nu}{4} g_0$. In the context of the Einstein-Hilbert truncation, this is the condition for finding a special kind of trajectory starting in the UVFP and ending exactly at the GFP where the limit $\Lambda = 0$ for $k \to 0$ can be accomplished, it is called the separatrix and it separates the flow into two different kinds of trajectories, the ones that run towards $\lambda \to -\infty$, and the ones running into the singular point $(\lambda = 1/2, g = 0)$. In the case of the R^2 truncation, following the analogous of the separatrix condition, leads to a logarithmic divergence for g_2 and again it is not possible to get the limit $k \to 0$.

In [79] the phase diagram for the R^2 theory is studied in a different parametrisation for the g_2 coupling. In that work, authors found a Gaussian fixed point sitting in the boundary of the system, and even though it was impossible for them to find a separatrix, they found some trajectories spending plenty of time in the classical regime. Their coupling corresponds to the reciprocal of g_2, and then the map

$$b = 1/g_2, \qquad \beta_b = -b^2 \beta_2, \tag{4.23}$$

show us that any logarithmic divergence encountered in the IR limit for β_2 will be compensated for the rapid decaying to zero of b^2 in the limit $k \to 0$. If this is a true Gaussian fixed point, it just means than in our present truncation it is located at $g_2 \to \infty$.

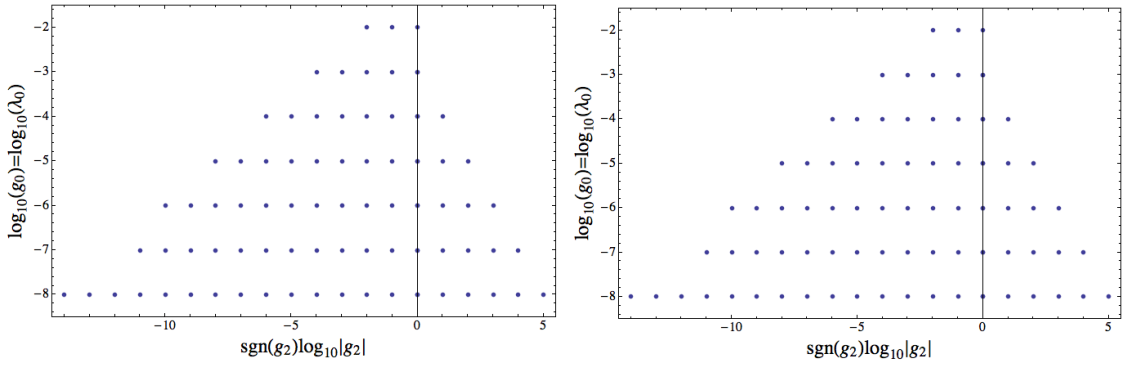

Figure 4.3: Domain of UV attraction. Vertical axis corresponds to *log* of the initial conditions for g and λ, and horizontal axis corresponds to initial conditions for g_2. $\lambda_0 = g_0$ ranges from 10^{-8} to 10^{-2}. In the case of g_2 initial conditions go from 10^0 to $\pm 10^{14}$. Each point represents an initial condition that is connected to the UV fixed point. Left panel corresponds to R^2 theory, right panel corresponds to $f(R)$ gravity (see text above).

Ultraviolet fixed point.

Apart from the GFP, we find a non-gaussian fixed point (NGFP) with coordinates and critical exponents

$$(\lambda, g, g_2) = (0.10137, 1.5293, 0.00318); \qquad \theta_{0,1} = 1.6317 \pm i\ 1.868, \quad \theta_2 = 29.3008, \quad (4.24)$$

and, with the following of the eigenvectors of the stability matrix

$$\begin{aligned} V_{0,1} &= (0.074789 \mp i\ 0.134847, -0.988038, 0.001795 \pm i\ 0.0004), \\ V_2 &= (0.6166, -0.78706, -0.01575) \end{aligned} \quad (4.25)$$

Note that this approximation leads to θ_2 of order 29. Same results for a large θ_2 value has been found in other studies [50, 19, 61], however, this value goes down to order 2 when higher derivative operators are added. Also, in [79], authors track back this big value to zero mode contributions for the beta functions. In our case, we will get a natural and accurate eigenvalue θ_2 after implementing a better approximation.

As it was reported in [50], the critical exponent θ_2 is so big that near the UVFP in the linearised regime, the corresponding factor $(\frac{k}{k_0})^{-\theta_2}$ decays so rapidly that it cancels the contribution from the eigenvector V_2, and hence, trajectories approaching the UVFP will behave exactly as in the Einstein-Hilbert case, and will be contained within a plane. When finally k^{θ_2} reaches unity, the flow is sufficiently far away from the UVFP.

Figure 4.1 shows the running of λ, g, and g_2. First we note that the cosmological constant coupling, and Newton's coupling gets the usual infrared behaviour near the point $(0, 0, 0)$, and even in the ultraviolet. Also, as there is no fixed point at the origin, for some

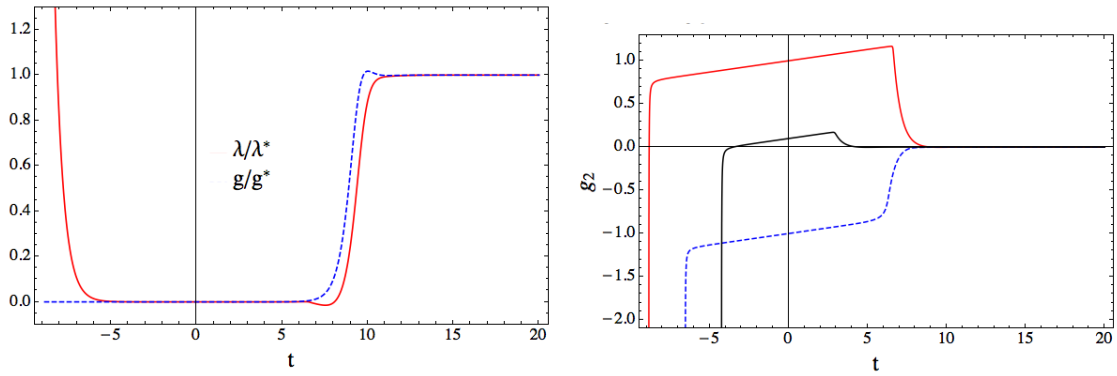

Figure 4.4: Left panel: Running of the λ (solid red line), and g (dashed blue line) coupling for R^2 theory with initial conditions (4.26). Right panel: Running of the g_2 coupling for different initial conditions, the red solid line corresponds to $(\lambda_0 = g_0 = 10^{-8}, g_{2,0} = 1)$, the black solid line to $(\lambda_0 = g_0 = 10^{-4}, g_{2,0} = -1/10)$, and the blue dashed line to $(\lambda_0 = g_0 = 0, g_{2,0} = 10^{-6}, -1)$

trajectories, λ can change sign near the origin. For g_2, in the UV trajectories start very close to the origin, as the usual fixed point value for this coupling is very small, then they grow (decay) rapidly to reach the logarithmic IR decay explained above, finally, after some RG time it decays sharply towards $g_2 \to \pm\infty$. For the cases where the trajectories run towards $\lambda \to -\infty$, g_2 decays logarithmically indefinitely.

4.4 f(R) theory

Next we discuss the impact of higher order interactions in $f(R)$ type theories. The primary idea here is to retain higher order couplings indirectly. There are several reasons for doing so. Firstly, it has been shown that higher order interactions are irrelevant in that they do not lead to further independent parameters. However, it was also found that higher order interactions are quantitatively important: they re-adjust lower order couplings, and strongly modify scaling exponents. Most notably, the R^2 approximation leads to an anomalously large value for the third relevant scaling exponent. However, as soon as higher order interactions are taken into account, the exponent becomes physically viable. For these reasons, we study $f(R)$ gravity in the approximation where only the relevant couplings (the vacuum energy, Newton'a coupling, and the R^2 interaction) are retained, whereas all higher order couplings are set onto their fixed point values.

Hence, in order to implement this idea, we will use the same procedure of last section, and start taking $N = 3$, but instead of using condition (4.10), we will use

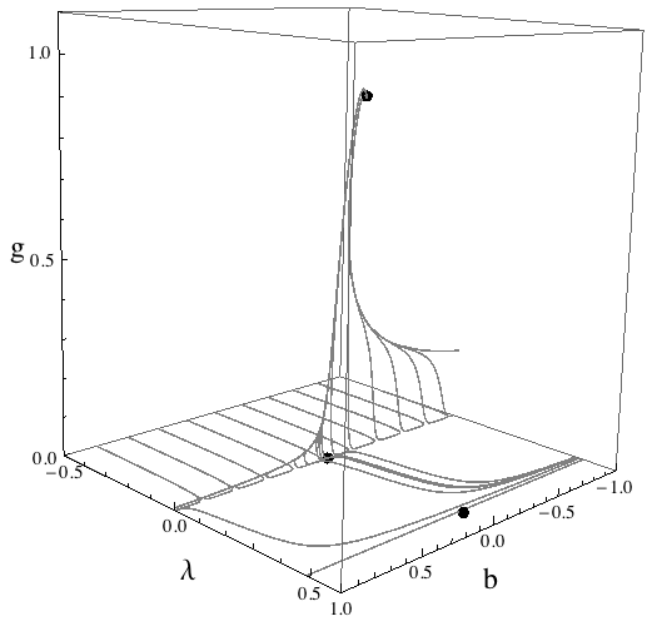

Figure 4.5: Flow for the $f(R)$ theory using the conditions (4.26). The black dots correspond to the ultraviolet fixed point, the absent Gaussian fixed point, and the singular point $(\lambda = 1/2, g = 0)$

$$g_3^* = -0.05723, \quad g_4^* = -8.3641, \quad \beta_3 = \beta_4 = 0, \tag{4.26}$$

these values were first obtained using $N = 71$, which means taking $g_{71} = g_{72} = 0 and \beta_{71} = \beta_{72} = 0$.

This will shift the position of the UVFP and the value of the critical exponents as if we included all orders in the expansion. Then, g_2, and g_3 provide our beta functions with information about all the other higher order couplings, up to g_{70}. This enhancement, is non-dynamical from the higher order couplings, implying that the phase space of the theory is described only by three dimensions as in the R^2 case.

Now, because of this improvement the location of the fixed point is exactly as that found in the whole truncation at order R^{70}:

$$(\lambda, g, g_2) = (0.11429, 0.92812, 0.0157), \quad \theta_{0,1} = 3.0230 \pm i\ 1.89368, \quad \theta_2 = 1.41293, \tag{4.27}$$

note the considerably smaller value for θ_2. Such value is comparable to the one found for more general truncations [19, 74, 61]. The corresponding eigenvectors are

$$\begin{aligned} V_{0,1} &= (0.0340345 \pm i\ 0.191504, -0.980855, 0.00942967 \mp i\ 0.00150789), \\ V_2 &= (0.386904, 0.915991, 0.10614). \end{aligned} \tag{4.28}$$

As the eigenvalue for the R^2 coupling is considerably smaller that in the former case, and being smaller than the real part of $\theta_{0,1}$, we expect a different behaviour close to the UVFP. However, deep in the infrared there are no qualitative differences between the two theories. This can be seen by comparing figures 4.4, 4.2, 4.1, and 4.5. The main difference is near the UVFP, in this new case, the spiralling due to the complex critical exponents has decreased.

In order to understand the differences respect to the previous case, we refer to figure 4.3. There we present a compendium of initial conditions for which the RG equations were integrated numerically. Each dot corresponds to the initial condition of a trajectory hitting the ultraviolet fixed point. The horizontal axis correspond to the initial condition $g_{2,0}$ expressed as the $log|g_2|$ multiplied by its sign. The vertical axis denotes the logarithm of the initial conditions for λ and g, for which we choose $\lambda_0 = g_0$.

As we can see from the figure, even though we have gotten a better result for the location of the UV fixed point and its critical exponents, the boundary of the system remains the same.

4.5 Discusion

In this chapter we implemented the renormalisation group equation derived in [87] in order to find the beta functions for the R^2 truncation. We confirmed the previous results about the non-existence of a Gaussian fixed point, and hence the lack of a separatrix [51]. However it is always possible to find a long classical regime for the cosmological constant and Newton's constant for different values of the R^2 coupling, leaving the possibility to find good constraints taken from Starobinsky's and $f(R)$ models for inflation[22]. In the ultraviolet practically there're no effects coming from the eigenvector V2 due to the large θ_2-value, that means that we are left only with the complex critical exponents (complex values indicate couple theories, in contrast with the case of diagonal stability matrices that appear for free theories).

In the the ultraviolet, the absence of the small value for the critical exponent θ_2 corresponding to R^2, leave us with a strongly coupled system.

In addition, we implemented a new idea where effectively for the first time we showed the phase space of an high order polynomial $f(R)$ theory. This based on the knowledge of the fixed point of higher order operators. With this conditions, we found a small value for the critical exponent of the R^2 operator, the infrared regime of this theory, keeps all the benefits from the previous picture, called, a long classical regime for the cosmological

constant and Newton's coupling. Also, and even though, the remaining critical exponents stayed complex, their effect in the deep UV is screened by strong effects coming from θ_2.

This findings open the possibility that trajectories in the 70 dimensional phase space of the full dynamical polynomial $f(R)$ theory, will behave in a similar way as the ones of the effective non-dynamical $f(R)$ found in this work. This should be true at least for the UV and IR regimes in a detached way. The other possibility is that if in the full theory, the UV critical surfaces is connected to the IR attractive critical surface near a Gaussian fixed point or any other infrared attractor, then the union of those spaces could be isomorphically represented by the domain of UV attraction of figure (4.3). Moreover, this technique to find beta functions from information of more general theories could be useful at the phenomenological level.

Chapter 5

IR fixed points of quantum gravity

5.1 Introduction

General relativity is the classical theory of gravitational interactions. Its domain of validity is remarkable as it extends over nearly thirty orders in magnitude starting at the submillimeter regime up to near-Hubble size scales. At smaller distances of about the Planck length l_{Pl}, quantum gravitational corrections are expected to set in. In the four-dimensional theory, the Planck length is of the order of $10^{-32}m$, although it could be significantly larger as suggested by extra-dimensional models and recent black hole studies with a large number of particle species beyond the standard model.

For gravity at short distances, RG results show that quantum fluctuations enforce an ultraviolet fixed point (UVFP) for the gravitational couplings as shown in the former chapters, thereby circumnavigating the virulent divergences of standard perturbation theory. In this context, gravity becomes asymptotically safe [91, 80, 36] and exists as a well-defined local quantum field theory, despite its perturbative non-renoralisability. A variety of renormalisation group studies in the continuum and numerical simulations on the lattice [47, 4] support the existence of this UV fixed point. One important feature that we will search for, is that the high-energy limit of the flow has to be connected to the low energy behaviour of gravity, i.e. its low energy behaviour has to yield Einstein's general relativity, and further more, it has to reproduce or explain the observed accelerated expansion of the Universe at distances compared to that of the Hubble scale.

Being $g = G_k k^2$ and $\lambda = \Lambda_k k^{-2}$, the dimensionless RG running of Newton's and of the cosmological constant, the RG flow for them is

$$\partial_t g = -2g + \text{quantum corrections}, \qquad \partial_t \lambda = 2\lambda + \text{quantum corrections}. \tag{5.1}$$

Hence, for small values of the couplings, g is attracted towards the gaussian fixed point

($\lambda_* = 0, g_* = 0$) where classical general relativity holds ($\Lambda = 0$), however (5.1) shows that λ behaves as an unstable IR operator, i.e. for small g the flow is driven away from the gaussian fixed point and strong RG corrections start setting in at the IR. In [82], the existence of an IR fixed point which would control the behaviour of the RG flow at large distances was conjectured, and in [12] this conjecture was taken seriously into account to prove that this model would give rise to an accelerated expansion of the late universe. Furthermore, some recent studies have tried to find evidence of the existence of IR fixed points in quantum gravity ranging from non-local extensions of Einstein-Hilbert theory [61], geometric flows [28], flow for the graviton propagator [17] and redefinition of couplings [70].

It is the purpose of this chapter to analyse the fate of RG trajectories which runs towards large λ, and for that end, we will recall the renormalisation group set-up as in the previous chapters and explicit flow equations for the gravitational couplings (Sect. 5.2). Then, we will highlight a degeneracy of fixed points (Sect. 5.4), and we will analyse the structure of the fixed points found and their critical exponents (Sect. 5.5). Finally, we will present our conclusions and discussions of the results and their physical implications (Sect.5.7).

5.2 Renormalisation group equations

Following Wilson's renormalisation group idea (i.e. changing the couplings for running couplings) and introducing an IR cutoff into the effective action we have that the scale behaviour of our running couplings G_k (Newton's constant) and Λ_k (cosmological constant) is dictated by means of the functional identity (2.35) [92]. Here we will use the Euclidean Einstein-Hilbert truncation

$$\Gamma_k = \int d^4x\sqrt{g}\frac{1}{16\pi G_k}\left(-R + 2\Lambda_k\right) + \cdots, \tag{5.2}$$

the ellipses in (5.2) denote the gauge fixing term (harmonic gauge as explained in chapter 3) and the ghost term. This truncation is enough to study the properties of gravity at large scale, since more general effects come from the RG picture. For example, in chapter 4, the picture we will show here also arises for the R^2 and R^3 truncations in the deep infrared.

The flow (2.35) describes the change of Γ_k upon integrating-out momentum degrees of freedom, and by construction it connects an initial effective action (Einstein-Hilbert) at $k = 0$ with the full quantum effective action Γ at some reference scale $k = \Lambda$. Here, we

will be exploring the possibility of getting a classical action with a different value for the gravitational coupling in the limit $k \to 0$.

We used the tensorial structure of [51] for the metric fluctuation. This structure correspond to the decomposition (3.3), (3.24), and the field redefinitions

$$\begin{aligned} &\xi_\mu \to \sqrt{-D^2 - R}\xi_\mu, \quad \sigma \to \sqrt{-D^2}\sqrt{-(D^2 - \frac{dR}{d-1}}\sigma, \\ &C \to \sqrt{-D^2}C, \quad \bar{C} \to \sqrt{-D^2}\bar{C}. \end{aligned} \tag{5.3}$$

These will give rise to no Jacobians in the functional measure. Also, we use a cutoff type I as described in (3.30), with the optimised scalar cutoff [53, 54]

$$r_k(z) = (1-z)\theta(1-z), \qquad z = \Delta = -D^2, \tag{5.4}$$

Then, the beta functions for the dimensionless couplings $g = k^2 G_k$ and $\lambda = k^{-2}\Lambda_k$ in (2.35) are

$$\partial_t g = \beta_g = (2 + \eta_N)g, \tag{5.5}$$

$$\partial_t \lambda = \beta_\lambda = (-2 + \eta_N)\lambda + g\left[a_1(\lambda, \alpha) - \eta_N a_2(\lambda, \alpha)\right] \tag{5.6}$$

where the graviton anomalous dimension $\eta_N = \partial_t(\ln G_k)$ is given by

$$\eta_N = \frac{g b_1(\lambda, \alpha)}{1 + g b_2(\lambda, \alpha)}, \tag{5.7}$$

The values of the a_i, and b_i functions are given in appendix D, and in general they will be gauge fixing parameter dependent ((3.2)).

Also, we will be working in two cases:

1. η_N approximated by its leading order (LO) in g, i.e. $b_2(\lambda) = 0$ (with $\alpha = 0$) in (5.7) [52]. As described in (3.75), this is a one-loop approximation, since the function $b_2(\lambda, \alpha)$ comes from the right hand side of the flow equation (2.35).

   In this case the anomalous dimension is

   $$\eta_N = \frac{g(4\lambda(33 - 25\lambda) - 81)}{24\pi(1 - 2\lambda)^2}. \tag{5.8}$$

   And the beta functions are

   $$\beta_\lambda = -2\lambda + \frac{g\left(100\lambda^2 - 132\lambda + 81\right)\left(g(4\lambda - 5) + (12\pi - 24\pi\lambda)\lambda\right)}{288\pi^2(2\lambda - 1)^3} + \\ + \frac{4g\lambda + g}{2\pi(1 - 2\lambda)} \tag{5.9}$$

   $$\beta_g = 2g - g\left(\frac{g\left(100\lambda^2 - 132\lambda + 81\right)}{24\pi(1 - 2\lambda)^2}\right). \tag{5.10}$$

2. Hartree-Fock resummation (HF) for η_N (with $\alpha \to \infty$, $\lambda \to \lambda/\alpha$, and $g \to 24\pi g/\alpha$) [55], the anomalous dimension here is

$$\eta_N = \frac{24g}{4g - (1-2\lambda)^2}, \tag{5.11}$$

while the beta functions are

$$\beta_\lambda = -2\lambda - \frac{24g(6g - 3\lambda + 1)}{4g - (1-2\lambda)^2} - 12g, \tag{5.12}$$

$$\beta_g = 2g + \frac{24g^2}{4g - (1-2\lambda)^2}. \tag{5.13}$$

In contrast to the leading order approximation this one consists in retaining higher loop corrections.

The gauge used in the first case (Landau gage), at the level of the action, means that the Newton's coupling (cosmological coupling) is dominated (suppressed) by the graviton vector and longitudinal scalar fluctuations, and the trace scalar part is completely suppressed. Meanwhile, for the second case, Newton's coupling and cosmological coupling are dominated by the graviton scalar and vector fluctuations, while the tensor mode and some of the scalar modes are parametrically suppressed. The choice of this gauges are such that the beta functions take their simplest form.

Both cases present a halt of the flow due to a singular behaviour; in the former, this occurs at the line $\lambda = 1/2$, meanwhile in the latter, it happens at a particular function of λ in the theory space. It was shown in [69] that the behaviour in this region is the same for a very wide range of regulators, concluding that the singularity is an universal feature of the system.

5.3 Nullclines and fixed points

One way to explore the fixed point structure of the flow is by looking at the intersections of the nullclines. We define $g_g(\lambda)$ as the integral curves for $\beta_g = 0$, and in a similar manner, $g_\lambda(\lambda)$ the integral curve for $\beta_\lambda = 0$, also, we define $g_b(\lambda)$ as the curves where the anomalous dimension diverge ($1/\eta_N = 0$).

In the LO approximation these nullclines take the form

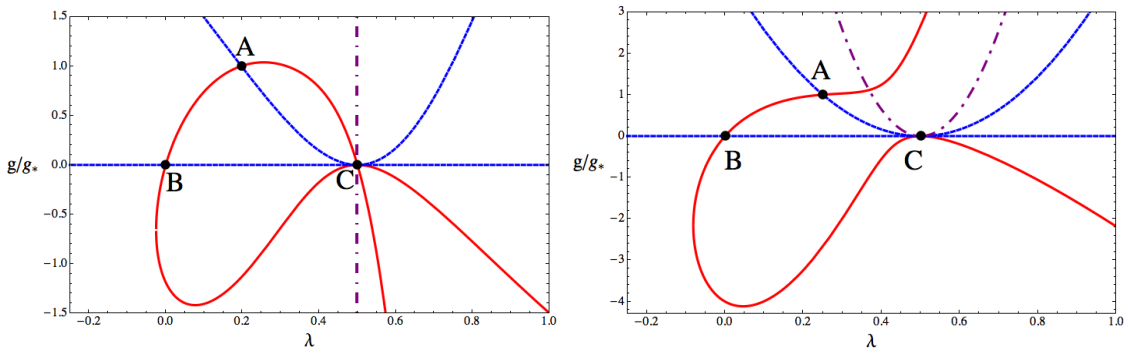

Figure 5.1: Nullclines of the linear approximation for the anomalous dimension (left) and for the Hartree-Fock resummation (right). Blue dashed lines correspond to nullclines g_g(from β_g), red lines correspond to nullclines g_λ (from β_λ), and purple dot-dashed lines indicates $1/\eta_N = 0$. Showing the UV fixed point A, the IR gaussian fixed point B, and the degenerated IR fixed point C.

$$g_\lambda = \pm\frac{6\pi\sqrt{(1-2\lambda)^2(\lambda(\lambda(8\lambda(25\lambda(50\lambda^2+28\lambda-133)+5179)-24591)+5112)+144)}}{(4\lambda-5)(4\lambda(25\lambda-33)+81)} - \frac{6\pi(+\lambda(81-2\lambda(2\lambda(50\lambda-43)+75))-12)}{(4\lambda-5)(4\lambda(25\lambda-33)+81)}, \tag{5.14}$$

$$g_g = 0, \quad \text{and} \quad g_g = \frac{48\pi(1-2\lambda)^2}{4\lambda(25\lambda-33)+81}, \tag{5.15}$$

$$g_b \to \lambda = \tfrac{1}{2}, \tag{5.16}$$

here the boundary of the system is given by the line $\lambda = 1/2$ for all g.

For the HF resummation these nullclines are:

$$g_\lambda = \tfrac{1}{96}(-3+4\lambda+12\lambda^2 \pm \sqrt{9+72\lambda-440\lambda^2+480\lambda^3+144\lambda^4}) \tag{5.17}$$

$$g_g = 0 \quad \text{and} \quad g_g = \tfrac{1}{16}(1-2\lambda)^2., \tag{5.18}$$

$$g_b = \tfrac{1}{4}\left(4\lambda^2-4\lambda+1\right), \tag{5.19}$$

unlike the previous case, here the boundary is a function of the cosmological constant λ.

Given the nullclines, now the λ-coordinate of the fixed points are simply solutions of the equations $g_\lambda(\lambda) - g_g(\lambda) = 0$, i.e the intersections of nullclines are fixed points.

5.3.1 UV fixed point

This is the very well stablished non-Gaussian fixed point. It has been studies throughly in several works [38, 36, 56, 55, 80, 51], through all this studies it has been found that this is a true fixed point describing gravity at very high energies, its stability has been shown for more general truncations, while it is also proven that is independent of the gauge and

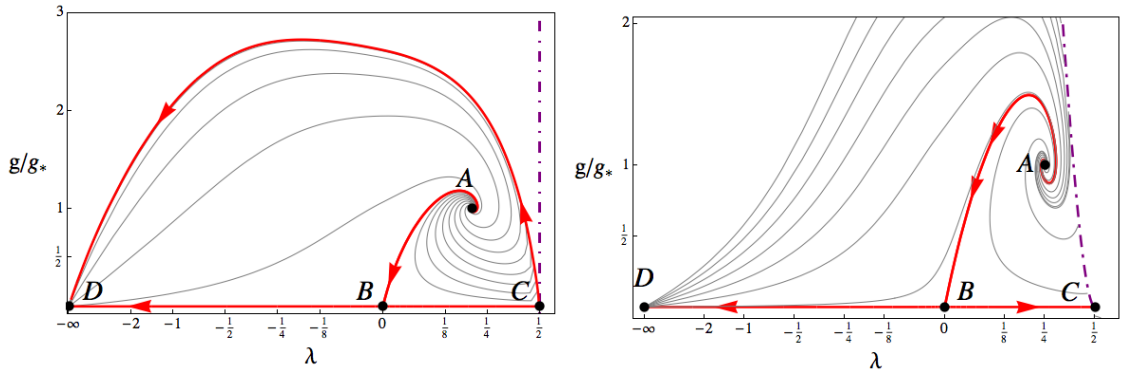

Figure 5.2: Global flows for the leading order approximation (left), and for the Hartree-Fock resummation (right). Purple dot-dashed lines indicates $1/\eta_N = 0$. Showing the UV fixed point A, the IR gaussian fixed point B, and the IR bifurcation C. Note that in the LO approximation all trajectories enclosed within the separatrix connecting C and D are globally safe, i.e. they do not run into the boundary of the system.

the definition of our cutoff. As the purpose of this chapter is to describe the IR limit of the theory, we will briefly comment the properties of this fixed point.

In figure 5.1 it is depicted as A, and it is the intersection of the non-trivial g_g and the positive branch of g_λ. Its coordinates for both approximations are given by

$$(\lambda^*_{LO}, g^*_{LO}) = (0.1971, 0.9401), \qquad (\lambda^*_{HF}, g^*_{HF}) = (1/4, 1/64). \tag{5.20}$$

The stability properties of the fixed point are given by the critical exponents θ_i. This are just the negative of the eigenvalues of the stability matrix

$$M_{ij} = \left.\frac{\partial \beta_i}{\partial g_j}\right|_{g^*_l}, \tag{5.21}$$

with $g_0 = \lambda$, and $g_1 = g$. For the UVFP we have

$$\theta^{LO}_{1,2} = 1.4887 \pm i2.6819, \qquad \theta^{HF}_{1,2} = \frac{5}{3} \pm i\frac{\sqrt{167}}{3}, \tag{5.22}$$

One can see that the real part of the eigenvalues is positive, and then, the non-Gaussian fixed point is UV attractive. The imaginary part give rise to a spiral behaviour for trajectories near the UVFP. Finally, we can see here that the critical exponents for lower order approximation are close to those of the full system.

5.3.2 Gaussian fixed point

In terms of the nullclines (5.14), (5.15), (5.18), and (5.18), this one correspond to the intersection of the positive branch g_λ and the line $g_g = 0$, and is situated at the origin of the theory space.

At the Gaussian fixed point, the critical exponents correspond minus the canonical mass dimension of the couplings, i.e. $\theta_1 = -2$, and $\theta_2 = 2$. Then, g is IR attractive, while λ is IR repulsive.

Near the Gaussian fixed point (GFP), the solution of the linearised system (2.5) is

$$g(k) = g_0 \left(\frac{k}{k_0}\right)^2 \tag{5.23}$$

$$\lambda(k) = \left(\lambda_0 - \frac{g_0\gamma}{4}\right)\left(\frac{k_0}{k}\right)^2 + \frac{g_0\gamma}{4}\left(\frac{k}{k_0}\right)^2 \tag{5.24}$$

where, $\lambda_0 = \lambda(k_0)$, $g_0 = g(k_0)$ and the positive constant γ depends on the case on consideration; for the leading order approximation we have $\gamma = 1/(2\pi)$, whie for the HF case is $\gamma = 12$. Solution (5.23) show that we can safely take the limit $k \to 0$, however (5.24) will diverge in such limit, unless $\lambda_0 = g_0\gamma/4$. Hence, for positive dimensionless Newton's constant, we can find three different types of trajectories as stated in [81]: Type Ia trajectories correspond to trajectories emanating from the UV fixed point with $\lambda \to -\infty$ when $k \to 0$, or $\lambda_0 < g_0\gamma/4$; the separatrix is referred as a trajectory of type IIa or trajectories sitting on $\lambda(k) = \gamma/4g(k)$; last but not least, trajectories type IIIa are those that run from the UV fixed point with positive values for λ, and end up in the boundary of the system. For the latter trajectories, the first term in (5.24) dominates the behaviour of λ, then solving $(k/k_0)^2$ in (5.23), and inserting this in (5.24) we get

$$\lambda \approx (\lambda_0 - \frac{g_0^2\gamma}{4})\frac{1}{g}, \tag{5.25}$$

then, in theory space, this are parabolas running towards fixed point C as depicted in figure 5.2.

Finally, note that in the LO case, the red line CD in the left panel of fig. (5.2) acts as an IR attractor shielding the flow from singularities and allowing trajectories with an extended semi-classical regime for positive, vanishing or negative λ. In [52], is shown that the phase space of (5.9), (5.10) is topologically equivalent to that of the conformally reduced gravity of [83], and it arises as a bifurcation, where the free parameter is the effective dimension n in which the conformal factor fluctuates. This picture follows for values bigger than the bifurcation point $n_c = 1.4715$. If this dimension is below the bifurcation point $n_c = 1.4715$, the phase space is that of the minisuperspace approximation [66] (where effectively the conformal mode fluctuates in one dimension), where UV and IR regimes connected via a limit cycle. Approaching n_c from above, the IR attractor CD becomes a separatrix connecting the fixed point C and the Gaussian fixed point B, and then, all trajectories connected to the UV fixed point approach the GFP arbitrarily close displaying the a

long semi-clasical regime. Finally, none of these asymptotically safe trajectories admit a negative cosmological constant. We will encounter an similar enclosure area of the phase space in next chapter after unfolding the degeneracy present on the point C.

5.3.3 Infrared fixed point

For both cases, we can easily recognise the special case of point C from the nullclines in figure 5.1. While all the other points correspond to a simple intersection, C corresponds to a tangential intersection of 3 lines plus the tangential intersection of the boundary of the flow where beta functions and the anomalous dimension diverge. Also, we have to note that at the point C the anomalous dimension is ill-defined. Along the horizontal line $g = 0$, $\eta_N = 0$, but for the curved line $g_g(\lambda)$ it must take the value $\eta_N = -2$, and furthermore, it diverges along the purple lines. Furthermore, the limit $(\lambda \to 1/2, g \to 0)$ for the eigenvalues of the stability matrix (5.21) does not commute. However, from the flow of the LO case, C would seem to be a well defined fixed point with an attractive and a repulsive IR directions.

If we forget for a minute about the boundary of the system, in general grounds [89], tangential nullclines correspond to the bifurcation at some value δ_c of an independent parameter δ. Furthermore, if we redefine our RG time as $t \to (1-2\lambda)^2 t$ for the LO case, and $t \to g_b t$ for the HF approximation, then restricting our analysis to HF case, the beta functions become

$$\begin{aligned} \beta_g \to g_b \beta_g &= 2g\left(16g - (1-2\lambda)^2\right), \\ \beta_\lambda \to g_b \beta_\lambda &= 2\left(-96g^2 + g\left(24\lambda^2 + 8\lambda - 6\right) + (1-2\lambda)^2\lambda\right), \end{aligned} \tag{5.26}$$

this system is topologically the same as the original system. Hence, the critical exponents for the fixed point C are $\theta_{1,2} = 0$. Zero eigenvalues like these are the result of the bifurcation of a saddle-node, otherwise called non hyperbolic fixed point [93, 89].

Then, from the discussion above we can think that C could be the result of a collapse of several fixed points (degenerated fixed point), and since is not lifted dynamically, the purpose of this chpater is to study the behaviour of the system by considering a small perturbation of the beta functions such that the nullclines intersect transversally generating new fixed points (Figure 5.3). Then to lift the degeneracy, we select a one parameter δ-transformation.

It was remarked in [82] that the divergence appearing at the point $(\lambda = 1/2, g = 0)$ is driven by unstable eigenmodes of the propagator for the transverse-traceless sector of the metric, when k^2 is sufficient small, and that the problem must be solved after using

a more general truncation. Similarly, we will assume here that the degeneracy would be lifted for a more general truncation and that the parameter δ accounts for the effects of this generalisation.

5.4 Degeneracy of Fixed Points

The small perturbation mentioned above is performed and controlled by introducing a small parameter δ as shown in (5.27) below (blowing-up method [31, 5, 32]), then the family of one-parameter beta functions is

$$\partial_t g = \beta_g(\lambda - \delta, g), \quad \partial_t \lambda = \beta(\lambda - \delta, g - b_\delta), \tag{5.27}$$

where b_δ is introduced in order to maintain the gaussian fixed point at the origin ($\lambda = 0, g = 0$). For the leading order approximation we have:

$$\begin{aligned} b_\delta \quad &= -6\pi \frac{\sqrt{144-4536\delta-44463\delta^2-160244\delta^3-290692\delta^4-277728\delta^5-118800\delta^6+17600\delta^7+40000\delta^8}}{405+984\delta+1028\delta^2+400\delta^3}, \\ &\quad +6\pi \frac{12+81\delta+150\delta^2+172\delta^3+200\delta^4}{405+984\delta+1028\delta^2+400\delta^3}, \end{aligned} \tag{5.28}$$

whilst for the HF resummation:

$$b_\delta = \frac{1}{96}\left(3 + 4\delta - 12\delta^2 - \sqrt{9 - 72\delta - 440\delta^2 - 480\delta^3 + 144\delta^4}\right) \tag{5.29}$$

The fixed point structure of (5.27) is shown in Figure 5.3. In both cases, we note the lifting of the divergence and the appearing of two new fixed points with $\lambda < 1/2$. The differences between cases is the shape of the boundary line where the anomalous dimension diverge ($1/\eta_N = 0$), and the level of degeneracy of the point C expressed as the number of new fixed points appearing: for the leading order approximation, the boundary (purple dashed line in Figure 5.3) is simply a line of constant λ, with three new fixed points to its right; whereas, for the Hartree-Fock approximation, the boundary is a parabola with two fixed points to its right.

The region with $\lambda > 1/2$ is of no physical interest since it has no connection to the fixed point A (UV). What is important to note is that, as we will show later, the fixed points C and C' are possible infrared fixed points. Fixed point C is sitting along the line $g = 0$, which, from (5.5), means that the anomalous dimension must be $\eta_N = 0$, meanwhile for C' must be $\eta_N = -2$.

One direct consequence is that, for small k, in the vicinity of C', since $g \neq 0$ and $G_k = g^*_{C'}/k^2$, we will see an increase in the value of the dimensionful Newton's constant G_k,

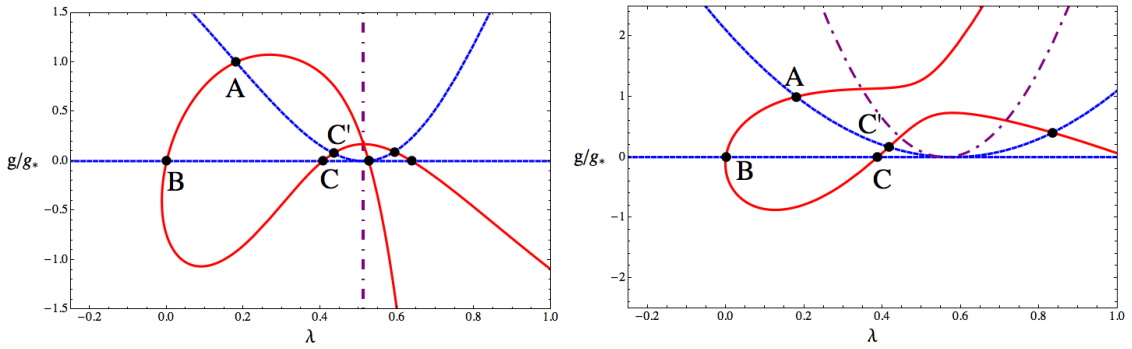

Figure 5.3: Lifting of the degeneracy and new fixed points and separatrices of system (5.27) in both cases. For the leading order approximation case (left) we use $\delta = 1/80$ and for the Hartree-Fock resummation (right) $\delta = 2/25$.

making gravity stronger; whereas, for C, Newton's constant coupling will get a constant value for the limit $k \to 0$

Of course, the position of all the fixed points in the system will get a $\delta-$dependence. Since $\delta_c = 0$ is a bifurcation point of the family (5.27), the local dynamics of the point $(\lambda = 1/2, g = 0)$ are not topologically equivalent if we move δ for positive or negative values, then for $\delta_c = 0$ the system (5.27) is structurally unstable around $\lambda = 1/2$ [46, 93]. The case $\delta > 0$ is the one of interest in our discussion, since the case $\delta < 0$ do not give rise to a new set of fixed points.

The fixed points for both cases are complicated but analytical functions in $\{0, 0.284976\}$, the explicit expressions around $\delta = 0$ are:

1. Leading order approximation:

   - FP A:

$$\lambda_A^* = 0.1971 - 1.1054\delta - 12.7287\delta^2, \tag{5.30}$$

$$g_A^* = 0.9401 + 9.95582\delta + 65.5671\delta^2. \tag{5.31}$$

   - FP B:

$$\lambda_B^* = 0, \tag{5.32}$$

$$g_B^* = 0. \tag{5.33}$$

   - FP C:

$$\lambda_C^* = \frac{1}{2} - \sqrt{\frac{5}{6}}\delta^{1/2} + \frac{5}{3}\delta, \tag{5.34}$$

$$g_C^* = 0. \tag{5.35}$$

- FP C':

$$\lambda^*_{C'} = \frac{1}{2} - \sqrt{\frac{5}{12}}\delta^{1/2} + \frac{13}{12}\delta - \frac{1427}{96\sqrt{15}}\delta^{3/2}, \tag{5.36}$$

$$g^*_{C'} = 2\pi\delta - \sqrt{\frac{12}{5}}\pi\delta^{3/2} + \frac{68\pi}{3}\delta^2, \tag{5.37}$$

2. Hartree-Fock resummation:

- FP A:

$$\lambda^*_A = \frac{1}{4} - \frac{2}{9}\delta - \frac{80}{27}\delta^2 - \frac{8344}{729}\delta^3 + \cdots, \tag{5.38}$$

$$g^*_A = \frac{1}{64} + \frac{11}{72}\delta + \frac{241}{324}\delta^2 + \frac{2362}{729}\delta^3 + \cdots. \tag{5.39}$$

- FP B:

$$\lambda^*_B = 0, \tag{5.40}$$

$$g^*_B = 0. \tag{5.41}$$

- FP C:

$$\lambda^*_C = \frac{1}{2} - \frac{1}{\sqrt{3}}\delta^{1/2} + 2\delta - \frac{31}{6\sqrt{3}}\delta^{3/2} + \cdots, \tag{5.42}$$

$$g^*_C = 0. \tag{5.43}$$

- FP C':

$$\lambda^*_{C'} = \frac{1}{2} - \frac{\sqrt{2}}{3}\delta^{1/2} + \frac{13}{9}\delta - \frac{8\sqrt{2}}{9}\delta^{3/2} + \cdots, \tag{5.44}$$

$$g^*_{C'} = \frac{1}{18}\delta - \frac{2\sqrt{2}}{27}\delta^{3/2} + \frac{28}{81}\delta^2 \cdots. \tag{5.45}$$

For both cases the distance between the fixed points C and C' is of order $\sqrt{\delta}/10$. Also, from these results one can show that in the limit $\delta \to 0$, C and C' go to $\lambda^* \to 1/2$ and $g^* \to 0$ without singularity problems, proving that C is a true bifurcating point of the theory.

5.5 Flow and Scaling

Similar to the fixed points, the critical exponents will be functions of the parameter δ.

1. Leading order approximation: After integrating numerically (5.27) we find an enclosed area of globally safe trajectories emanating from the UV fixed point attracted towards C' and finally repelled to fixed point D, the line $C'D$ here is an attractor as

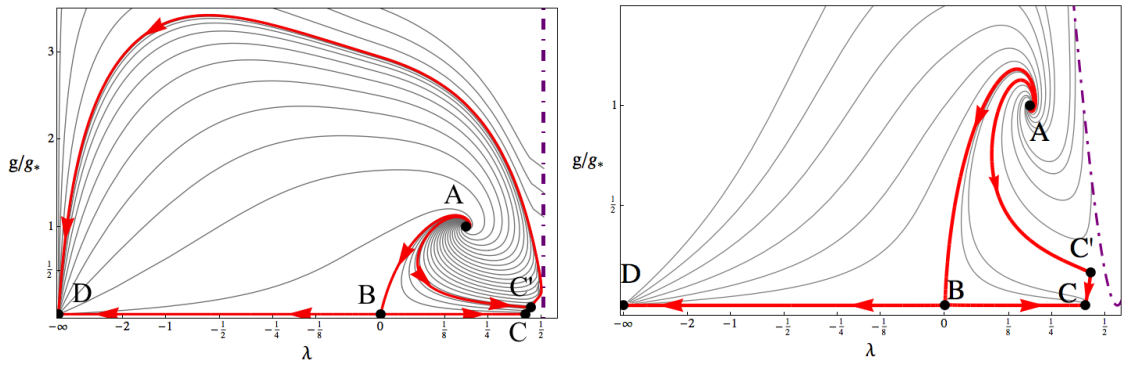

Figure 5.4: Global flows for the leading order approximation (left, $\delta = 1/80$) and Hartree-Fock resummation (right, $\delta = 2/25$). The red lines are the different separatrices, meanwhile dot-dashed purple line are the boundaries of the system in each case.

the line CD explained at the end of subsection 5.3.3. We also find another globally safe section of the phase space where all trajectories finish at fixed point C when $k \to 0$, and where only positive λ is admitted.

In this case the critical exponents are:

- FP A:

$$Re[\theta] = 1.4887 + 12.6979\delta - 51.0579\delta^2 + 1433.87\delta^3, \tag{5.46}$$

$$Im[\theta] = 2.6820 - 13.8357\delta - 89.4567\delta^2 - 1757.48\delta^3. \tag{5.47}$$

- FP B:

$$\theta_1 = -2 \tag{5.48}$$

$$\theta_2 = 2 - \frac{3}{2}\delta - \frac{961}{12}\delta^2. \tag{5.49}$$

- FP C:

$$\theta_1 = -\frac{8}{5} - \sqrt{\frac{24}{5}}\delta^{-1/2} + \frac{941}{10\sqrt{30}}\delta^{1/2} + \frac{121}{3}\delta + \frac{616673}{480\sqrt{30}}\delta^{3/2}, \tag{5.50}$$

$$\theta_2 = -2. \tag{5.51}$$

- FP C':

$$\theta_1 = 4 - \frac{28}{\sqrt{15}}\delta^{1/2} + \frac{132}{5}\delta - \frac{4739}{120\sqrt{15}}\delta^{3/2}, \tag{5.52}$$

$$\theta_2 = -\frac{12}{5} - \frac{4\sqrt{3}}{\sqrt{5}}\delta^{-1/2} + \frac{659\sqrt{3}}{20\sqrt{5}}\delta^{1/2} + \frac{7103}{300}\delta - \frac{11248859}{2400\sqrt{15}}\delta^{3/2}. \tag{5.53}$$

2. Hartree-Fock resummation: In this case a section of the phase space where trajectories, either finish at fixed point D or become singular on the boundary of the flow. A second section is found, this is a basin of attraction where all trajectories end at C when $k \to 0$. In this basin of attraction only positive values of the cosmological constant are allowed. Comparing this case with the case $\delta_c = 0$, we note that trajectories type Ia and type IIIa are still found here, but in addition we find two new separatrices.

   The δ dependence of the universal eigenvalues is as follows:

   - FP A:

$$Re[\theta] = \frac{5}{3} + \frac{20}{9}\delta + \frac{12736}{243}\delta^2 + \cdots, \tag{5.54}$$

$$Im[\theta] = \frac{\sqrt{167}}{3} + \frac{1124}{9\sqrt{167}}\delta - \frac{28525760}{40581\sqrt{167}}\delta^2 + \cdots. \tag{5.55}$$

   - FP B:

$$\theta_1 = 2 + 4\delta - 8\delta^2 + \cdots, \tag{5.56}$$

$$\theta_2 = -2. \tag{5.57}$$

   - FP C:

$$\theta_1 = -\frac{8}{3} - \frac{4}{\sqrt{3}}\delta^{-1/2} - \frac{14}{3\sqrt{3}}\delta^{1/2} + 8\delta^2 + \cdots, \tag{5.58}$$

$$\theta_2 = -2. \tag{5.59}$$

   - FP C':

$$\theta_1 = -\frac{8}{3} - 2\sqrt{2}\delta^{-1/2} + \frac{40\sqrt{2}}{9}\delta^{1/2} - \frac{256}{9}\delta + \cdots, \tag{5.60}$$

$$\theta_2 = 4 - \frac{16\sqrt{2}}{3}\delta^{1/2} + \frac{80}{3}\delta - \frac{160\sqrt{2}}{3}\delta^{3/2} + \cdots. \tag{5.61}$$

5.5.1 Gaussian fixed point and UV fixed point

One of the goals of this work was to unfold the degenerate fixed point C while at the same time the structure of the UV and Gaussian fixed points was preserved. From the expressions for the critical exponents and fixed points we see that this is the case. However, the critical exponents for the UVFP and GFP are modified by a factor of order $\mathcal{O}(\delta)$. In spite of this, we will choose as a physical just the case for very small values of δ, and then, the effects on the GFP and UVFP are negligible. Apart from this subtlety, the analysis of the previous section is valid here as well.

5.5.2 Infrared fixed points C and C'

First we note that one of the critical exponents of point C is exactly -2 (attractive IR direction) with no δ dependence; a similar result was reported in [13] for a hypothetical IR fixed point, however, in that work the other critical exponent was found to be margina, i.e. $\theta_2 = 0$. Our case is compeltely opposite to this result because θ_2 is of order $1/\sqrt{\delta}$, making C completely IR attractive. For C' we find a similar result as for C, the first eigenvalue is order $\sqrt{\delta}$ while the second is order $1/\sqrt{\delta}$. These mean that for small δ there is a direction in which trajectories are pulled strongly towards their IR values.

Now we compute the normalised eigenvectors in order to understand which direction is the one for which trajectories are attracted with "strength" $1/\sqrt{\delta}$. We will restrict the following analysis to the HF case.

1. For C:

$$V_1 = (1, 0), \tag{5.62}$$

$$V_2 = \left(\frac{\sqrt{3}}{\sqrt{\delta}} - \frac{9}{2} + \frac{19\sqrt{\delta}}{4\sqrt{3}} + \frac{313\delta}{8}, 1\right). \tag{5.63}$$

2. For C':

$$V_1 = \left(-\frac{9}{2\delta} + 10 - \frac{9\sqrt{2}}{\sqrt{\delta}}, 1\right)., \tag{5.64}$$

$$V_2 = \left(\frac{3}{\sqrt{2}\sqrt{\delta}} - 10 + \frac{58\sqrt{2}\sqrt{\delta}}{3}, 1\right). \tag{5.65}$$

Now it is clear that trajectories are pulled strongly in the direction perpendicular to λ for both fixed points. To understand even further this we can compute the solution of the linearised system taking into account only the leading order in δ for the fixed points, critical exponents and eigenvalues.

Fixed point C

$$\begin{aligned}\lambda(k) =& \frac{1}{2} - \frac{1}{\sqrt{3}}\delta^{1/2} + \left[\lambda_0 - \frac{1}{2} + \frac{1}{\sqrt{3}}\delta^{1/2} - g_0\sqrt{3}\delta^{-1/2}\right]\left(\frac{k}{k_0}\right)^{\frac{4}{\sqrt{3}}\delta^{-1/2}} + \\ &+ g_0\sqrt{3}\delta^{-1/2}\left(\frac{k}{k_0}\right)^2,\end{aligned} \tag{5.66}$$

$$g(k) = g_0\left(\frac{k}{k_0}\right)^2. \tag{5.67}$$

Where $\lambda_0 = \lambda(k_0)$, and $g_0 = g(k_0) > 0$. Since the separation of C and C' is of order $\delta^{1/2}/10$, then $g_0 < \delta^{1/2}/10$. Then, the combination $g_0\delta^{-1/2}\sqrt{3}$ appearing in (5.66) is at

most order $\sqrt{3}/10$. Now, since the second term of (5.66) is proportional to k^{θ_1}, this means that it is strongly suppressed for small values of δ, and hence, the dominant terms of (5.66) are the first and third ones. Now, from (5.67) by solving (k/k_0) in terms of $g(k)$ and substituting this value in (5.66), and avoiding the second term we get

$$\lambda(k) = \lambda^*_C + \sqrt{3}\delta^{-1/2} g(k) \tag{5.68}$$

this is the equation for the separatrix connecting C and C'. Clearly, the slope in the phase space connecting these fixed points is $\sqrt{3}\delta^{-1/2}$. Let us note that we didn't need to fix the initial conditions for λ_0 to get this result, then the line CC' acts like an attractor. From (5.66) we conclude also, that trajectories close to CC' approach the fixed point C with strength 2, i.e. much more slowly than they approach CC' perpendicularly to λ.

The dimensionful Newton's coupling and the dimensionful cosmological constant are (setting $k_0 = 1$)

$$G(k) = g_0, \tag{5.69}$$

$$\Lambda(k) = \lambda^*_C k^2 + g_0\sqrt{3}\delta^{-1/2}k^4 + \mathcal{O}(k^{\theta_1}+2), \tag{5.70}$$

Since the cosmological constant now is proportional to k^2, then it means that the fixed point C determines the value of the cosmological constant in the deep infrared regime of the theory. Moreover, the value for Newton's constant will be a constant value.

Fixed point C'

$$\lambda(k) = \lambda^*_{C'} - c_0\frac{9}{2\delta}\left(\frac{k_0}{k}\right)^{2\sqrt{2}\delta^{1/2}} + c_1\frac{3}{\sqrt{2}}\delta^{-1/2}\left(\frac{k}{k_0}\right)^{4-\mathcal{O}(\delta^{1/2})}, \tag{5.71}$$

$$g(k) = g^* + c_0\left(\frac{k_0}{k}\right)^{2\sqrt{2}\delta^{1/2}} + c_1\left(\frac{k}{k_0}\right)^{4-\mathcal{O}(\delta^{1/2})}. \tag{5.72}$$

For $k < k_0$ the second terms of (5.71), and (5.72) dominate. In this case if we neglect the second terms we get what we will call trajectories **type Ic**

$$\begin{aligned} g(k) &= g^*_{C'} + (\lambda^*_{C'} - \lambda(k))\frac{2}{9}\delta \\ &= \frac{1}{18}\delta + (\frac{1}{2} - \frac{\sqrt{2}}{3}\delta^{1/2} - \lambda(k))\frac{2}{9}\delta \end{aligned} \tag{5.73}$$

this is the equation for the separatrix joining A and C' near C', and since it does not depend on the sign of either c_0 or c_1, then it is valid for $\lambda > \lambda^*_{C'}$. Now we have three cases depending on the sign of c_0:

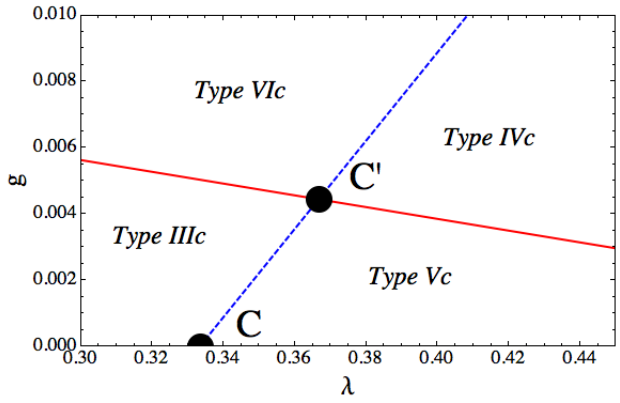

Figure 5.5: Classification of the different types of trajectories near the fixed point C') (see text).

- **Type IIc**: For this we solve $(k/k_0)^{\theta_2}$ from (5.71) in terms of $\lambda(k)$ and substitute the result in (5.72), then we get the separatrix connecting C and C',

$$g(k) = (\lambda(k) - \lambda^*_{C'})\frac{\sqrt{2}}{3}\delta^{1/2} + g^*, \tag{5.74}$$

  and similar to the separatrix type Ic, this result does not depend on the sign of c_1, and then it is valid for values $\lambda(k) > \lambda^*_{C'}$. Hence, the separatrices type Ic and IIc divide the phase space around C' in 4 quadrants.

- **Type IIIc**, $a^2 = c_1 < 0$: These trajectories are the asymptotic safe ones connecting the UVFP with the fixed point C.

- **Type Ivc**, $b^2 = c_1 > 0$: These correspond to trajectories approaching C' from the right and ending in the boundary of the system above C'.

Now, if we go back to (5.71) and (5.72), and neglect the last terms, then we have two cases for c_0

- **Type Vc**, $A^2 = c_0 < 0$: Trajectories in this case approach C' from the right and finishing at $k \to 0$ in fixed point C.

- **Type VIc**, $B^2 = c_0 > 0$: We find two kind of trajectories in this type, all of them start at the UVFP, then they are well defined in the limit $k \to \infty$, after that they either end in the singular boundary, or end at D with a well defined limit $k \to 0$ with $\lambda \to -\infty$.

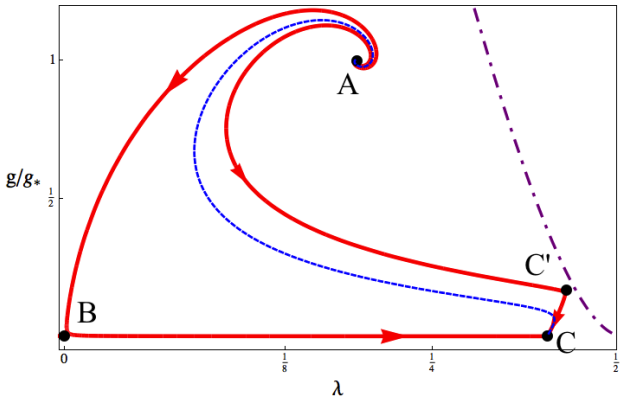

Figure 5.6: Schematic trajectory of the δ-modified system ($\delta = 2/25$) (see text).

All these type of trajectories are depicted in figure 5.5. Also, we note that through the analysis of the vicinity of fixed point C' we have characterised all the possible trajectories of the system.

The description of a typical trajectory of type IIIc is as follows (Figure 5.6):

- Starting at $k >> M_{Pl}$ in A, the trajectory is repelled towards the fixed point B
- It remains some time in the vicinity of B, i.e., classical gravity sets in.
- After the classical regime, it gets strongly attracted towards C'.
- Then, it spends some time in the vicinity of C' in a strongly coupled phase, and it is slowly repelled towards C.
- Finally, it is attracted to C with strength 2 and ends with $k = 0$, $\Lambda_k^* = 0$, and $G_k^* > G_N$.

Due to the δ^{-1} dependence in θ_2, all trajectories leaving B will be dragged rapidly towards C and C' .The presence of C' causes a very steep grow in the value of Newton's running coupling, driving an accelerated universe in the very deep IR scales, as was noted in [12] (Figure 5.7). Finally, in Figure 5.7, we plot the value of G_k for a typical trajectory in the δ-modified system, and we show its different behaviours around the vicinity of the different fixed points.

5.6 Gauge independence.

As the introduction of the δ parameter is not fundamental, we should worry about the gauge dependence of the fixed points and critical exponents. Even more, we should worry

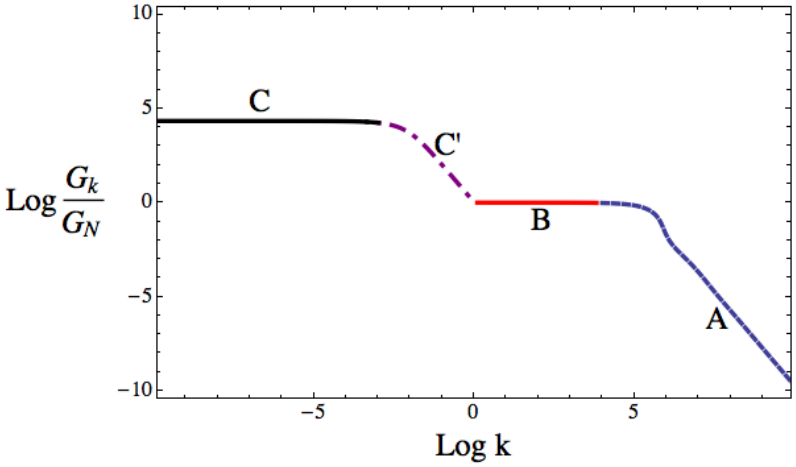

Figure 5.7: Log plot of typical behaviour for the running Newton's coupling G_k over Newton's constant as measured at terrestrial scales. Full lines correspond to classical regimes for terrestrial distances (red, fixed point B) and cosmological distances (black, fixed point C). Dashed blue line and dot-dashed purple line correspond to strong coupling behaviour, in the UV (fixed point A) and IR (fixed point C'), respectively ($\delta = 1/100000$).

about the stability of the results in the HF resumption case, as we only choose the limit $\alpha \to \infty$ in order to simply the equations. With this in mind, we repeated the computations for $0 \leq \alpha \leq 1$, which is a better choice from the physical point of view.

The gauge fixing parameter α enters in the renormalisation group equations in the form $1/(1-2\alpha\lambda)$, hence, imposing new boundaries to the flow for $\alpha > 1$. In Table 5.1 we show the mean value and the standard deviation for the different fixed points and their corresponding critical exponents for $0 \leq \alpha \leq 1$. We observe that, the relative standard deviations of the different quantities range from 0.22% for $\lambda_{C'}$ to 9.06% for $Re(\theta_A)$ in the leading order approximation case, and from 0.06% for $\lambda_{C'}$ to 6.54% for g_A, i.e., there is a low variability in α.

5.7 Conclusions

One of the consequences of the mass dimension of the cosmological constant coupling is that near the GFP it acts as an IR repulsive operator, hence leading to the IR fixed point model [12], which is a viable alternative to the best-fit FRW model in reproducing the supernova and radio source data. We have shown in this work that for two different approximations (Hartree-Fock resummation and a leading order) the problem in the boundary point ($\lambda = 1/2, g = 0$) in the IR of Einstein-Hilbert theory can be seen as a degeneracy of fixed points. Also, to study the nature of these fixed points we have taken

	λ_A	g_A	θ_A^{Re}	θ_A^{Im}	λ_C	g_C	θ_C^1	θ_C^2	$\lambda_{C'}$	$g_{C'}$	$\theta_{C'}^1$	$\theta_{C'}^2$
$\langle X_{LO}\rangle$	0.1972	0.9124	1.3943	2.5287	0.4316	0	-27.0797	-2	0.4513	0.0424	3.5088	-38.1576
$\langle \Delta X_{LO}\rangle$	0.0040	0.0053	0.1264	0.0355	0.0010	0	0.3064	0	0.001	0.0003	0.0338	0.2687
$\langle X_{HF}\rangle$	0.1651	0.8362	1.909	2.5061	0.4635	0	-31.7670	-2	0.4692	0.0126	3.5554	-38.1802
$\langle \Delta X_{HF}\rangle$	0.0018	0.0547	0.0926	0.0752	0.0003	0	0.2688	0	0.0003	0.0001	0.0319	0.3591

Table 5.1: Mean value and standard deviation for the fixed points and corresponding critical exponents for $\delta = 1/300$ for HF, and $\delta = 1/150$ for OL with $0 \leq \alpha \leq 1$. The subscripts LO and HT stand for leading order approximation and Hartree-Fock resummation.

an appropriate perturbation of the system by modifying the beta functions of the theory, giving rise to two new physically relevant infrared fixed points, whilst we maintain the UV fixed point and gaussian in the picture. First, the nature of the non-perturbative infrared point C' is the same as the nature of the conjectured fixed point in [82] and [12] which drives an accelerated expanding of the late Universe. Second, the fixed point C is located at $g* = 0$ and two infrared attractive directions, hence, trajectories ending here will describe classical gravity for some value of Newton's constant greater than the one measured at terrestrial scales. Within this picture the hypothetical infrared fixed point first suggested in [82] corresponds to our fixed point C'. Another infrared fixed point was found in [61] after including the non-local term $ln(R)$ to the Einstein-Hilbert action, the only drawback there is that the UVFP developed by the system is situated at $g < 0$, and then, the connection with UV physics is no reliable [80].

It is believed that Einstein-Hilbert theory is just the first term in a derivative expansion going from the low to the high-energy regime. In general, higher order quantum corrections to gravity can be found in the literature (e.g. [38]). However, this high derivative theories are expected to be successful at small distances, hence, one can reinterpret our results in the sense that our approach allow us to build a model for the deep IR expecting that the full theory would lift the degeneracy without the introduction of the small parameter δ. By now interacting fixed points have been found along several directions.

For example, in [17, 16] authors found globally safe trajectories by studying the renormalisation group equations arising from the graviton propagator. Another infrared fixed point was found in [28] in the grounds of a fully differmorphism-invariant RG group approach. And finally, in [70] a coupling redefinition similar to (5.26) helps to extract some information about the infrared fixed point.

More work will be required to firmly establish their existence, and to evaluate its impact for cosmology.

Chapter 6

Conclusions

In this thesis we have tried to answer open questions within the asymptotic safety program to quantise gravity in a non-perturbative approach [91, 80]. The philosophy behind was to provide insights for these questions without getting too involved with severe complexities to describe our systems (to get more from less). As the main goal is to get the UV completion for gravity, the fundamental and stable picture that we require all the time, is for the renormalisation group equations to drive the system into an interacting fixed point provided with a finite and positive number of relevant operators.

In higher order theories such as $f(R)$, one of the problems is to find a scaling solution for the functions f, and whether such solution is valid for the entire domain of background Ricci curvature. The latter point arises since the appearance of poles in the equations at fixed curvature is found to be related to the addition of redundant operators into the theory [27, 26]. Another open question in this context is whether the UV degeneracy of the critical exponents found in the vast majority of the literature can lifted for more general truncations. In chapter 3, we have exploited spectral sums without any further approximations. Most notably, we also reproduced the results from heat kernels at small curvature. Our approach therefore offers malleable ways of going beyond the heat kernel and to explore the impact from large Ricci curvature onto the RG evolution of couplings. Next, we defined a new way to project the renormalisation group equations. This idea will allow us to interpolate (and control the background) between the usual way to project the flow about $R = 0$ and the one performed about the equations of motion, i.e. $R = 4\Lambda$, this is done by introducing a interpolating parameter c, such that $R = 4c\Lambda$. Then, we learnt first that a fixed point solution can always be found for different values of c, then due to the $1/c$ asymptotic behaviour of λ^* we found that effectively we explored the values of the curvature $0 < R < 2$. Secondly, by varying c the critical exponents split from a com-

plex conjugated pair into two real independent components, and furthermore, the critical exponent present a minimum around the on shell condition $c = 1$. Stated differently, our findings suggest that complex critical exponents are an artefact of expanding the underlying renormalisation group flow around vanishing curvature, rather than around solutions to its own equation of motion. For more studies finding real critical exponents we refer to [8], where a scaling solution is found for the asymptotic limit $R \to \infty$; [87] for studies of gravity with matter; [23] for Einstein-Hilbert in three dimensions; [10, 11] for inclusion of fourth order derivative couplings; [33] for unimodular gravity. Future work in this direction corresponds to improving our background field technique by using the exponential parametrisation [35] rather than the linear splitting (3.1), and with these tools to perform a systematic study for higher order theories.

Chapter (3) corresponds to the study of the deep UV regime of gravity. Effective theories rely on the input of initial conditions in order to make predictions, and since most of the physical information in gravity comes from the small energy world, then we should be concerned about the connection of the deep UV with the classical regime. With this motivation in chapter 4 first we study the phase space of the R^2 theory, where we find a very large value for the critical exponent corresponding to the square of the Ricci curvature , which in turn causes that the flow near the ultraviolet fixed point behaves effectively as in the Einstein-Hilbert case. Then with the help of what was called non-perturbative boundary conditions, we computed our RG equations,. This condition entails we introduced as initial conditions the best known values (the value found at order R^{70} [87]) for the fixed point for the couplings of the operators R^3 and R^4, this gives non-dynamical background information to the system about higher order operators. Even though we did not find a Gaussian fixed point to connect the non-Gaussian fixed point, we can always find a long classical regime for the cosmological constant and Newton's coupling.

Finally, in the last chapter 5, the question of whether RG equations describe the deep infrared physics for gravity is addressed. Here, in the Einstein-Hilbert theory we showed that on top of the divergent IR point $(\lambda, g) = (1/2, 0)$ there is a degenerated true fixed point of the theory. Then, using tools from dynamical systems we successfully lifted the degeneracy while the local behaviour of the ultraviolet and Gaussian fixed points remained parametrically untouched. Two new infrared fixed points were found: an interacting one, with one infrared attractive and one infrared repulsive directions, and a new fully attractive classical fix point. Finally, we found a set of trajectories as the possible true reliable

physical ones. It would be interesting to check whether one of this trajectories matches with the data available in the very deep infrared at cosmological scales. If it happens that there is a single trajectory describing our universe, and the cosmological constant is the one responsible for the late accelerated expansion of the universe, then this kind of models could, speculatively predict a final stage of the universe as a non-accelerating one where we ran out of dark energy, i.e. where the cosmological coupling vanishes. This is the final stage of this work and correspond to the deep IR regime of gravity.

As final statement it will be interesting to see whether the ideas and techniques developed here can be put forward for more advanced studies of quantum gravity in the future.

Bibliography

[1] L.F. Abbott. The background field method beyond one loop. *Nuclear Physics B*, 185(1):189 – 203, 1981. 14

[2] Stephen L. Adler. Einstein gravity as a symmetry-breaking effect in quantum field theory. *Rev. Mod. Phys.*, 54:729–766, Jul 1982. 14

[3] Toshiaki Aida and Yoshihisa Kitazawa. Two loop prediction for scaling exponents in (2+epsilon)-dimensional quantum gravity. *Nucl. Phys.*, B491:427–460, 1997. 6

[4] Jan Ambjørn, S. Jordan, J. Jurkiewicz, and R. Loll. Second-order phase transition in causal dynamical triangulations. *Phys. Rev. Lett.*, 107:211303, Nov 2011. 51

[5] D.K Arrowsmith. The singularity xt6y. *Journal of Differential Equations*, 34(2):153 – 166, 1979. 59

[6] C. Bagnuls and C. Bervillier. Exact renormalization group equations. An Introductory review. *Phys. Rept.*, 348:91, 2001. 4

[7] Dario Benedetti. Asymptotic safety goes on shell. *New J.Phys.*, 14:015005, 2012. 13, 17, 26, 36

[8] Dario Benedetti. On the number of relevant operators in asymptotically safe gravity. *Europhys.Lett.*, 102:20007, 2013. 1, 40, 71

[9] Dario Benedetti and Francesco Caravelli. The Local potential approximation in quantum gravity. *JHEP*, 1206:017, 2012. 1, 12, 13, 26, 39, 40

[10] Dario Benedetti, Pedro F. Machado, and Frank Saueressig. Asymptotic safety in higher-derivative gravity. *Mod. Phys. Lett.*, A24:2233–2241, 2009. 71

[11] Dario Benedetti, Pedro F. Machado, and Frank Saueressig. Taming perturbative divergences in asymptotically safe gravity. *Nucl. Phys.*, B824:168–191, 2010. 71

[12] Eloisa Bentivegna, Alfio Bonanno, and Martin Reuter. Confronting the IR fixed point cosmology with high redshift supernova data. *JCAP*, 0401:001, 2004. 52, 67, 68, 69

[13] Alfio Bonanno, Giampiero Esposito, Claudio Rubano, and Paolo Scudellaro. The Accelerated expansion of the Universe as a crossover phenomenon. *Class.Quant.Grav.*, 23:3103–3110, 2006. 64

[14] Jens Braun, Holger Gies, and Daniel D. Scherer. Asymptotic safety: a simple example. *Phys. Rev.*, D83:085012, 2011. 6

[15] I.L. Buchbinder, S. Odintsov, and L. Shapiro. *Effective Action in Quantum Gravity*. Taylor & Francis, 1992. 18

[16] Nicolai Christiansen, Benjamin Knorr, Jan M. Pawlowski, and Andreas Rodigast. Global Flows in Quantum Gravity. 2014. 69

[17] Nicolai Christiansen, Daniel F. Litim, Jan M. Pawlowski, and Andreas Rodigast. Fixed points and infrared completion of quantum gravity. *Phys.Lett.*, B728:114–117, 2014. 52, 69

[18] Alessandro Codello and Giulio DOdorico. Scaling and Renormalization in two dimensional Quantum Gravity. *Phys. Rev.*, D92(2):024026, 2015. 6

[19] Alessandro Codello, Roberto Percacci, and Christoph Rahmede. Ultraviolet properties of f(R)-gravity. *Int. J. Mod. Phys.*, A23:143–150, 2008. 1, 40, 46, 48

[20] Alessandro Codello, Roberto Percacci, and Christoph Rahmede. Investigating the Ultraviolet Properties of Gravity with a Wilsonian Renormalization Group Equation. *Annals Phys.*, 324:414–469, 2009. 1, 12, 19, 26, 40

[21] Edmund J. Copeland, Christoph Rahmede, and Ippocratis D. Saltas. Asymptotically Safe Starobinsky Inflation. *Phys. Rev.*, D91(10):103530, 2015. 1

[22] Antonio De Felice and Shinji Tsujikawa. f(R) theories. *Living Rev. Rel.*, 13:3, 2010. 49

[23] Maximilian Demmel, Frank Saueressig, and Omar Zanusso. Fixed-Functionals of three-dimensional Quantum Einstein Gravity. *JHEP*, 11:131, 2012. 71

[24] Maximilian Demmel, Frank Saueressig, and Omar Zanusso. A proper fixed functional for four-dimensional Quantum Einstein Gravity. *JHEP*, 08:113, 2015. 40

[25] B. S. DeWitt. *Quantum gravity: the new synthesis.*, pages 723–725. Cambridge Unive. Press, 1979. 81

[26] Juergen A. Dietz and Tim R. Morris. Asymptotic safety in the f(R) approximation. *JHEP*, 01:108, 2013. 1, 40, 70

[27] Juergen A. Dietz and Tim R. Morris. Redundant operators in the exact renormalisation group and in the f(R) approximation to asymptotic safety. *JHEP*, 07:064, 2013. 40, 70

[28] Ivan Donkin and Jan M. Pawlowski. The phase diagram of quantum gravity from diffeomorphism-invariant RG-flows. 2012. 52, 69

[29] Pietro Don, Astrid Eichhorn, and Roberto Percacci. Matter matters in asymptotically safe quantum gravity. *Phys. Rev.*, D89(8):084035, 2014. 1

[30] Djamel Dou and Roberto Percacci. The running gravitational couplings. *Class.Quant.Grav.*, 15:3449–3468, 1998. 1, 12, 26

[31] Freddy Dumortier. Singularities of vector fields on the plane. *Journal of Differential Equations*, 23(1):53 – 106, 1977. 59

[32] E. Gonzalez-Olivares E. Saez. Dynamics of a predator-prey model. *SIAM Journal on Applied Mathematics*, 59(5):1867–1878, 1999. 59

[33] Astrid Eichhorn. The Renormalization Group flow of unimodular f(R) gravity. *JHEP*, 04:096, 2015. 1, 71

[34] K. Falls. Asymptotic safety and the cosmological constant. 2014. 24, 26, 34, 36

[35] K. Falls. On the renormalisation of Newton's constant. *Phys. Rev.*, D92:124057, 2015. 14, 36, 71

[36] K. Falls, Daniel F. Litim, Konstantinos Nikolakopoulos, and Christoph Rahmede. Further evidence for asymptotic safety of quantum gravity. 2014. 12, 13, 37, 39, 40, 41, 51, 55

[37] K. Falls, Daniel F. Litim, and Aarti Raghuraman. Black Holes and Asymptotically Safe Gravity. *Int. J. Mod. Phys.*, A27:1250019, 2012. 1

[38] K. Falls, D.F. Litim, K. Nikolakopoulos, and C. Rahmede. A bootstrap towards asymptotic safety. 2013. 1, 55, 69

[39] Sarah Folkerts, Daniel F. Litim, and Jan M. Pawlowski. Asymptotic freedom of Yang-Mills theory with gravity. *Phys. Lett.*, B709:234–241, 2012. 1

[40] E.S. Fradkin and A.A. Tseytlin. Renormalizable asymptotically free quantum theory of gravity. *Nuclear Physics B*, 201(3):469 – 491, 1982. 18

[41] Filipe Freire, Daniel F. Litim, and Jan M. Pawlowski. Gauge invariance and background field formalism in the exact renormalization group. *Phys.Lett.*, B495:256–262, 2000. 10

[42] K. Gawedzki and A. Kupiainen. RENORMALIZING THE NONRENORMALIZABLE. *Phys. Rev. Lett.*, 55:363–365, 1985. 6

[43] Murray Gell-Mann and F. E. Low. Quantum electrodynamics at small distances. *Phys. Rev.*, 95:1300–1312, 1954. 6

[44] Marc H. Goroff, Augusto Sagnotti, and Augusto Sagnotti. Quantum gravity at two loops. *Physics Letters B*, 160(13):81 – 86, 1985. 5

[45] David J. Gross and Frank Wilczek. Ultraviolet Behavior of Nonabelian Gauge Theories. *Phys. Rev. Lett.*, 30:1343–1346, 1973. 5

[46] John Guckenheimer and Philip Holmes. *Nonlinear oscillations, dynamical systems, and bifurcations of vector fields.* Applied mathematical sciences. Springer, New York, 2002. 60

[47] Herbert W. Hamber. Gravitational scaling dimensions. *Phys. Rev. D*, 61:124008, May 2000. 36, 51

[48] Falls K. *Asymptotic safety and black holes.* PhD thesis, University of Sussex, May 2013. 39, 40, 41

[49] Hikaru Kawai, Yoshihisa Kitazawa, and Masao Ninomiya. Ultraviolet stable fixed point and scaling relations in (2+epsilon)-dimensional quantum gravity. *Nucl. Phys.*, B404:684–716, 1993. 6

[50] O. Lauscher and M. Reuter. Flow equation of quantum Einstein gravity in a higher derivative truncation. *Phys. Rev.*, D66:025026, 2002. 2, 4, 12, 26, 43, 46

[51] O. Lauscher and M. Reuter. Ultraviolet fixed point and generalized flow equation of quantum gravity. *Phys.Rev.*, D65:025013, 2002. 1, 4, 9, 12, 27, 43, 49, 53, 55, 86

[52] Daniel Litim and Alejandro Satz. Limit cycles and quantum gravity. 2012. 53, 57

[53] Daniel F. Litim. Optimization of the exact renormalization group. *Phys.Lett.*, B486:92–99, 2000. 2, 22, 40, 53, 90

[54] Daniel F. Litim. Optimized renormalization group flows. *Phys.Rev.*, D64:105007, 2001. 2, 22, 40, 53, 90

[55] Daniel F. Litim. Fixed Points of Quantum Gravity and the Renormalisation Group. *PoS*, QG-Ph:024, 2007. 1, 54, 55

[56] Daniel F. Litim. Renormalisation group and the Planck scale. *Phil.Trans.Roy.Soc.Lond.*, A369:2759–2778, 2011. 55

[57] Daniel F. Litim, Matin Mojaza, and Francesco Sannino. Vacuum stability of asymptotically safe gauge-Yukawa theories. 2015. 6

[58] Daniel F. Litim and Tilman Plehn. Virtual gravitons at the LHC. In *SUSY 2007 proceedings, 15th International Conference on Supersymmetry and Unification of Fundamental Interactions, July 26 - August 1, 2007, Karlsruhe, Germany*, 2007. 1

[59] Daniel F. Litim and Tilman Plehn. Signatures of gravitational fixed points at the LHC. *Phys. Rev. Lett.*, 100:131301, 2008. 1

[60] Daniel F. Litim and Francesco Sannino. Asymptotic safety guaranteed. *JHEP*, 12:178, 2014. 6

[61] Pedro F. Machado and Frank Saueressig. On the renormalization group flow of f(R)-gravity. *Phys.Rev.*, D77:124045, 2008. 1, 12, 26, 40, 46, 48, 52, 69

[62] Elisa Manrique and Martin Reuter. Bimetric Truncations for Quantum Einstein Gravity and Asymptotic Safety. *Annals Phys.*, 325:785–815, 2010. 12

[63] Elisa Manrique, Martin Reuter, and Frank Saueressig. Bimetric Renormalization Group Flows in Quantum Einstein Gravity. *Annals Phys.*, 326:463–485, 2011. 12

[64] Pawel O. Mazur and Emil Mottola. ABSENCE OF PHASE IN THE SUM OVER SPHERES. 1989. 9, 14, 20, 81, 84

[65] Pawel O. Mazur and Emil Mottola. The path integral measure, conformal factor problem and stability of the ground state of quantum gravity. *Nuclear Physics B*, 341(1):187 – 212, 1990. 9, 14, 20, 81

[66] Charles W. Misner. Quantum cosmology. i. *Phys. Rev.*, 186:1319–1327, Oct 1969. 57

[67] Tim R. Morris. The Exact renormalization group and approximate solutions. *Int. J. Mod. Phys.*, A9:2411–2450, 1994. 4

[68] Emil Mottola. Functional integration over geometries. *J.Math.Phys.*, 36:2470–2511, 1995. 9, 14, 81

[69] S. Nagy, B. Fazekas, L. Juhasz, and K. Sailer. Critical exponents in quantum Einstein gravity. 2013. 54

[70] S. Nagy, J. Krizsan, and K. Sailer. Infrared fixed point in quantum Einstein gravity. *JHEP*, 1207:102, 2012. 52, 69

[71] Konstantinos Nikolakopoulos. *Quantum gravity and the renormalisation group: theoretical advances and applications*. PhD thesis, University of Sussex, November 2013. 39

[72] Andreas Nink. Field Parametrization Dependence in Asymptotically Safe Quantum Gravity. *Phys. Rev.*, D91(4):044030, 2015. 6

[73] Nobuyoshi Ohta. Beta Function and Asymptotic Safety in Three-dimensional Higher Derivative Gravity. *Class. Quant. Grav.*, 29:205012, 2012. 26

[74] Nobuyoshi Ohta, Roberto Percacci, and Gian Paolo Vacca. Renormalization Group Equation and scaling solutions for f(R) gravity in exponential parametrization. 2015. 1, 40, 48

[75] Roberto Percacci and Daniele Perini. Asymptotic safety of gravity coupled to matter. *Phys. Rev.*, D68:044018, 2003. 1

[76] Michael Edward Peskin and Daniel V. Schroeder. *An introduction to quantum field theory*. Advanced book program. Westview Press Reading (Mass.), Boulder (Colo.), 1995. Autre tirage : 1997. 4

[77] Joseph Polchinski. Renormalization and effective lagrangians. *Nuclear Physics B*, 231(2):269 – 295, 1984. 4

[78] H. David Politzer. Reliable Perturbative Results for Strong Interactions? *Phys. Rev. Lett.*, 30:1346–1349, 1973. 5

[79] Stefan Rechenberger and Frank Saueressig. The R^2 phase-diagram of QEG and its spectral dimension. *Phys. Rev.*, D86:024018, 2012. 2, 45, 46

[80] M. Reuter. Nonperturbative evolution equation for quantum gravity. *Phys.Rev.*, D57:971–985, 1998. 1, 4, 12, 26, 51, 55, 69, 70

[81] M. Reuter and Frank Saueressig. Renormalization group flow of quantum gravity in the Einstein-Hilbert truncation. *Phys. Rev.*, D65:065016, 2002. 1, 12, 57

[82] M. Reuter and H. Weyer. Quantum gravity at astrophysical distances? *JCAP*, 0412:001, 2004. 1, 52, 58, 69

[83] Martin Reuter and Holger Weyer. Background Independence and Asymptotic Safety in Conformally Reduced Gravity. *Phys. Rev.*, D79:105005, 2009. 57

[84] Mark A. Rubin and Carlos R. Ordonez. EIGENVALUES AND DEGENERACIES FOR n-DIMENSIONAL TENSOR SPHERICAL HARMONICS. 1983. vii, 19, 22

[85] Mark A. Rubin and Carlos R. Ordonez. Symmetric Tensor Eigen Spectrum of the Laplacian on n Spheres. *J.Math.Phys.*, 26:65, 1985. vii, 19, 22

[86] Michael M. Scherer, Holger Gies, and Stefan Rechenberger. An Asymptotic-safety mechanism for chiral Yukawa systems. *Acta Phys. Polon. Supp.*, 2:541, 2009. 6

[87] Jan Schröder. *Aspects of quantum gravity and matter.* PhD thesis, University of Sussex, May 2015. 39, 40, 41, 49, 71

[88] Alexei A. Starobinsky. A New Type of Isotropic Cosmological Models Without Singularity. *Phys. Lett.*, B91:99–102, 1980. 38

[89] S.H. Strogatz. *Nonlinear Dynamics And Chaos.* Studies in nonlinearity. Sarat Book House, 2007. 58

[90] Gerard 't Hooft and M. J. G. Veltman. One loop divergencies in the theory of gravitation. *Annales Poincare Phys. Theor.*, A20:69–94, 1974. 5

[91] Steven Weinberg. *Ultraviolet divergences in quantum theories of gravitation*, pages 790–831. Cambridge Unive. Press, 1979. 1, 5, 51, 70

[92] Christof Wetterich. Exact evolution equation for the effective potential. *Phys.Lett.*, B301:90–94, 1993. 4, 39, 52

[93] Stephen Wiggins. *Introduction to applied nonlinear dynamical systems and chaos.* Texts in applied mathematics. Springer-Verl, New York, Berlin, Paris, 1990. 58, 60

[94] K. G. Wilson and John B. Kogut. The Renormalization group and the epsilon expansion. *Phys. Rept.*, 12:75–200, 1974. 1, 4

[95] Kenneth G. Wilson. The Renormalization Group and Strong Interactions. *Phys. Rev.*, D3:1818, 1971. 5

[96] Kenneth G. Wilson. The Renormalization Group: Critical Phenomena and the Kondo Problem. *Rev. Mod. Phys.*, 47:773, 1975. 1, 4

[97] James W. York. Conformally invariant orthogonal decomposition of symmetric tensors on riemannian manifolds and the initial-value problem of general relativity. *Journal of Mathematical Physics*, 14(4):456–464, 1973. 15

[98] J. Zinn-Justin. *Quantum Field Theory and Critical Phenomena*. International series of monographs on physics. Clarendon Press, 1996. 4

Appendix A

Jacobians for the TT decomposition

Here we will compute the correct functional integral according to [68, 65, 64]. The result here assumes that Minkowski spacetime is the true vacuum of quantum gravity. The analysis starts from a lorentzian formulation to determine the correct euclidean action by analytic continuation.

Classical general relativity is invariant under infinitesimal general coordinate transformations (diffeomorphisms group $Diff(\mathcal{M})$)

$$x^\mu \to x^\mu + \epsilon^\mu(x). \tag{A.1}$$

These symmetry is something we want to preserve in the quantum theory as well, and for that purpose we start defining the inner product in the space of infinitesimal metrics $\delta g_{\mu\nu} \equiv h_{\mu\nu}$ by

$$\langle h, h\rangle_T = \int d^dx\sqrt{-g}h_{\mu\nu}(x)G^{\mu\nu\rho\sigma}h_{\rho\sigma}(x), \tag{A.2}$$

where the subscript T indicates that the product is for tensors. (A.1) on the spacetime manifold corresponds to

$$h_{\mu\nu} \to h_{\mu\nu} + D_\mu\xi_\nu + D_\nu\xi_\mu. \tag{A.3}$$

With this in mind, the measure on the space of metrics must be invariant under (A.1) and (A.3), i.e. G in (A.2) must be a purely local function of the coordinates of the space of metrics $\mathcal{M}$ (without derivatives). The most general metric on $\mathcal{M}$ with this characteristics is of the form

$$G^{\mu\nu\rho\sigma} = \frac{1}{2}(g^{\mu\rho}g^{\nu\sigma} + g^{\mu\sigma}g^{\nu\rho} + Cg^{\mu\nu}g^{\rho\sigma}), \tag{A.4}$$

where C is a constant to determine [25].

Now, we will define the measure of $\mathcal{M}$ by a Gaussian normalisation condition:

$$\int \mathcal{D}h_{\mu\nu} exp(-\frac{i}{2}\langle h,h\rangle)_T = 1. \tag{A.5}$$

To understand the meaning of the constant C, let us decompose the tensor $h_{\mu\nu}$ into its trace-free and trace parts

$$h_{\mu\nu} = h^{TF}_{\mu\nu} + \frac{1}{d} h g_{\mu\nu}, \tag{A.6}$$

with $h = h^{\mu}_{\mu}$. Operating each part with the super metric (A.4), we see first that for the trace-free part $G^{\mu\nu\rho\sigma} h^{TF}_{\mu\nu} = h^{TF\rho\sigma}$ is mapped into itself independently of C. While for the scalar trace mode we have

$$(G^{\mu\nu\rho\sigma})\frac{g_{\mu\nu}}{d} h = (1 + \frac{Cd}{2})\frac{g^{\rho\sigma}}{d} h,$$

and hence it has an eigenvalue dependent on C. This means that for $C > -d/2$, the signature of G in the scalar trace tensor is positive, and negative for $C < -d/2$. If $C = -d/2$, the metric is basically the projector onto the trace-free subspace.

Once the measure for $\mathcal{M}$ is defined, we still have to subtract the infinite gauge orbit volume from it. Let us start with a change of coordinates in the tangent space of $\mathcal{M}$ at $g_{\mu\nu}$:

$$h_{\mu\nu} = h^{\perp}_{\mu\nu} + (L\xi)_{\mu\nu} + (2\sigma + \frac{2}{d} D_\lambda \xi^\lambda) g_{\mu\nu}, \tag{A.7}$$

where L maps vectors into traceless symmetric tensors,

$$(L\xi)_{\mu\nu} \equiv D_\mu \xi_\nu + D_\nu \xi_\mu - \frac{2}{d} D_\lambda \xi^\lambda g_{\mu\nu}. \tag{A.8}$$

$L\xi$ spans all symmetric tensors which are gauge transformations of $h^{TF}_{\mu\nu}$, i.e. the traceless part of $h_{\mu\nu}$. σ and $h^{\perp}_{\mu\nu}$ are the gauge invariant pieces of the trace part and the trace-free part $h^{TF}_{\mu\nu}$ respectively. From here, we choose $h^{\perp}_{\mu\nu}$ to be an orthogonal part to L, with requires $(L^\dagger h^\perp)_\mu = -2D^\nu h^{\perp}_{\mu\nu} = 0$. Also, $h^\perp$ may be required to satisfy an arbitrary gauge condition

$$(F \cdot h^\perp)_\mu = F^\nu h^{\perp}_{\mu\nu} = 0, \tag{A.9}$$

the only condition we require for (A.9) is for the operator $F \circ L$ to be locally invertible in order to find uniquely a solution for ξ.

The scalar part σ is a gauge invariant quantity since we have subtracted from the trace part of $h_{\mu\nu}$ the piece generated by infinitesimal coordinate transformations according to

$$\frac{h}{d} \equiv 2\sigma + \frac{2}{d} D_\mu \xi^\mu \tag{A.10}$$

In order to subtract the infinite gauge orbit volume generated by ξ_μ, we need to find the Jacobian of the transformation to the new field coordinates $(h^\perp, \xi, \sigma)$, i.e.

$$\mathcal{D}h_{\mu\nu} = J_1 \mathcal{D}h^\perp_{\mu\nu} \mathcal{D}\xi_\mu \mathcal{D}\sigma. \tag{A.11}$$

First, we substitute (A.7) into (A.2) to get

$$\langle h, h\rangle_T = \left\langle h^\perp, h^\perp \right\rangle_T + \left\langle \xi, L^\dagger L \xi \right\rangle_V + \frac{2+dC}{2d} \langle h, h\rangle_S \,, \tag{A.12}$$

where we have defined the inner product for vectors and scalars as

$$\langle v, v\rangle_V = \int d^dx \sqrt{-g} v^\mu g_{\mu\nu} v^\nu, \qquad \langle h, h\rangle_S = \int d^dx \sqrt{-g} h^2. \tag{A.13}$$

It is easy to prove the mixing terms in (A.12) vanish simply by using the transverse and traceless properties of $h^\perp$.

The vector operator acting on vector modes appearing in (A.12) is

$$(\tilde{\Delta}_1 \xi)_\mu \equiv (L^\dagger L \xi)_\mu = -2(\delta_\mu{}^\nu D^2 + (1 - \frac{2}{d}) D_\mu D^\nu + R_\mu{}^\nu)\xi_\nu, \tag{A.14}$$

moreover, since $\tilde{\Delta}_1$ is the product of an operator and its adjoint then the Euclidean continuation has no negative modes, and its only zero modes come purely from L itself. These zero modes are conformal Killing vectors (CKV), which span a finite dimensional subspace of $Diff(\mathcal{M})$. For the sphere S^d there are $d(d+1)/2$ Killing vectors corresponding to the infinitesimal generators of $SO(d+1)$.

We will subtract explicitly this finite dimensional subspace from the definition of σ, hence, these scalar gauged modes are by definition not included in the gauge-independent space of fluctuations σ.

Now, we are ready to compute the Jacobian appearing in (A.11). From (A.12) we note that there are no derivatives of $h^\perp$ and σ, then in the same fashion as (A.5) we are free to choose

$$\int \mathcal{D}\sigma \exp(-\frac{i}{2} \langle \sigma, \sigma\rangle) = 1, \qquad \int \mathcal{D}h^\perp_{\mu\nu} \exp(-\frac{i}{2} \left\langle h^\perp, h^\perp \right\rangle) = 1, \tag{A.15}$$

and by choosing

$$\int \mathcal{D}\xi_\mu \exp(-\frac{i}{2} \langle \xi, \xi\rangle) = 1, \tag{A.16}$$

we finally can write (A.11) as

$$\mathcal{D}h_{\mu\nu} = J_1 [Vol(CKV)]^{-1} \mathcal{D}\sigma \mathcal{D}\xi_\mu \mathcal{D}h^\perp_{\mu\nu} \tag{A.17}$$

with the Jacobian being

$$J_1 = [det'(L^\dagger L)]^{1/2} \equiv [det'(\tilde{\Delta}_1)]^{1/2}. \tag{A.18}$$

The prime in the determinant denotes that zero modes of $\tilde{\Delta}_1$ have to be excluded (these modes simply give rise to the volume factor $Vol(CKV)$).

In order to evaluate the Jacobian (A.18) we decompose the space of vectors into transverse and longitudinal vectors according to

$$\xi_\mu = \xi_\mu^\perp + D_\mu \psi, \tag{A.19}$$

Operating $\tilde{\Delta}_1$ into this decomposition and commuting covariant derivatives gives

$$(\tilde{\Delta}_1 \xi^\perp)_\mu = 2(\Delta \xi_\mu^\perp - R_\mu{}^\nu \xi_\nu^\perp) \tag{A.20}$$

$$(\tilde{\Delta}_1 \psi)_\mu = 4 \left[D_\mu \left(1 - \frac{1}{d} \right) \Delta - \frac{1}{d} R_\mu{}^\nu \right] \psi, \tag{A.21}$$

with these expressions we now can rewrite the Jacobian for a maximally symmetric space as [64]

$$J_1 = [det'_V \tilde{\Delta}_1]^{1/2} = \left[det'_{\perp V} (\Delta - \frac{R}{d}) \right]^{1/2} \left[det''_S (\Delta - \frac{R}{d-1}) \right]^{1/2}, \tag{A.22}$$

where $\Delta = -D^2$, and the primes indicate that we need to remove the negative mode and zero mode of $\Delta - R/(d-1)$, and the zero mode of $\Delta - R/d$. The subscripts means that the operators act either on transverse vectors or scalars respectively.

Appendix B

Het Kernel techniques

From (3.32) we have

$$\begin{aligned}\sum_i S_i =& \frac{1}{2}\mathrm{Tr}\left[\frac{\partial_t R_{\perp,k}}{\frac{1}{4}Z_k(\Delta+\frac{2}{d(d-1)}R+2(\frac{d-2}{2d}R-\Lambda_k))+R_{\perp,k}}\right]\\ &+\frac{1}{2}\mathrm{Tr}''\left[\frac{\partial_t R_{\sigma,k}}{\frac{(2-d)(d-1)}{4d^2}Z_k[\Delta-\frac{R}{d-1}+\frac{d}{d-1}(\frac{d-2}{2d}R-\Lambda_k)]+R_{\sigma,k}}\right]\\ &-\frac{1}{2}\mathrm{Tr}''\left[\frac{\partial_t R_{0,k}}{\frac{(d-1)}{d}Z_k[\Delta-\frac{R}{d-1}]+R_{0,k}}\right]\\ &-\frac{1}{2}\mathrm{Tr}'\left[\frac{\partial_t R_{1,k}}{2Z_k[\Delta-\frac{R}{d}]+R_{1,k}}\right]+\frac{1}{2}\left[\frac{\partial_t R_{-,k}}{Z_k a_- + R_{-,k}}\right],\end{aligned} \tag{B.1}$$

with $a_- = \frac{R}{d-1} - \frac{d}{d-1}(\frac{d-2}{2d}R - \Lambda_k)$, $\Delta = -\nabla^2$ and the index i taking the values $0, 1\sigma, 2$. We will choose $R_{i,k}$ such that the denominator of each term has the form $\Delta + \cdots + r_{i,k}$, where $r_{i,k}$ is defined by

$$R_{i,k}(z) = Z_k r_{i,k}(z) \tag{B.2}$$

Each of the traces in (B.1) are functions of the modified laplacian Δ_i, $f(\Delta_i = -\nabla^2 + U_i(R, \Lambda_k))$, with each "potential" term as follow

$$\begin{aligned}U_\perp &= \frac{2}{d(d-1)}R - 2\left(\Lambda_k - \frac{d-2}{2d}R\right), \qquad U_1 = -\frac{R}{d}, \qquad U_0 = -\frac{R}{d-1}\\ U_\sigma &= -\frac{1}{d-1}R - \frac{d}{d-1}\left(\Lambda_k - \frac{d-2}{2d}R\right)\end{aligned} \tag{B.3}$$

We can express the traces in terms of the heat kernel anti-Laplace transform with respect to Δ_i and expand in the early time s. Hence

$$S = \mathrm{Tr}[W(\Delta)] = \int ds \mathrm{Tr}[e^{-\Delta s}]\tilde{W}(s) \approx \frac{1}{(4\pi)^{d/2}}\sum_{n=0}^{\infty} Q_{\frac{d}{2}-n}[W]A_n(R,\Lambda_k) \tag{B.4}$$

The Seeley-DeWitt coefficients coming from the expansion of the heat kernel are $A_{i,n} =$

$\int d^dx\sqrt{g}a_{i,n}$, with [51]

$$
\begin{aligned}
&a_{0,0}=a_{\sigma,0}=1, \qquad a_{1,0}=d-1, \qquad a_{\perp,0}=\frac{(d-2)(d+1)}{2}\\
&a_{0,1}=\frac{d+5}{6(d-1)}R, \qquad a_{\sigma,1}=\frac{d+5}{6(d-1)}R+\frac{d}{d-1}\left(\Lambda_k-\frac{d-2}{2d}R\right),\\
&a_{1,1}=\frac{d^2+5d-12+6\delta_{d,2}}{6d}R,\\
&a_{\perp,1}=\frac{d(d+1)(d+2)(d-5+3\delta_{d,2})-12(d-2)(d+1)}{12d(d-1)}R+(d-2)(d+1)\left(\Lambda_k-\frac{d-2}{2d}R\right).
\end{aligned}
\tag{B.5}
$$

Also, we have the terms giving rise to R^2-terms

$$
\begin{aligned}
a_{0,2}&=\frac{-6+133d+48d^2+5d^3}{-360d(d-1)^2}R^2,\\
a_{\sigma,2}&=\frac{-6+133d+48d^2+5d^3}{360d(d-1)^2}R^2+\left(\Lambda_k-\frac{d-2}{2d}R\right)\left(\frac{d+5}{6(d-1)}R+\frac{1}{2}\left(\Lambda_k-\frac{d-2}{2d}R\right)\right),\\
a_{1,2}&=\frac{(d-3)(-240+d(202+d(63+5d)))+360(2\delta_{4,d}+\delta_{2,d})}{360d^2(d-1)}R^2\\
a_{\perp,2}&=\frac{(d+1)((d-2)(d-1)(-720+d(-234+d(-7+5d)))+3240\delta_{4,d})}{720d^2(d-1)^2}R^2+\\
&+\left(\Lambda_k-\frac{d-2}{2d}R\right)\left(\frac{(d+1)(12+d(-16+(-3+d)d))}{6d(d-1)}R+\frac{(d+1)(d-2)}{2}\left(\Lambda_k-\frac{d-2}{2d}R\right)\right).
\end{aligned}
\tag{B.6}
$$

And the functionals $Q_m[W]$ for $m>0$ are given by the Mellin transform

$$
Q_m[W]=\frac{1}{\Gamma(m)}\int_0^\infty dz z^{m-1}W(z), \tag{B.7}
$$

where we have to identify z to the corresponding Laplacians for the different spin fields. Also, for $Q_{-m}[W]$ with $m\leq 0$

$$
Q_{-m}[W]=(-1)^m\frac{d^mW(z)}{dz^m}|_{z=0}. \tag{B.8}
$$

Since all the $W(z)$ terms contain the derivative in the regulator, and z depends on Λ_k , for a regulator of the form $R_k(z)=\frac{1}{G_k}r_k(z)$, we can brake down (B.7) in three parts by considering

$$
\partial_t R_{k,i}(z)=\frac{1}{G_k}(-\eta_N r_{k,i}(z)+\dot{r}_{k,i}(z)+r'_k(z)\dot{U}_i), \tag{B.9}
$$

where the anomalous dimension is $\eta_N=\partial_t G_k/G_k$, and dot means derivative respect t. Hence, (B.7) for $m>0$ can be written in a dimensionless way as

$$
Q_{m,i}=\frac{(-1)^{[i]}}{2\cdot\Gamma(m)}k^{2m}(\phi_m[r_{k,i}]-\eta_N\tilde{\phi}_m[r_{k,i}]+\dot{U}_i(R,\Lambda_k)\hat{\phi}_m[r_{k,i}]), \tag{B.10}
$$

the index $[i]$ is defined as $[2] = [\sigma] = 0$, and $[1] = [0] = 1$, and the threshold functions are defined as

$$\phi_m = \int_0^\infty dz z^{m-1} \frac{\dot{r}_{k,i}(z)}{z + r_{k,i}(z)}, \quad \tilde{\phi}_m = \int_0^\infty dz z^{m-1} \frac{r_{k,i}(z)}{z + r_{k,i}(z)} \quad \hat{\phi}_m = \int_0^\infty dz z^{m-1} \frac{r'_{k,i}(z)}{z + r_{k,i}(z)}. \tag{B.11}$$

For $m = 0$ we have

$$Q_{0,i}[W] = W(z)|_{z=0} = \frac{(-1)^{[i]}}{2} \left(\frac{\dot{r}_{k,i}(z)}{r_{k,i}(z)} - \eta_N + \frac{r'_{k,i}(z)\dot{U}_i}{r_{k,i}(z)} \right) \Bigg|_{z=0}. \tag{B.12}$$

In four dimensions, using the exponential shape function (3.37), $\bar{V} = k^4 \int d^d x \sqrt{g}$, and the dimensionless quantities $R \to k^2 R$, $\lambda = k^{-2}\Lambda_k$ the different traces of the RHS of the flow equation are

$$\begin{aligned}
S_0 &= \frac{-2160\zeta(3) + 540\eta_G + 90(3\eta_G - \pi^2)R + 269(\eta_G - 2)R^2}{17280\pi^2} \bar{V}, \\
S_\sigma/\bar{V} &= \frac{8\lambda\left(6\gamma(\beta\lambda + 2\lambda) + 8\lambda(\beta\lambda + 2\lambda + 3) + 3\pi^2\right) + 6\left(\pi^2 - 6\right)\beta\lambda - 3\eta(4\lambda(8\lambda + 3) + 9)}{864\pi^2} \\
&\quad + \frac{-72\lambda + 108\zeta(3)}{864\pi^2} + R\frac{4(8\lambda + 3\gamma)(\beta\lambda + 2\lambda) - 3\eta(16\lambda + 3) + 96\lambda + 3\pi^2}{1728\pi^2} \\
&\quad + R^2\frac{29(2\beta\lambda - 3\eta + 4\lambda + 6)}{51840\pi^2} \\
S_1/\bar{V} &= \frac{-2160\zeta(3) + 540\eta_G + 60(3\eta_G - \pi^2)R + 109(\eta_G - 2)R^2}{5760\pi^2} \bar{V}, \\
S_2/\bar{V} &= \frac{5\left(4\lambda\left(3(2\lambda + \gamma)(\beta\lambda + 2\lambda) + 12\lambda + \pi^2\right) + \left(\pi^2 - 6\right)\beta\lambda - 3\eta\left(8\lambda^2 + 2\lambda + 1\right)\right)}{96\pi^2} \\
&\quad + \frac{5\left(-12\lambda + 12\zeta(3)\right)}{96\pi^2} - R\frac{25\left(6((4\lambda + \gamma)(\beta\lambda + 2\lambda) + 8\lambda) - 3\eta(8\lambda + 1) + \pi^2\right)}{576\pi^2} \\
&\quad - R^2\frac{719(-\beta\lambda + \eta - 2(\lambda + 1))}{3456\pi^2}
\end{aligned} \tag{B.13}$$

Appendix C

f(R) theory

The functions and functionals appearing on (4.7)

$$\partial_t f - 2Rf' + 4f = I_0[f] + I_1[f] \cdot \partial_t f' + I_2[f] \cdot \partial_t f'',$$

are

$$I_0[f] = \left[P_0^S + P_0^V + \frac{P_0^{T1} \cdot f' + P_0^{T2} \cdot R \cdot f''}{D^T} + \frac{P_0^{S1} \cdot f' + P_0^{S2} \cdot f'' + P_0^{S3} \cdot R \cdot f'''}{D^S} \right] \tag{C.1}$$

$$I_1[f] = \left[\frac{P_1^T}{D^T} + \frac{P_1^S}{D^S} \right] \tag{C.2}$$

$$I_2[f] = \frac{P_2^S}{D^S} \tag{C.3}$$

The f-dependent denominators of $I_i[f]$ are

$$D^T[f] = 3f - (R-3)f' \tag{C.4}$$

$$D^S[f] = 2f + (3-2R)f' + (3-R)^2 f''. \tag{C.5}$$

The numerators are

$$P_0^S = \frac{271}{90}R^2 - 12R - 12 \tag{C.6}$$

$$P_0^V = \frac{191}{30}R^2 - 24R - 36 \tag{C.7}$$

$$P_c^V = \frac{607}{15}R^2 - 24R - 144, \tag{C.8}$$

$$P_c^S = \frac{511}{30}R^2 - 12R - 36, \tag{C.9}$$

$$P_0^{T1} = \frac{311}{756}R^3 - \frac{1}{3}R^2 - 90R + 240, \tag{C.10}$$

$$P_0^{T2} = -\frac{311}{756}R^3 + \frac{1}{6}R^2 + 30R - 60, \tag{C.11}$$

$$P_0^{S1} = \frac{37}{756}R^3 + \frac{29}{15}R^2 + 18R + 48, \tag{C.12}$$

$$P_0^{S2} = -\frac{37}{756}R^4 - \frac{29}{10}R^3 - \frac{121}{5}R^2 - 12R + 216, \tag{C.13}$$

$$P_0^{S3} = \frac{181}{1680}R^4 + \frac{29}{15}R^3 + \frac{91}{10}R^2 - 54, \tag{C.14}$$

$$P_1^T = \frac{311}{1512}R^3 - \frac{1}{12}R^2 - 15R + 30, \tag{C.15}$$

$$P_1^S = \frac{37}{1512}R^3 + \frac{29}{60}R^2 + 3R + 6, \tag{C.16}$$

$$P_2^S = -\frac{181}{3360}R^4 - \frac{29}{30}R^3 - \frac{91}{20}R^2 + 27. \tag{C.17}$$

Appendix D

RG Flows in Einstein-Hilbert gravity

The coefficients appearing in (5.6) and (5.7)

$$a_1(\lambda) = f_1\phi^1_{d/2}(-2\lambda)) + f_2\phi^1_{d/2}(-2\alpha\lambda) + f_3\phi^1_{d/2}(0), \tag{D.1}$$

$$a_2(\lambda) = \frac{1}{2}\left\{f_1\hat{\phi}^1_{d/2}(-2\lambda) + f_2\hat{\phi}^1_{d/2}(-2\alpha\lambda)\right\}, \tag{D.2}$$

$$\begin{aligned} b_1(\lambda) = {} & f_4\phi^1_{d/2-1}(-2\lambda) + f_5\phi^1_{d/2-1}(-2\alpha\lambda) + f_6\phi^2_{d/2}(-2\lambda) + f_7\phi^2_{d/2}(-2\alpha\lambda) \\ & + f_8\phi^1_{d/2-1}(0) + f_9\phi^2_{d/2}(0) + f_{10}\phi\delta_{d,2}\left(\frac{1}{1-2\lambda} - \frac{1}{1-2\alpha\lambda}\right) \end{aligned} \tag{D.3}$$

$$\begin{aligned} b_2(\lambda) = {} & \frac{1}{2}f_4\hat{\phi}^1_{d/2-1}(-2\lambda) + \frac{1}{2}f_5\hat{\phi}^1_{d/2-1}(-2\alpha\lambda) + \frac{1}{2}f_6\hat{\phi}^2_{d/2}(-2\lambda) \\ & + \frac{1}{2}f_7\hat{\phi}^2_{d/2} + \frac{1}{2}f_{10}\delta_{d,2}\left(\frac{1}{1-2\lambda} - \frac{1}{1-2\alpha\lambda}\right) \end{aligned} \tag{D.4}$$

where the threshold functions are

$$\begin{aligned} \phi^n_m(w) &= \frac{1}{\Gamma(m)}\int_0^\infty dy y^{m+1}\frac{-r'(y)}{(y(1+r(y))+w)^n}, \\ \hat{\phi}^n_m(w) &= \frac{1}{\Gamma(m)}\int_0^\infty dy y^{m+1}\frac{r'(y)}{(y(1+r(y))+w)^n}, \end{aligned} \tag{D.5}$$

in this work we use the optimised cutoff $r = (k^2 - q^2)\theta(k^2 - q^2)$ [53, 54]. With this choice the threshold functions are:

$$\phi^n_m(w) = \frac{1}{\Gamma(m+1)(1+w)^n}, \qquad \hat{\phi}^n_m(w) = \frac{1}{\Gamma(m+2)(1+w)^n} \tag{D.6}$$

the coefficients f_i which only depends on the gauge fixing parameter α and the dimension of the space-time are

$$
\begin{aligned}
&f_1 = d(d-1)f_0, \quad f_2 = 2df_0, \quad f_3 = -4df_0, \quad f_4 = \frac{d^3-2d^2-11d-12}{d}f_0, \\
&f_5 = 2\frac{d^2-6}{3d}f_0, \quad f_6 = -2\frac{d^3-4d^2+7d-8}{d-1}f_0, \quad f_7 = 4\frac{d+1-\alpha d(d-2)}{d}f_0, \\
&f_0 = (4\pi)^{1-d/2}, \quad f_8 = -2f_5, \quad f_9 = -\frac{8}{d}(d+1)f_0, \quad f_{10} = 12f_0.
\end{aligned}
\tag{D.7}
$$